Benjamin Josef Sorgmann, BSc

Development of Aluminium doped Zinc Oxide by Plasma-Enhanced Atomic Layer Deposition

MASTER'S THESIS

to achieve the university degree of

Diplom-Ingenieur

Master's degree programme: Advanced Materials Science

submitted to

Graz University of Technology

Supervisor

Assoc.-Prof. Dr. Anna Maria Coclite

Institute of Solid State Physics

Univ.-Prof. Ph.D. Peter Hadley
Institute of Solid State Physics

Graz, April 2018

AFFIDAVIT

I declare that I have authored this thesis independently, that I have not used other than the declared sources/resources, and that I have explicitly indicated all material which has been quoted either literally or by content from the sources used. The text document uploaded to TUGRAZonline is identical to the present master‘s thesis.

Date

Signature

ABSTRACT

Zinc oxide is a wide direct band gap semiconductor that crystallizes in a hexagonal wurtzite-structure. Zinc oxide thin films have been used for several applications such as transparent conductive oxide (TCO), ultraviolet light emitters, solar cell windows, bulk acoustic wave devices [1-4] and many more. For such TCOs, the resistivity has to be low. For zinc oxide, a reduction of the resistivity can be achieved via aluminium doping.

For depositing the thin films, plasma-enhanced atomic layer deposition (PEALD), a self-limiting process that allows sub-monolayer thickness control as well as conform and uniform coatings, is used. In the process oxygen-plasma is used as the co-reactant, enabling depositions at room temperature. Most often water is used as a co-reactant, but it requires high temperatures (>300 °C) to oxidize the precursor. Trimethylaluminium (TMA) is used to deposit aluminium oxide layers, whereas Diethylzinc (DEZ) is used to deposit zinc oxide layers. By alternating those precursors, so called super-cycles are created with different aluminium contents in the thin films while changing the number of DEZ-cycles followed by one TMA-cycle.

This work comprises the upgrading of the ALD-setup (adding a line for TMA) and the optimization of the dopant content for the best electrical properties. The thin films are characterized by spectroscopic ellipsometry, x-ray fluorescence, x-ray photoelectron spectroscopy, x-ray diffraction and 4-point probe.

The results show that the aluminium-content can be controlled by changing the number of DEZ-cycles, followed by one TMA-cycle. The variation of the aluminium content pointed out a minimum of the resistivity as well as a change in the inter-planar distance and of the crystallite size.

KURZFASSUNG

Zinkoxid ist ein Halbleiter mit einer großen, direkten Bandlücke, der in einer hexagonalen Wurtzite-Struktur kristallisiert. Dünnschichten von Zinkoxid haben viele Anwendungsbereiche wie transparente und leitfähige Oxide, UV-Lichtemitter, Solarzellen-Fenster, akustische Volumenwellenvorrichtungen und einige mehr. Für diese Oxide ist niedriger spezifischer Widerstand essenziell. Eine Reduktion des spezifischen Widerstandes von Zinkoxiden kann mittels Aluminium-Doping erreicht werden.

Plasmaunterstützte Atomlagenabscheidung (PEALD) wird zur Herstellung der Dünnschichten verwendet. Das ist ein selbstlimitierender Prozess, welcher eine Dickenkontrolle im Submonolagenbereich sowie das Auftragen von konformen und homogenen Schichten ermöglicht. Diesbezüglich verwendet man Sauerstoff-Plasma als Co-Reaktant, was Depositionen bei Raumtemperatur ermöglicht. Meistens jedoch wird Wasser als Co-Reaktant verwendet, was aber hohe Temperaturen (>300 °C) benötigt um die chemischen Vorprodukte zu oxidieren. TMA wird verwendet um Aluminiumoxidschichten aufzutragen, wohingegen DEZ verwendet wird um Zinkoxidschichten herzustellen. Durch das Wechseln der chemischen Vorprodukte werden sogenannte Super-Zyklen abgeschieden, was zu einem unterschiedlichen Aluminiumgehalt der Dünnschichten führt. Dies wird durch das Ändern der Anzahl der DEZ-Zyklen, gefolgt von einem TMA-Zyklus erreicht.

Diese Arbeit beinhaltet die Erweiterung des ALD-Aufbaus (Hinzufügen einer TMA-Leitung) und der Optimierung des Doping-Gehalts für die besten elektrischen Eigenschaften. Die Dünnschichten werden mittels spektroskopischer Ellipsometrie, Röntgenfluoreszenz, Röntgenphotoelektronenspektroskopie, Röntgenbeugung und 4-Punkt Probe charakterisiert.

Die Ergebnisse zeigen, dass mittels dieses Verfahrens der Aluminiumgehalt durch die Änderung der Anzahl der DEZ-Zyklen, gefolgt von einem TMA-Zyklus, kontrolliert werden kann. Diese Änderung des Aluminiumgehalts weist ein Minimum des spezifischen Widerstandes auf. Auch kann diesbezüglich eine Änderung der Kristallit-Größe und des Abstandes zwischen parallelen Gitterebenen festgestellt werden.

ACKNOWLEDGMENTS

I am very grateful to my supervisor Ass.Prof. Anna Maria Coclite for guiding me through my master thesis and for always finding some time when I needed help. I am also thankful for the nice experiences I had with her and Dorr. Mag Alberto Perrotta during our travel to Elettra in Trieste.

It was a privilege to share the office with Paul Christian, Julian Pilz, Marianne Kräuter, Fabian Muralter and Katrin Unger. I am especially grateful to Paul Christian for his great inputs, Fabian Muralter for helping me with chemical difficulties and Julian Pilz for his all-time support.

Julian Pilz and Alberto Perrotta have been a great help for the experimental part as well as data analysis.

I want to thank my co-supervisor Univ.-Prof. Ph.D. Peter Hadley for introducing me to 4-point probing.

I am grateful to Prof. Roland Resel and his group members for helping me with the analysis of the XRF-Data.

I would like to thank all of them for the great time I have had during my master thesis.

I want to thank my family for their financial and scientific support as well as for being there whenever I need them. Thanks a lot to Josef, Waltraud, Nathalie, Christoph and Helene Sorgmann as well as to Günther and Annemarie Eberhard.

I want to mention the great discussions with my father Josef Sorgmann, which have helped me a lot with the solution of physical and mathematical problems during my whole study.

Last but not least, I want to thank my friends Richard Berger and Anna Gruber for the adjustments of my master thesis.

CONTENTS

LIST OF FIGURES

LIST OF TABLES

ACRONYMS

Al	Aluminium
ALD	Atomic Layer Deposition
AZO	Aluminium doped Zinc Oxide
Al_2O_3	Aluminium oxide
C	Carbon
CPS	Counts Per Second
CVD	Chemical Vapour Deposition
DEZ	Diethylzinc
GPC	Growth Per Cycle
PEALD	Plasma Enhanced Atomic Layer Deposition
QCM	Quartz Crystal Microbalance
RT	Room Temperature
SE	Spectroscopic Ellipsometry
Si	Silicon
SiO2	Silicon dioxide
TMA	Trimethylaluminium
XRD	X-ray Diffraction
XRF	X-ray Fluorescence
XPS	X-ray Photoelectron Spectroscopy
Zn	Zinc
ZnO	Zinc oxide

1) INTRODUCTION

Zinc oxide (ZnO) is a II-VI binary compound semiconductor with a wide direct band gap of about 3.4 eV [5]. Aluminium doped ZnO (AZO) thin films have a great potential in many applications like transparent conductive oxide (TCO), ultraviolet light emitters, solar cell windows and bulk acoustic wave devices, to name only a few [1-4]. Aluminium creates a n-type semiconductor due to its donor character while being incorporated into the wurtzite-structure of ZnO.

To achieve a defined aluminium doping concentration, atomic layer deposition (ALD) is chosen as the deposition method. Repeating a so-called cycle (section 2.2) while working in saturation regime (Figure 2) leads to a self-limiting process achieving a thickness control of the deposited layers in the range of Angstrom (Å). The deposited aluminium content can be controlled precisely using different processes, aluminium oxide and zinc oxide, and varying their cycle ratios leading to super-cycles (section 2.5.2). Another benefit of ALD is the uniform and conformal layer growth leading to the same doping concentration on large area or multiple samples. Plasma-enhanced atomic layer deposition (PEALD) is a sub-process of ALD, using plasma species as the co-reactant.

The goal of the master thesis is the optimization of AZO deposition obtaining low resistivity films by using PEALD. To determine the aluminium content of the deposited AZO thin films, X-ray fluorescence and X-ray photoelectron spectroscopy were used. X-ray diffraction was carried out for various aluminium content samples to investigate the crystal structure, the crystallite size, and the inter-planar distance. For such deposited super-cycles also the growth per cycle and the refractive index were investigated. 4-point probe measurements were done to investigate the resistivity dependency on the aluminium content. All investigations were done at two different deposition temperatures, room temperature and 150 °C. It is shown that the resistivity decreases with increasing deposition temperature. Moreover, the influence of the annealing process on the resistivity of the AZO thin films, deposited at room temperature, is discussed.

The master thesis consists of three different parts. The first part describes the principles of ALD as well as the modifications on the setup to obtain doping. Furthermore, the fundamentals, applications and properties of aluminium oxide, zinc oxide and aluminium doped zinc oxide thin films are explained.

The second part contains the used setup for depositing AZO thin films via PEALD as well as an overview of the experimental plan. The adopted characterisation methods are also described.

The third part is about the results obtained from the different characterisation techniques.

Part I

FUNDAMENTALS

The first part of “FUNDAMENTALS” describes the principles of atomic layer deposition (ALD) based on the common ALD method, referred as thermal ALD. Furthermore, the differences between thermal ALD and plasma-enhanced ALD (PEALD) are discussed.

The second part comprises some fundamentals, applications and properties of aluminium oxide, zinc oxide and aluminium doped zinc oxide thin films. Additionally, some growth characteristics depending on the used amount of aluminium doping concentration are described.

2) ATOMIC LAYER DEPOSITION

This chapter describes the principles of atomic layer deposition (ALD) and the doping process related to this method. It comprises the characteristics of ALD, the process leading to layer-by-layer deposition, all kinds of materials that can be used and some demands on the used precursors. Furthermore, the difference between thermal ALD and the used method of plasma-enhanced ALD is explained. At the end of the chapter, a further main topic, "DOPING", is treated.

As mentioned in the previous work "Plasma-enhanced atomic layer deposition of zinc oxide thin films" by Dipl. Ing. Julian Pilz, more details on ALD can be found in the book chapter "Atomic Layer Deposition" by Harm Knoops et al. [6] and in the book "Atomic layer deposition of nanostructured materials" edited by Nicola Pinna and Mato Knez [7].

For more details on doping, look at the supporting Documents "Oberflächen- und Dünnschichtphysik" by Assoc. Prof. Dr. Anna Maria Coclite [8], or at the webpage "https://www.halbleiter.org/en/waferfabrication/doping/" [9]. A deeper introduction on the ALD method is given by the paper "Structural, electrical, and optical properties of atomic layer deposition Al-doped ZnO films" by Parag Banerjee et al [5].

2.1 INTRODUCTION

Atomic layer deposition (ALD), a subclass of chemical vapour deposition (CVD), is a thin film method in which a film is grown on a substrate by exposing its surface to sequentially alternating precursors. The precursor flows into the reactor are separated by a non-reactive gas purge and for that reason they react only with the surface of the sample and not with themselves. Those steps are repeated cyclically. A cycle consists of introducing a first precursor, which is often a metal-organic one acting as metal source, a second one (also referred as co-reactant), which is mostly a gas showing chemical surface reactions like oxidation, hydrolysis or reduction, and their separation steps.

To be able to deposit the precursors via ALD, they have to fulfil some demands. They have to have a high vapour pressure leading to full saturation in the vacuum chamber, a good thermal stability avoiding decompositions during the deposition process and they have to be able to chemisorb on the substrate surface to enable the growth of the layers.

Theoretically one ALD cycle should lead to the deposition of a full monolayer. Practically, though, the precursor molecules absorbed on the active sites may hinder a uniform coverage by steric hindrance. As a consequence, only sub-monolayers can be deposited within one cycle. A great thickness control can be obtained. To achieve such self-limiting processes, the exposure of all of the steps, precursor and purging doses, have to be in saturation. Saturation means that the exposure times for the precursors have to be long enough to cover the whole substrate and the purging times have to be long enough to avoid intermixing of precursors

residues from previous doses, which would end up in a CVD-like growth. This leads to a uniform and conformal growth.

The benefits of ALD, like the described conformality, uniformity and thickness control (Figure 1), lead to many possibilities as coating of organic substrates, 3D structures or large areas.

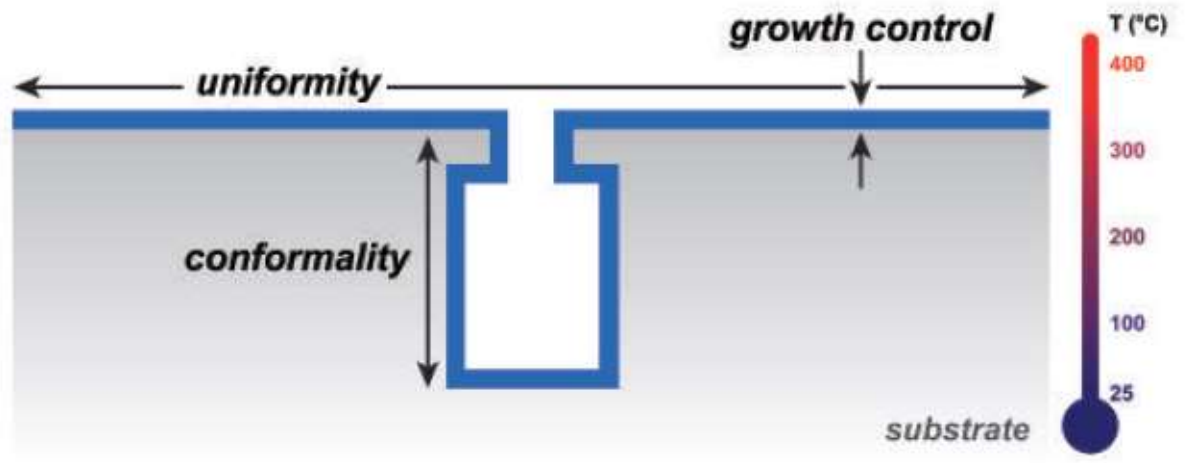

Figure 1: Desired characteristics of thin film growth. Image reprinted from [6]

2.2 THE ALD PROCESS

The process mentioned in section 2.1 consists of the following four parts leading to two half-cycles (Figure 2): The precursor dose and the purging step after the precursor dose as well as the co-reactant dose and the purging step after the co-reactant dose. In the middle, the four parts of the cycle are drawn to picture the cycle by cycle growth. Furthermore, arrows are used to indicate the saturation. The explanation for each of those parts are given below.

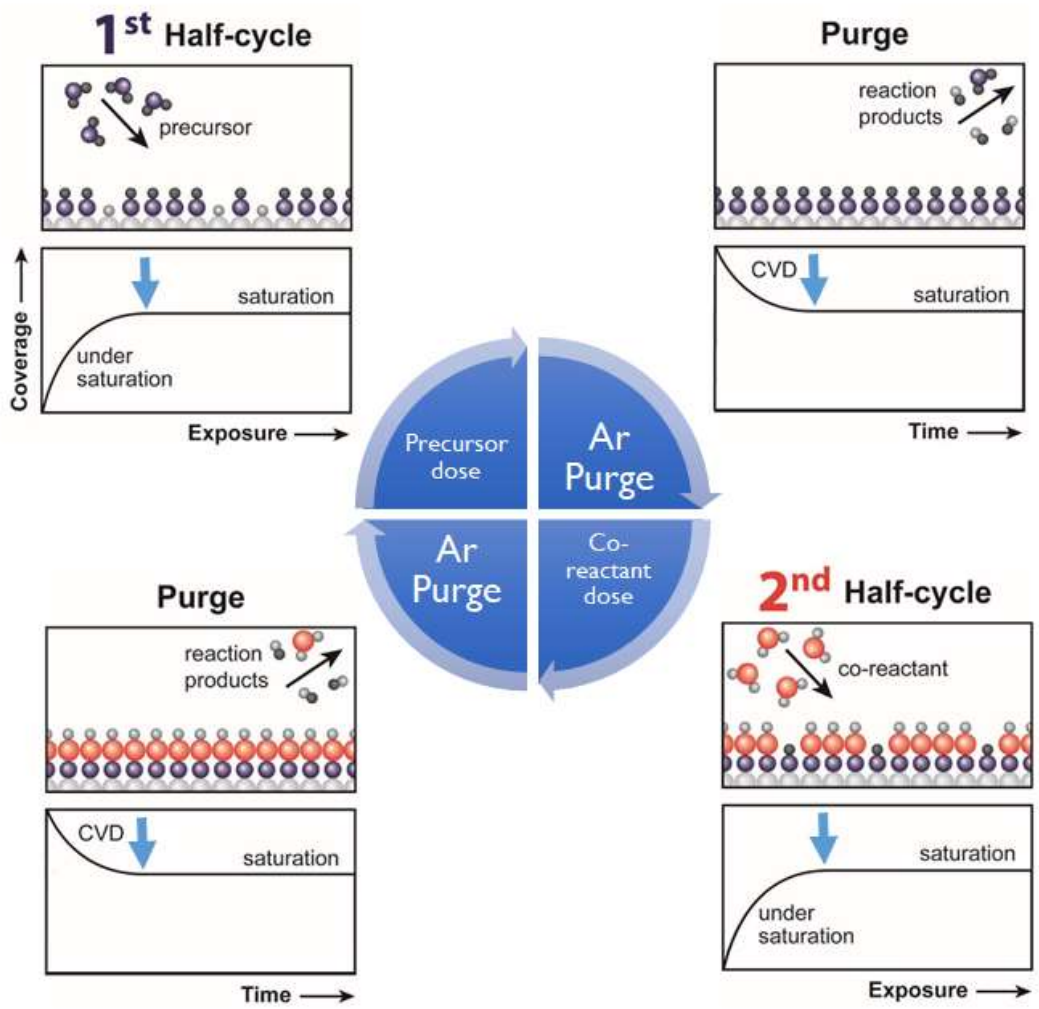

Figure 2: Basic scheme of the ALD process. Image reprinted from [6] and modified

The first half-cycle consists of the metalorganic precursor and the purging step afterwards.

1. **Precursor dose:** The precursor is pulsed into the reactor via opening and closing of a valve. The dose has to be long enough to fully cover the substrate surface leading to one monolayer or even one sub-monolayer. The precursor molecules chemisorb only on so-called active sites, functional groups and/or defects created by heat or plasma, on the substrate. The growth rate is limited by the number of active sites and determined by the nature of the precursor-surface interaction.

2. **Purging after precursor dose:** The purging time has to be long enough to remove the by-products that are created during the chemisorption of the precursor as well as the excess of the molecules itself. Otherwise not only the chemisorbed precursor, but also the excess of it and the produced by-products react with the following co-reactant molecules, which corresponds to a CVD-like growth and not a self-limited ALD process.

The second half-cycle consists of the co-reactant and the following purging step.

3. **Co-reactant dose:** Also the co-reactant is pulsed into the vacuum chamber to react with the deposited precursor molecules. The dose has to be long enough to fully oxidize or hydrolyse the precursor to create the desired layer.

4. **Purging after co-reactant dose:** This purging step is also done to avoid a CVD-like growth by removing the by-products and the exceeded co-reactant.

Those two half-cycles lead, due to its self-limiting surface reactions, to a characteristic growth per cycle (GPC) resulting in the desired thickness of the deposited layer by repeating the whole cycle. In the ideal case, the GPC is one monolayer, but a steric hindrance results in a GPC lower than that. The steric hindrance comes into play when the distance between the active sites is smaller than the dimensions of a precursor molecule. This results into not having every active site available for the deposition process. However, such hindrance does not affect the self-limiting and dense packing of the deposited thin film.

To further illustrate the 2 half-cycles of the ALD process, the two reactions (1 and 2), occurring thereby, are displayed below. The surface (s) with surface groups (Y), the precursor (AX_2) and the co-reactant (BY_2) have to be considered to result in by-products (XY), intermediate (AX) and after finishing one cycle in the desired layer (ABY). The surface groups that are involved into the reactions, are acting as this so-called active sites. The precursor and co-reactant consist of the desired elements A and B, while having 2-ligands attached to each of those. Such a reaction can be considered for example having an ALD process with diethylzinc ($Zn(Et)_2$) as precursor and water (H_2O) as co-reactant.

$$s - Y_{(ad)} + AX_{2(g)} \rightarrow s - AX_{(ad)} + XY_{(g)} \quad (1)$$

$$s - AX_{(ad)} + BY_{2(g)} \rightarrow s - ABY_{(ad)} + XY_{(g)} \quad (2)$$

2.3 MATERIALS AND PRECURSORS

The different materials marked in the periodic table (Figure 3) can be deposited in an ALD process. By modifying the process, adding half-cycles, a deposition of compounds with a higher order can be done as well. Furthermore, doped thin films can be created (section 2.5.2). To achieve the desired layer via ALD, the corresponding precursor, one of the marked elements in Figure 3, have to fulfil some requirements:

- The precursor has to be sufficiently volatile to enable sequentially pulsing.
- The precursor has to be reactive only to the created surface groups, to avoid undesirable side reactions.
- The reaction with the surface groups has to be terminated by them, to achieve a self-limiting process resulting in a characteristic GPC.
- The decomposition temperature of the precursor has to be very high, to enable the chemisorption process.
- The by-products have to be volatile to be able to purge them, so a CVD-like growth can be avoided.
- The by-products have to have a lower reactivity, so that they do not influence the precursor chemisorption process on the whole surface.

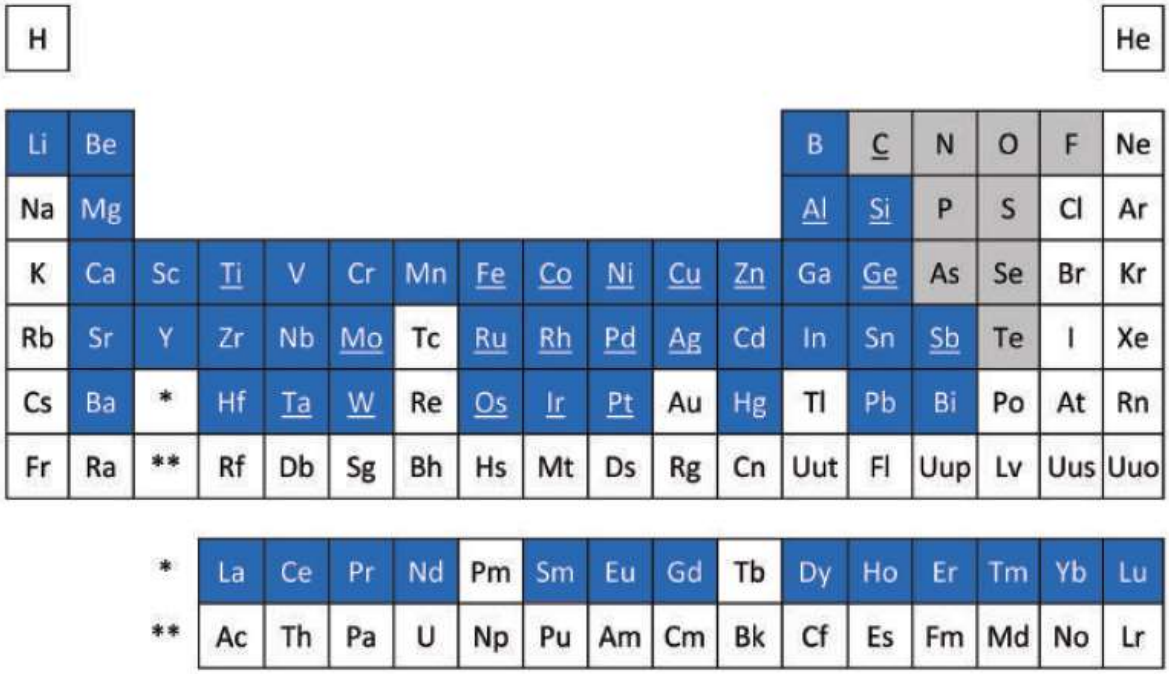

Figure 3:Materials that have been deposited by ALD (by 2015). Blue marked elements are those which have been deposited in a compound such as oxides, nitrites, carbides etc. The grey elements serve as the non-metallic component. Underlined elements have also been deposited purely. Image reprinted from [6]

Due to the requirements on the thermal stability of the precursor, it can be suggested that there exists an optimal temperature window for ALD processes. This temperature window depending on the precursor is shown in Figure 4. If the temperature is too low, condensation resulting in an increased GPC can occur. In contrast, the GPC can be reduced if the reactivity is lowered by decreasing the temperature. If the deposition temperature is higher than the decomposition temperature, the process results in a higher GPC, due to decomposition before reacting with the surface. On the other hand, also desorption resulting in a decrease of the GPC can happen.

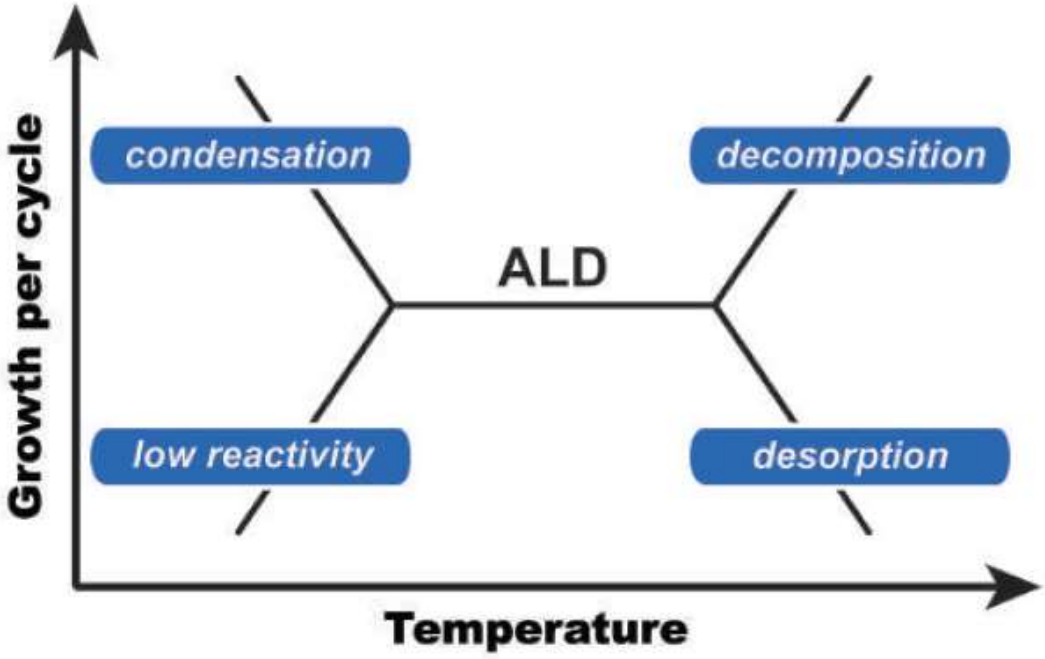

Figure 4: Growth per cycle as a function of substrate temperature in a thermal ALD process. Image reprinted from [6]

2.4 THERMAL AND PLASMA-ENHANCED ATOMIC LAYER DEPOSITION

Until now, the common atomic layer deposition (ALD), referred as thermal ALD, has been discussed. Consequently, this section contains the main difference to PEALD exhibiting a different behaviour of the deposited film.

The main difference is the driving force of the surface reaction. While the common ALD uses thermal energy to create reactive species, for PEALD it is the plasma. Plasma combined with typical gases like O_2, N_2 or H_2 is used as the co-reactant. Due to the high reactivity of the plasma radicals, the temperature window is extended to lower temperatures, which results in a greater choice of precursors and materials as well as the possibility of doing depositions even like room temperature. Due to several plasma parameters that can be changed, the possibility to tune the material properties are given as well. Nevertheless, PEALD results in a denser packed thin film with less impurity content and a reduced defect density. This leads to a higher resistivity, which is for example reported on ZnO-films in the paper “Structural, optical, electrical and resistive switching properties of ZnO thin films deposited by thermal and plasma-enhanced atomic layer deposition” by Jian Zhang et al. [10].

Plasma in general is defined as a collection of electrons, neutral atoms, positive and negative charged ions as well as neutral and charged molecules. So plasma generates via accelerating electrons through an electric field excited and reactive species (radicals). Due to the different flux rates, the central role in inducing surface reaction by plasma is done by its radicals.

2.5 DOPING

This section gives a short introduction into the doping process including some general properties and methods. More information about this topic can be found in the supporting documents “Oberflächen- und Dünnschichtphysik” by Assoc. Prof. Dr. Anna Maria Coclite [8] and on the internet using the following link “https://www.halbleiter.org/en/waferfabrication/doping/” [9]. Furthermore, the doping process for the atomic layer deposition method is specified by underlying self-drawn figures. Information about doping in relation to ALD can be found in the paper “Structural, electrical, and optical properties of atomic layer deposition Al-doped ZnO films” by Parag Banerjee et al [5].

2.5.1 INTRODUCTION INTO DOPING

It is common to dope semiconductors in order to change their conductivity. Doping is achieved by enhancing the impurities in the crystal structure by taking an element that has a different amount of electrons in the valance shell compared to the basic material. As a consequence, an excess of electrons (n-type semiconductor) or a deficiency of electrons (p-type semiconductor) is created.

To introduce such impurities, foreign substances and different techniques are used. Depending on the doping procedure, a partial or uniform doping concentration over the whole sample can be achieved. The first one occurs for example via photolithography using masks or via ion implanting, while the second one normally appears during the fabrication of the semiconductors.

The main mechanism for doping is diffusion. Thus, the impurities diffuse into the basic material. Diffusion is influenced by many factors like the concentration gradient, the dopant and substrate used themselves, the crystallographic orientation of the substrate due to different packing densities along different crystallographic orientations and the deposition temperature. Increasing the deposition temperature and the concentration gradient via adding more impurities results in a higher diffusion and moreover in a higher doping.

In contrast to uniform doping occurring during the fabrication, PEALD leads to a non-uniform one. Operating with layer-by-layer deposition (section 2.2) and at low temperatures (section 2.4) results in a decreased diffusion and as a result into a doping not distributed over the whole super-cycle (section 2.5).

2.5.2 DOPING VIA ATOMIC LAYER DEPOSITION

Figure 5 shows the cycle process for depositing a pure material. The sequential pulsing of the different parts of the cycle are displayed. For simplicity, the pulse times are equal. Furthermore, the two different purging steps are not shown as separate lines due to the equal pulsing times.

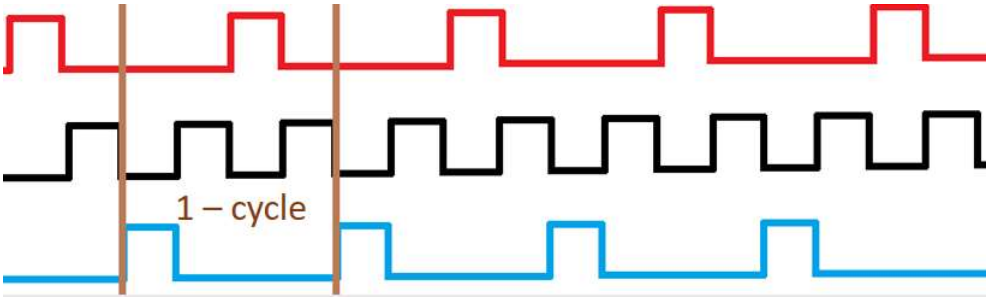

Figure 5: Schematic of depositing one cycle (brown) of zinc oxide using diethylzinc (blue) as a precursor, oxygen - plasma as co-reactant (red) and argon as purging gas (black).

The two different precursors used (described in section 4.1.3) were: diethylzinc (DEZ), shown in blue (Figure 5 and Figure 6), for depositing zinc oxide (ZnO) layers and trimethylaluminium (TMA), shown in green (Figure 6), for depositing aluminium oxide (Al_2O_3) layers. In ALD doping occurs via substituting one of the DEZ pulses through one TMA pulse. This leads to so-called super-cycles, depositing n-ZnO layers followed by one Al_2O_3 layer on top. For example, Figure 6 shows the sequential pulsing of the different precursors using a 2:1 cycle ratio due to substituting every third pulse of DEZ by TMA. Decreasing the cycle ratio leads to an increased Al-content corresponding to a reduction of the percentage of ZnO cycles deposited. While doping, the desired thickness is achieved by repeating these super-cycles, shown in the schematic diagram (Figure 7).

Each of those processes (Figure 5 and Figure 6) starts with the second half-cycle, the co-reactant dose. The reason for that is to create a surface with surface groups, the active sites as mentioned in section 2.2, to get the possibility to deposit the used precursors and attach them to the surface.

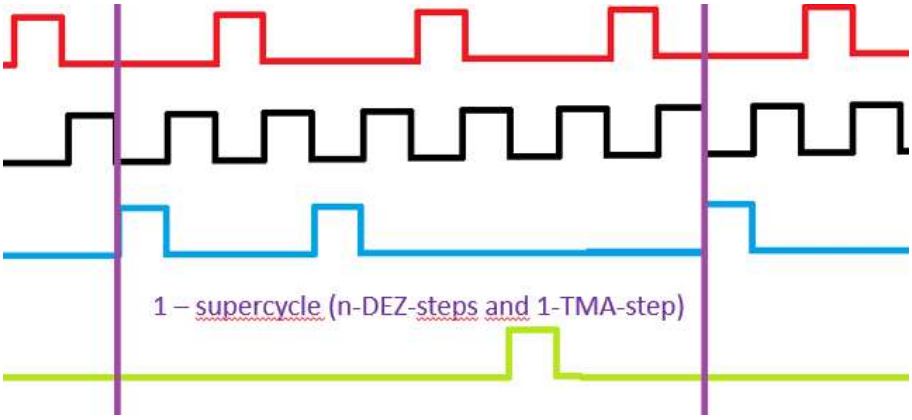

Figure 6: Schematic of depositing one super-cycle (violet) of aluminium doped zinc oxide using diethylzinc (blue) and trimethylaluminium (green) as a precursor, oxygen - plasma as co-reactant (red) and argon as purging gas (black)

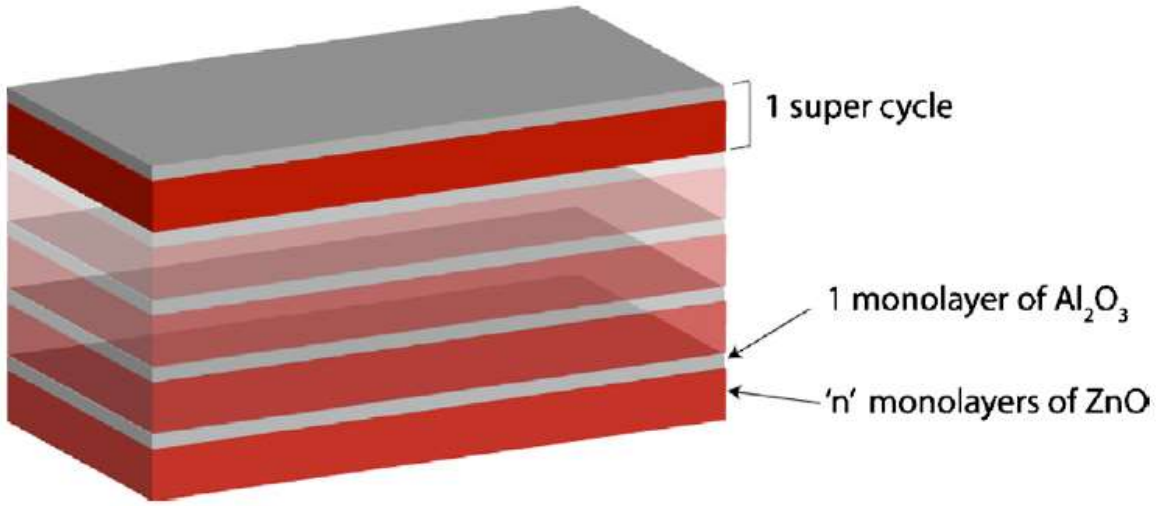

Figure 7: Schematic diagram of the film stack used to make various aluminium doped zinc oxide thin films by atomic layer deposition, where n-zinc oxide cycles (red) deposited followed by one aluminium oxide cycle deposited on top (grey) resulting in a super-cycle structure. Image reprinted from [5]

3) PROPERTIES AND BEHAVIOUR OF ALUMINIUM DOPED ZINC OXIDE

This chapter explains some properties and behaviours of aluminium doped zinc oxide (AZO) with an additional focus on the different growth rates of zinc oxide and aluminium oxide while changing the amount of aluminium doping concentration based on the paper "Growth of ZnO/Al_2O_3 Alloy Films Using Atomic Layer Deposition Techniques" by J. W. Elam and S. M. George [11]. To study the behaviour and the properties, the papers "Studies on optical, structural and electrical properties of atomic layer deposited Al-doped ZnO thin films with various Al concentrations and deposition temperatures" by W J Maeng et al. [12] and "Structural, electrical, and optical properties of atomic layer deposition Al-doped ZnO films" by Parag Banerjee et al. [5], are used.

Beforehand a short overview of some properties of zinc oxide (ZnO) and aluminium oxide (Al_2O_3) using the following papers is done: "Structural, optical, electrical and resistive switching properties of the properties of ZnO thin films deposited by thermal atomic layer deposition thermal and plasma-enhanced atomic layer deposition" by Jian Zhang et al. [10] and "Plasma-enhanced and thermal atomic layer deposition of Al_2O_3 using dimethylaluminium isopropoxide, $[Al(CH_3)_2(\mu\text{-}O^iPr)]_2$, as an alternative aluminium precursor" by Stephen E. Potts et al. [13].

3.1 ZINC OXIDE AND ALUMINIUM OXIDE

This chapter comprises some fundamentals of zinc oxide (ZnO) and aluminium oxide (Al_2O_3) like their structure as well as their electrical and optical properties. For ZnO the following paper, "Structural, optical, electrical and resistive switching properties of the properties of ZnO thin films deposited by thermal atomic layer deposition thermal and plasma-enhanced atomic layer deposition" by Jian Zhang et al. [10] is used. Further information and details about ZnO can be found in the book "Zinc Oxide: Fundamentals, Materials and Device Technology." by Hadis Moroç and Ümit Özgür [14]. For Al_2O_3 thin films deposited via thermal ALD and PEALD the paper "Plasma-enhanced and thermal atomic layer deposition of Al_2O_3 using dimethylaluminium isopropoxide, $[Al(CH_3)_2(\mu\text{-}O^iPr)]_2$, as an alternative aluminium precursor" by Stephen E. Potts et al. is made use of [13].

3.1.1 ZINC OXIDE

Zinc oxide (ZnO), a so called II-VI binary compound semiconductor with a wide direct band gap of about 3.4 eV, has due to its excellent optical, electrical and piezoelectric properties many various applications such as solar cells [15], transparent thin film transistors [16] or UV-laser [17], to name only a few. Furthermore, it has a large exciton binding energy of about 60 meV at room temperature and crystallizes under ambient conditions in a thermodynamic stable wurtzite structure for which a schematic is shown in Figure 8.

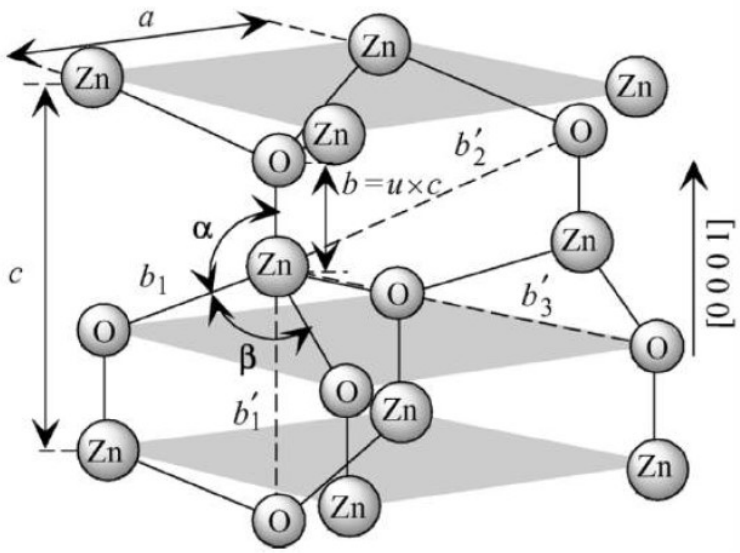

Figure 8: Schematic representation of the ZnO wurtzite crystal structure. Image reprinted from [14]

Figure 9 points out some characteristics of ZnO deposited by ALD and PEALD. The growth per cycle for ZnO depends on the temperature. Increasing the deposition temperature up to 150 °C results in an increase of the growth per cycle (GPC). Afterwards, by further increasing, the GPC decreases. Comparing thermal ALD to PEALD, a higher growth rate for PEALD can be observed. The differences are resulting from the different driving forces leading to a shift of the temperature window to lower deposition temperatures as mentioned in section 2.4.

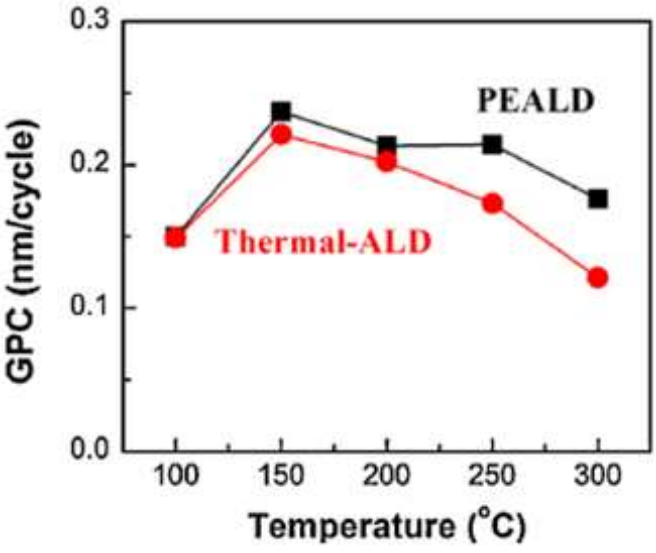

Figure 9: ZnO growth rate as a function of deposition temperature. Image reprinted from [10]

Moreover, the crystallographic structure changes for the deposited ZnO thin films at various temperatures as mentioned in the paper “Structural, optical, electrical and resistive switching properties of ZnO thin films deposited by thermal atomic layer deposition thermal and plasma-enhanced atomic layer deposition” by Jian Zhang et al. [10]. While at low temperatures (100 °C) a polycrystalline structure possessing different orientations like (100), (002) and (110) is shown, higher temperatures lead to a preferential orientation in the (002) direction. Such a change is even faster for PEALD compared to thermal ALD to achieve the same amount of the (002) preferential orientation. The same behaviour can be also recognized for aluminium doped zinc oxide thin films mentioned in section 3.2. Additionally, an increase of the deposition temperature results in a highly ordered crystallographic structure, having larger grains.

Due to the aim of the master thesis, a look on the electrical properties of ZnO are done. The resistivity, inversely proportional to the conductivity, is shown in Figure 10. While increasing the deposition temperature, the resistivity for thermal ALD shows a minimum at 200 °C. Only the resistivity for ZnO deposited via thermal ALD is represented due to PEALD grown thin films depicted much higher resistivities (> 10^4 Ωcm). Referring to this, the density of defects, such as oxygen vacancies, which are mainly accountable for the high conductivity, and the low resistivity, is low for PEALD.

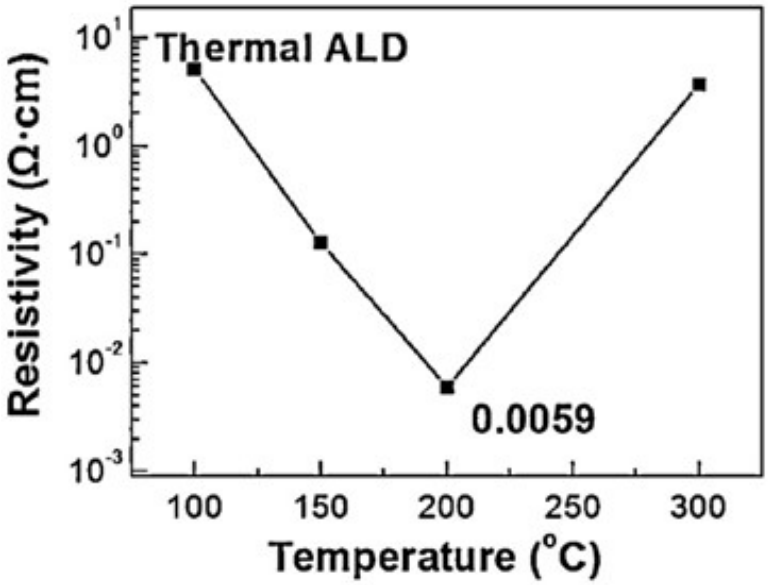

Figure 10: The resistivity as a function of substrate temperature of zinc oxide films deposited by thermal atomic layer deposition on glass substrates. Image reprinted from [10]

3.1.2 ALUMINIUM OXIDE

The second layer deposited to achieve AZO thin films are Al_2O_3 layers leading to a discussion about some behaviours of them while using ALD and furthermore some applications they are used for, like acting as a passivation layer in solar cells [18], anti-corrosion coatings for metallic substrates [19], medium-k dielectrics [20] and many more. Moreover, Al_2O_3 layers, an amorphous material and insulator with a band gap of about 8.7 eV, are used to dope the ZnO thin films via using different cycle-ratios (section 2.5.2). To do some investigation on its behaviour, the information provided from the paper "Plasma-enhanced and thermal atomic layer deposition of Al_2O_3 using dimethylaluminium isopropoxide, $[Al(CH_3)_2(\mu\text{-}O^iPr)]_2$, as an alternative aluminium precursor" by Stephen E. Potts et al. [13] is taken into account.

In contrast to ZnO (Figure 9), Al_2O_3 shows for PEALD a decrease of the growth rate, while increasing the deposition temperature to 150 °C (Figure 11). A further increase of the deposition temperature leads to a reduction of the GPC for both materials.

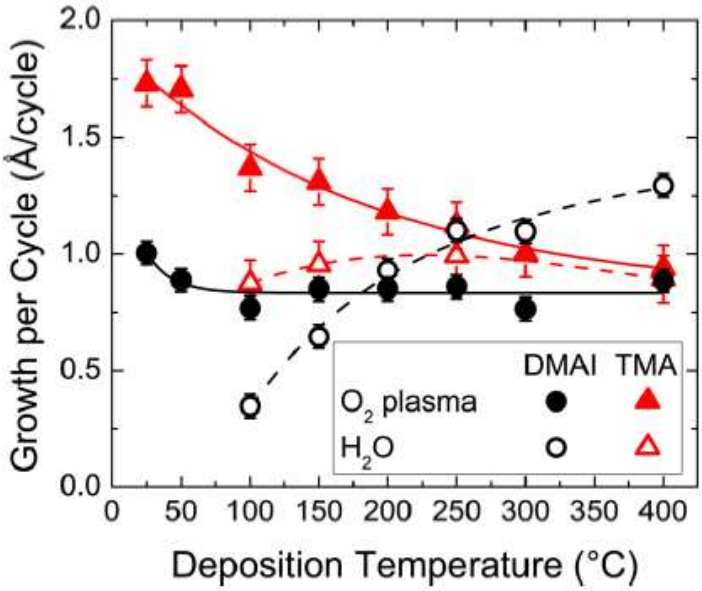

Figure 11: Growth per cycle as a function of deposition temperature for the plasma-enhanced and thermal ALD of Al_2O_3 using DMAI and TMA as precursors. Image reprinted from [13]

Varying the deposition temperature also influences the stoichiometry, which is considered ideal during the analysis of the XRF measurements (section 5.3.3). Figure 12(a) shows the approximation to the ideal stoichiometry, the O/Al ratio decreases to 1.5, while increasing the deposition temperature. In contrast, the mass density (Figure 12 (b)) increases thereby and is described in the paper "Plasma-enhanced and thermal atomic layer deposition of Al_2O_3 using dimethylaluminium isopropoxide, $[Al(CH_3)_2(\mu\text{-}O^iPr)]_2$, as an alternative aluminium precursor" by Stephen E. Potts et al [13] as coincidence with the approach to the ideal stoichiometry of the Al_2O_3 layer.

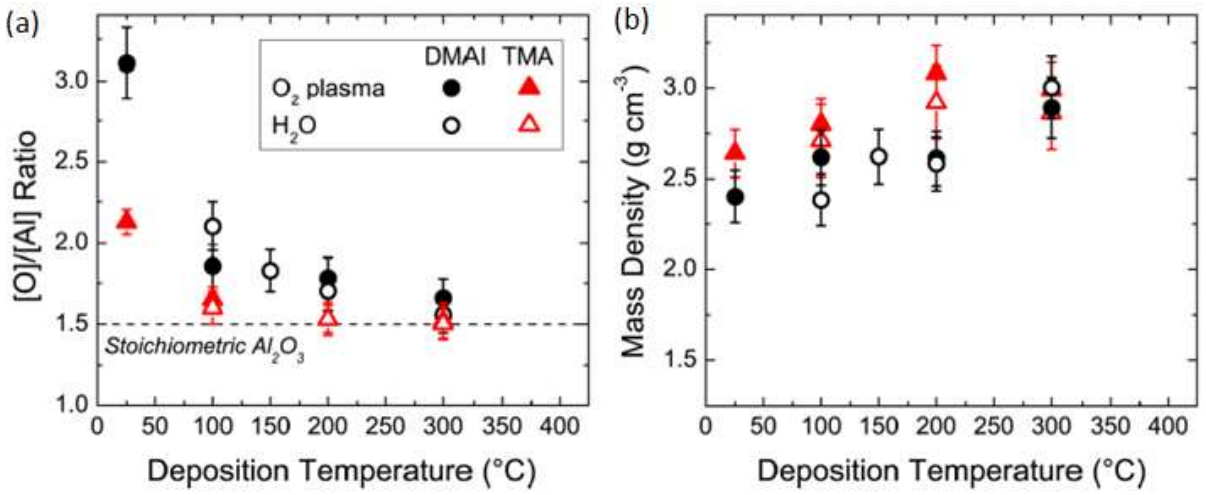

Figure 12: Film composition as a function of deposition temperature obtained using Rutherford backscattering spectrometry and elastic recoil detection. (a) the O/Al ratio and (b) the mass density of the films. Images reprinted from [13]

3.2 ALUMINIUM DOPED ZINC OXIDE

This section explains some behaviour of aluminium doped zinc oxide thin films with support of the results of the papers "Studies on optical, structural and electrical properties of atomic layer deposited Al-doped ZnO thin films with various Al concentrations and deposition temperatures" by W J Maeng et al. [12] and "Structural, electrical, and optical properties of atomic layer deposition Al-doped ZnO films" by Parag Banerjee et al. [5]. Also a subchapter describing the different growth rates of ZnO and Al_2O_3 while changing the amount of aluminium doping concentration based on the results of the paper "Growth of ZnO/Al_2O_3 Alloy Films Using Atomic Layer Deposition Techniques" by J. W. Elam and S. M. George [11] is discussed.

ZnO-based thin films are used for many applications. Nevertheless, via doping a change of the conductivity can be achieved. Aluminium is mainly used to create a n-type semiconductor due to the donor character of aluminium while being incorporated into the wurtzite-structure of ZnO. Aluminium doped zinc oxide (AZO) is mostly utilised as a thin film having a great potential in many applications like transparent conductive oxide (TCO), ultraviolet light emitters, solar cell windows and bulk acoustic wave devices to name only a few of them [1-4]. For TCO a high conductivity and a high transmittance (> 80%) in the visible range are necessary. Such requirements are mentioned in the paper "Studies on optical, structural and electrical properties of atomic layer deposited Al-doped ZnO thin films with various Al concentrations and deposition temperatures" by W J Maeng et al [12]. To achieve high conductivity, low resistivity, the amount of aluminium used for doping has to be chosen carefully. However, the transparency of ZnO thin films is about 90% even if they are highly doped with aluminium [31].

AZO thin films have the same crystal structure, the thermodynamic stable wurtzite structure (Figure 8), as the pure zinc oxide ones. The characteristic of the crystal structure depends on the amount of aluminium oxide (Al_2O_3) deposited. The effects are shown in the paper "Studies on optical, structural and electrical properties of atomic layer deposited Al-doped ZnO thin

films with various Al concentrations and deposition temperatures" by W J Maeng et al [12]. Those experiments are done by thermal ALD leading to different electrical properties compared to deposit the thin films by PEALD. As mentioned in section 3.1.1, PEALD results for pure ZnO thin films in a denser packed one with a higher resistivity. Due to the deposition method is not changed, the same should be true for AZO.

As shown in the figures (Figure 13 and Figure 14), the doping concentration and the deposition temperature have an impact on the crystal structure of AZO thin films.

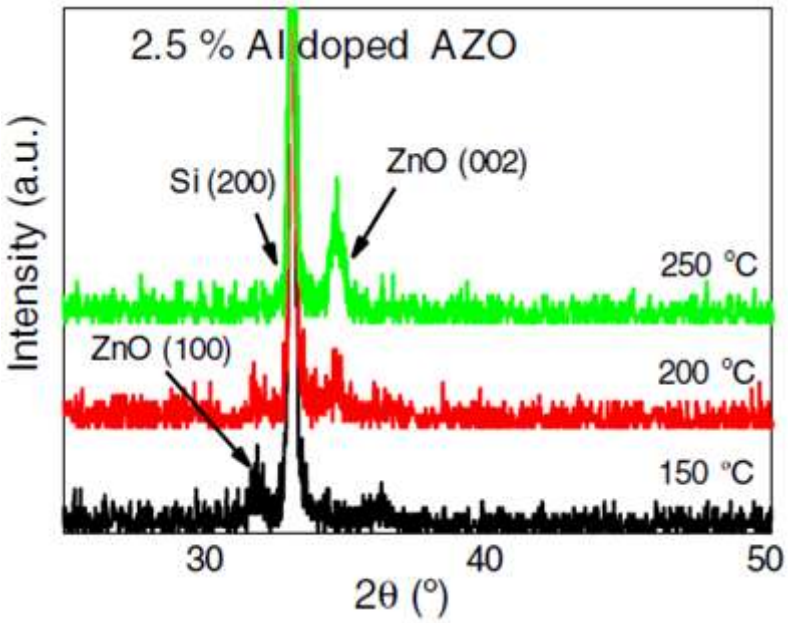

Figure 13: XRD data for 2.5 at% Al-doped ZnO films at growth temperatures of 150 °C, 200 °C and 250 °C. Image reprinted from [12]

Figure 13 points out the same behaviour for AZO as for pure ZnO (plots for this can be found in [10]) for increasing the temperature (described in section 3.1.1). A polycrystalline film with a preferential orientation change from (100) to (002) while increasing the temperature is shown.

The influence of the aluminium content is pictured in Figure 14. Due to the high deposition temperature of 250 °C, the preferential orientation for all various aluminium doping concentrations of ZnO thin films is (002). While increasing the doping content to 4 at%, the AZO shows an increase of intensity of the (002) peak whereas afterwards a decrease happens. This behaviour is explained in the paper "Studies on optical, structural and electrical properties of atomic layer deposited Al-doped ZnO thin films with various Al concentrations and deposition temperatures" by W J Maeng et al. [12], as due to the formation of non-conductive Al_2O_3 clusters, that acts instead of an electron donor more as a charge carrier trap. Below 4 at%, the Al^{3+} ions provide a donor character due to the tendency of being incorporated at interstitial or substitutional sites. If the doping concentration exceeds a certain amount, the resistivity increases due to acting as a charge carrier trap. Another investigation via a transmission electron microscopy image points out that the average grain size is reduced while increasing the aluminium content further to 12.5 at%. On the other hand, an Al-content of 2.5 at% exhibits a bigger one than undoped thin films. The resulting impact on the mobility out of it is shown in Figure 15.

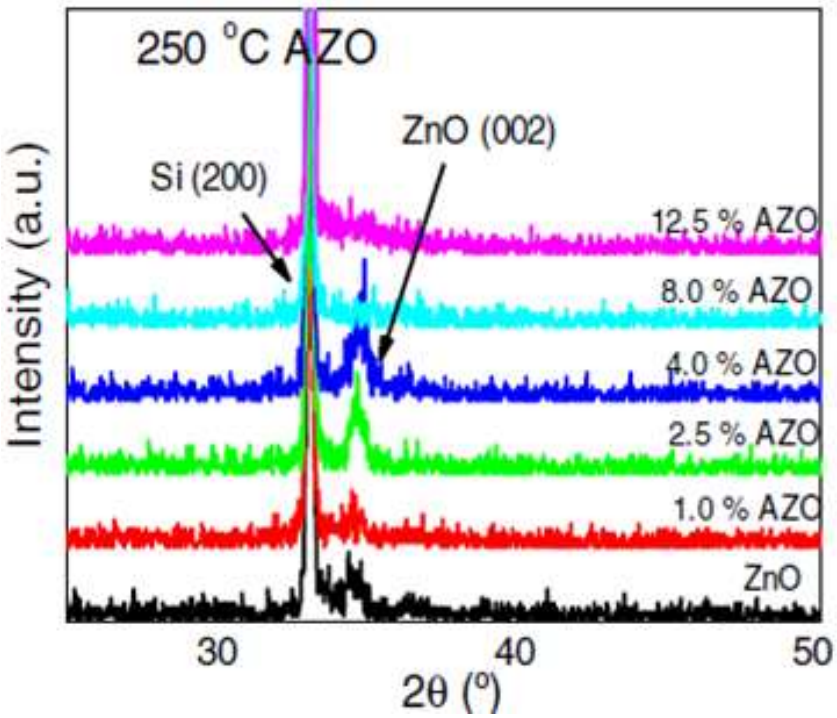

Figure 14: XRD data for undoped ZnO and AZO films with 1-12.5 at% Al at a growth temperature of of 250 °C. Image reprinted from [12]

The resistivity can be mainly reduced by choosing the right doping amount and the depositing temperature preferring the (002) orientation (compare Figure 15 to Figure 13). In the paper "Studies on optical, structural and electrical properties of atomic layer deposited Al-doped ZnO thin films with various Al concentrations and deposition temperatures" by W J Maeng et al. [12], the lowest resistivity is found at a doping concentration of about 2.5 at%, which corresponds to a cycle ratio of 30:1 at a deposition temperature of 250 °C. The mobility and the carrier concentration, which are inverse proportional to the resistivity dependences on the deposition temperature and the aluminium doping concentration are shown in Figure 15. Increasing the mobility and/or the charge carrier concentration leads to a decrease of the resistivity. This is achieved by enhancing the temperature while choosing the right aluminium doping concentration. By comparing Figure 15 to Figure 13, it can be concluded that a preferential (002) orientation results in a lower resistivity.

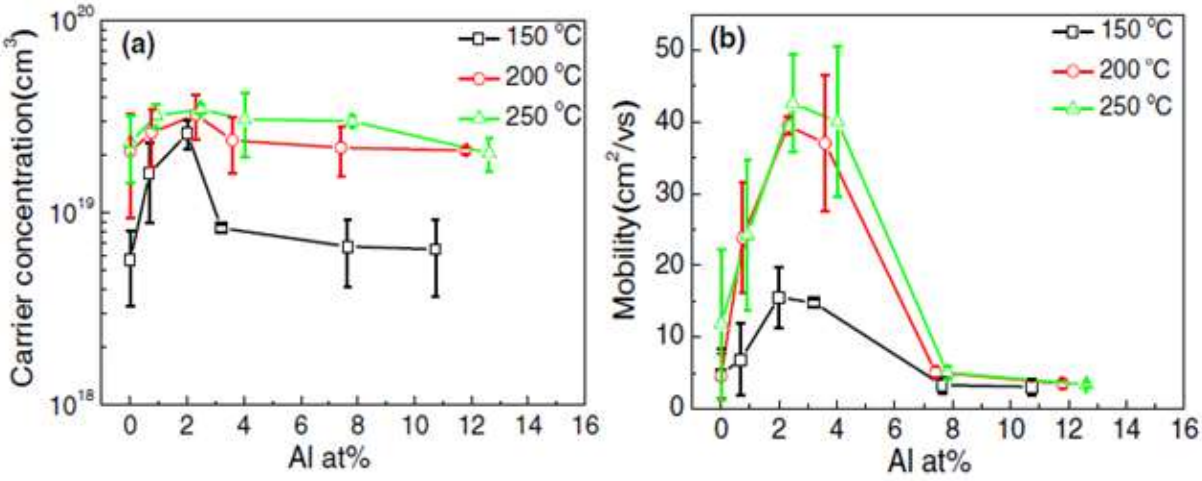

Figure 15: (a) carrier concentration and (b) Hall mobility data as a function of Al concentration for various growth temperatures. Images reprinted from [12]

In the paper "Structural, electrical, and optical properties of atomic layer deposition Al-doped ZnO films" by Parag Banerjee et al. [5] the lowest resistivity is found for 3 at%, which correspond to a cycle ratio of 20:1. The plot for the resistivity depending on the Al-doping concentration (at%) is shown in Figure 16. This investigation has been done at a deposition temperature of 150 °C. That results in a XRD-pattern having the (100) orientation as the preferential one. A change in the peak position of the (100) peak corresponding to a change of the inter-planar distance of the planes (discussed in sections 10.1.1 and 10.3.1) has been found. Furthermore, a decrease of the d-spacing along the [100] direction while increasing the aluminium content is illustrated. As reported in that paper, a stretching along the c-axis, [002]-direction, with a smaller Al^{3+} ionic radius results in a decrease of the a-axis, [100]-direction.

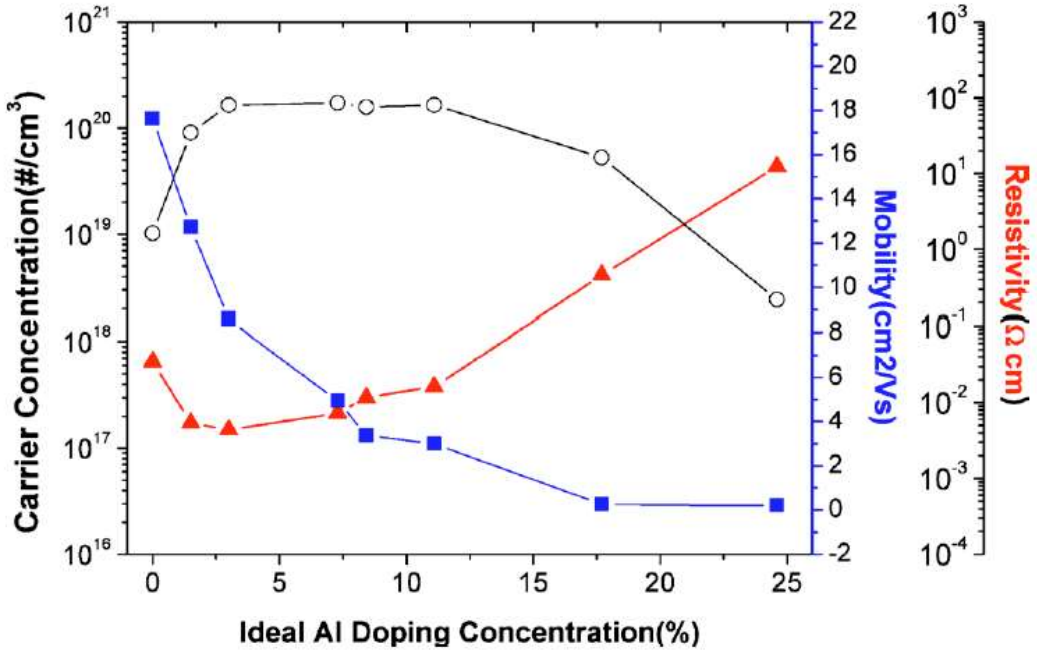

Figure 16: Room temperature carrier concentration (black), mobility (blue), and resistivity (red) as a function of at% Al-doping for aluminium doped zinc oxide films. Image reprinted from [5]

3.2.1 GROWTH OF ALUMINIUM DOPED ZINC OXIDE

To be able to interpret the results gained during this thesis, the knowledge of the growth according to different amounts of aluminium doping is provided in the paper "Growth of ZnO/Al_2O_3 Alloy Films Using Atomic Layer Deposition Techniques" by J. W. Elam and S. M. George [11] due to some in-situ measurements with a quartz crystal microbalance (QCM). Moreover, some ex-situ measurements to determine the Zn film content with inductively coupled plasma atomic emission spectroscopy and to determine the thickness via ellipsometry and stylus profilometry are done. This section comprises some of their results and conclusions.

As mentioned in section 2.1, thin films grown by ALD occurs by using different sequential pulsed precursors. For the doping process, to obtain various aluminium doping concentrations, super-cycles containing different cycle ratios have to be produced. The cycle ratio can be also expressed as a percentage of ZnO cycles (%). A cycle ratio of 2:1, which leads to a super-cycle consisting 3 cycles in total and is shown in Figure 6, results in a percentage of ZnO cycles of 67 %.

To determine the Zn film content, the "rule of mixtures" is used. This prediction is shown in Figure 17(a) as a dashed line. The measured zinc film content is determined using inductively coupled plasma atomic emission spectroscopy and represented via the black dots. Figure 17(a) points out a perfect match for a percentage of ZnO cycles above 90 % and a great deviation otherwise. A highly negative slope of the Zn film content between 75 % and 86 % percentage of ZnO cycles indicated as a grey region is illustrated. Comparing this to the thickness measurements done via ellipsometry and stylus profilometry shown in Figure 17(b), a decrease of the thickness in the same region is represented. The AB-cycles corresponds to the exposure of the different precursors to the surface (A = precursor, B = co-reactant).

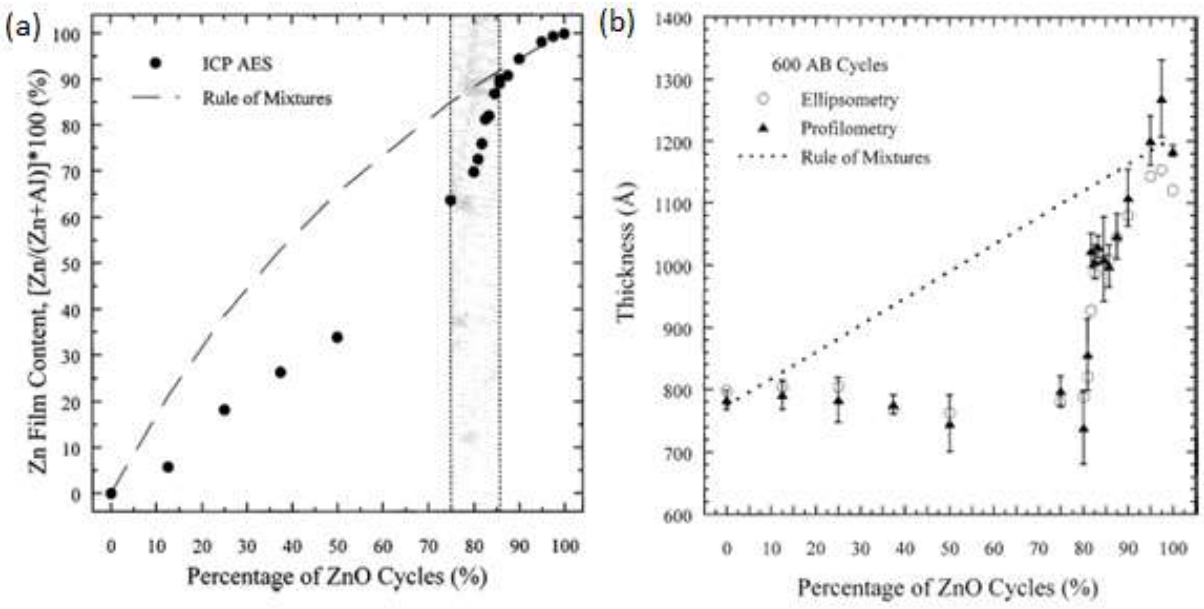

Figure 17: (a) Zinc film content versus percentage of zinc oxide cycles used to grow the zinc oxide/aluminium oxide alloy film. The zinc film content was determined using inductively coupled plasma atomic emission spectroscopy. (b) Thickness after 600 AB cycles versus percentage of zinc oxide cycles used to grow the zinc oxide/aluminium oxide alloy film. The film thickness was measured using ellipsometry (open circles) and stylus profilometry (solid triangles). Images reprinted from [11]

The decrease of the Zn film content and the thickness is explained with some etching due to the observed negative growth (Figure 18(e) and Figure 18(f)) via in-situ QCM measurements. In the paper "Growth of ZnO/Al_2O_3 Alloy Films Using Atomic Layer Deposition Techniques" by J. W. Elam and S. M. George [11] two different possible driving forces are mentioned that may influence this etching process. On the one hand the abstraction of Zn from the hydroxylated ZnO surface is brought by the formation of $Zn(CH_3)_2$ and on the other hand the formation of $ZnAl_2O_3$ spinel having a Zn content of 33% leads to a removal of Zn from the ZnO/Al_2O_3 alloy having a higher Zn content.

The results of the deposited thin films having different percentage of ZnO cycles are shown in Figure 18. While alternating the two different layers, aluminium oxide and zinc oxide, the first cycle of Al_2O_3 deposited after a ZnO cycle is lower than the growth rate of depositing pure Al_2O_3 (Figure 18(a)). A similar behaviour for the deposited ZnO layers occurs, resulting in a lower growth rate for the first 4-6 cycles of ZnO after a deposited Al_2O_3 layer compared to depositing only ZnO cycles (Figure 18(i)). Furthermore, the growth rate of the following deposited ZnO layers exceeds the expected one. This leads to the possibility that the deposited AZO layers can be thicker than anticipated. Such a behaviour can be seen in Figure 17(b) for the aluminium doped zinc oxide film consisting of 97.5 % of percentage of ZnO cycles (Figure 18(h)). 97.5 % of percentage of ZnO cycles corresponds to a cycle ratio of 39:1.

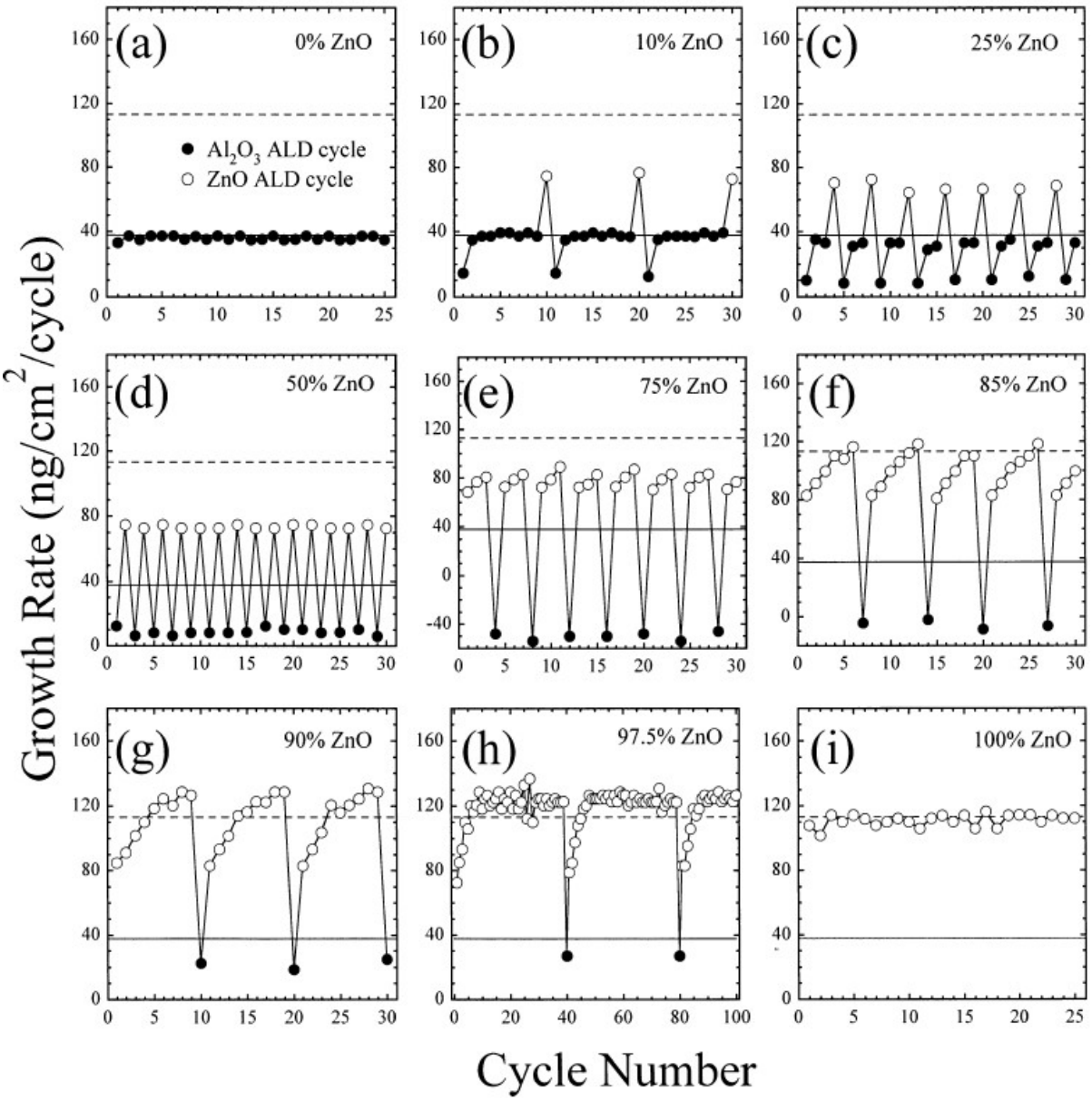

Figure 18: Growth rates obtained from in-situ quartz crystal measurements during the atomic layer deposition of various zinc oxide/aluminium oxide alloy films prepared using different percentages of zinc oxide cycles. The horizontal dashed lines show the average atomic layer deposition growth rates measured for pure zinc oxide and aluminium oxide, respectively. Image reprinted from [11]

Part II

EXPERIMENTAL

This first part describes the setup for the plasma-enhanced atomic layer deposition including the main parts. A main focus on the ALD-MLD-controller program enables the regulating of the deposition procedure of aluminium doped zinc oxide (AZO) thin films. The saturation curves for depositing aluminium oxide resulting in the optimum recipe is presented. The AZO depositions done at room temperature and elevated deposition temperature of 150 °C are described. A short explanation of the annealing process for the AZO thin films deposited at room temperature is given.

The second part contains the characterisation techniques for the investigation of the deposited AZO thin films. Those are spectroscopic ellipsometry, X-ray fluorescence, X-ray photoelectron spectroscopy, X-ray diffraction and 4-point probe. A short description of the used setup and the method to analyse the measurements is also added.

4) SETUP AND EXPERIMENTS

4.1 EXPERIMENTAL SETUP

This section describes the experimental setup used to deposit the aluminium doped zinc oxide (AZO) thin films. A schematic of the experimental setup is shown in Figure 19. The different components of the setup are listed in Table 1.

Table 1: Instruments for experimental setup

DEVICE	MODEL
Arduino	Arduino Uno
Relays module	
RF power generator	Advanced Energy Cesar 13.560 MHz
Matching network	Advanced Energy Navio
Multi gas controller	MKS 647C
ALD valves	Swagelok ALD 3
Mass flow controller	MKS MF1-C
Butterfly valve	
Pneumatic valve	Burkert Solenoid Valve 125301
Turbo molecular pump	Pfeiffer Vacuum TMH071P
Rotary vane pump	Pfeiffer Vacuum DUO5M
Pressure gauge	mks BARATRON CAPACITANCE MANOMETER G233834G10 626B01TDE9

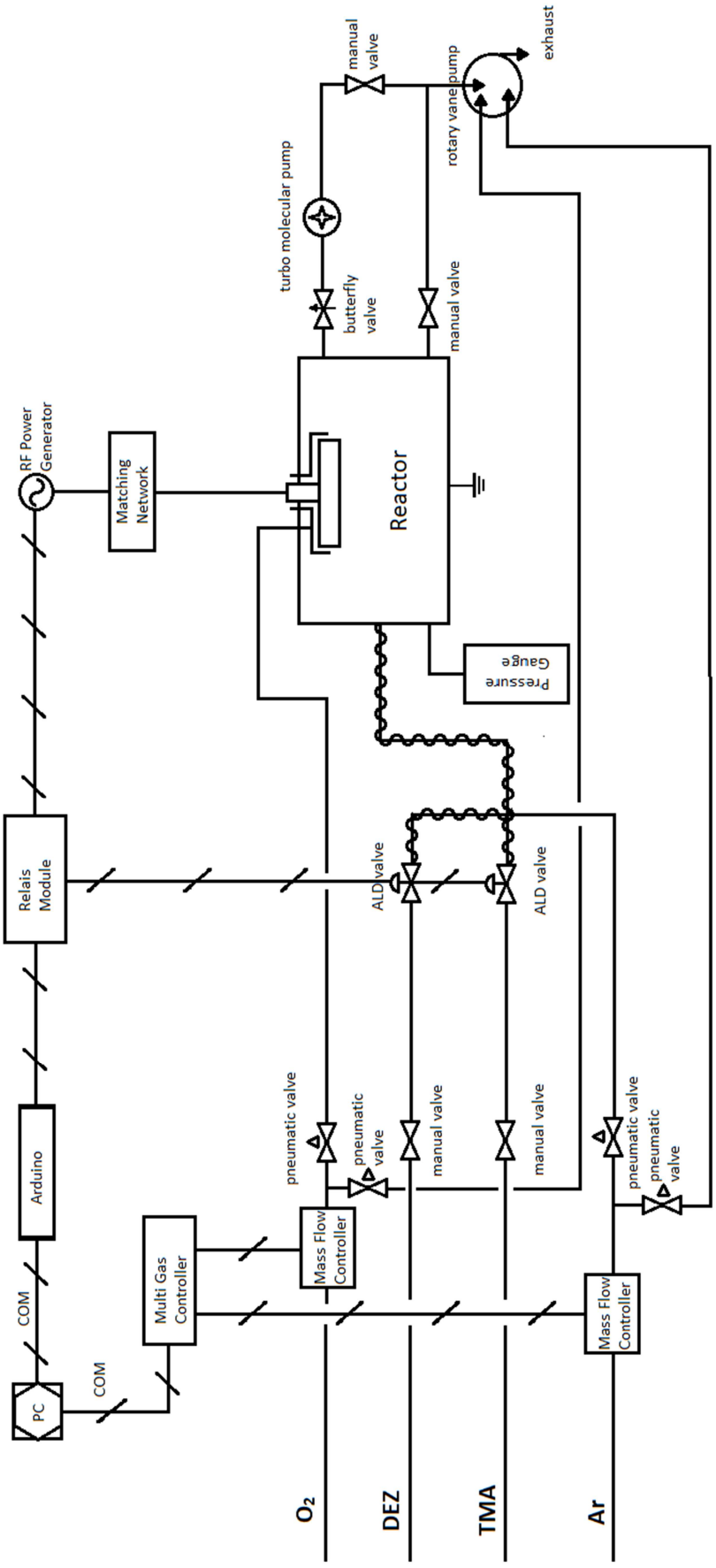

Figure 19: Schematic of experimental setup. Crossed lines correspond to signal transmission lines, sinusoidal line corresponds to heated line.

Most of the components are precisely described in the master thesis of “Plasma-enhanced atomic layer deposition of zinc oxide thin films” by Dipl. Ing. Julian Pilz [21]. In this chapter, the old components are briefly described, together with the additional components used for introducing the doping second precursor.

As described in chapter 2), atomic layer deposition is a technique where via repeating the cycle or super-cycle a layer-by-layer deposition is achieved. All the steps of such a cycle have to be pulsed. These requirements are fulfilled by running the ALD-MLD-controller program on the PC. The program is connected to an Arduino and a multi gas controller. The Arduino, which is connected to the relays module, controls the on-off-switching of the RF-generator and the ALD-valves, which are connected to the precursor-reservoirs, diethylzinc (DEZ) and trimethylaluminium (TMA). The multi gas controller is on the one hand connected to the mass flow controllers, that takes care of the desired flow rates, and on the other hand to the pneumatic valves, which close or open the line. To achieve such an atomic layer-by-layer deposition, a vacuum system is needed as well. The vacuum system of the custom-built reactor has a turbo molecular pump and a vane rotary pump as a booster pump. The turbo molecular pump rotates at 1500 Hz and the butterfly valve, which is the connection between the reactor and the turbo molecular pump and which has a specific opening angle to do the depositions at the desired working pressure inside the reactor. A detailed explanation of the most important parts like the custom-built reactor, the ALD valve, the precursors, which are used for depositing aluminium doped zinc oxide (AZO) thin films, and a detailed explanation of the ALD-MLD-controller program are given in the following sections.

4.1.1 REACTOR

The reactor, shown in Figure 20, hosts a heating stage for depositions at elevated substrate temperature, and a top electrode grid connected via a coaxial cable to the power generator and the matching network. The power generator is used to generate a capacitively-coupled plasma at a radio frequency of 13.56 MHz. The reactor bottom serves as the ground electrode. The substrates are either placed on the reactor bottom, during depositions at room temperature, or at the heating stage, while depositing at an elevated one. The heating stage is 1 cm above the reactor bottom, but still connected via a weld seam. Furthermore, a connection to the heating device exists, which are isolated with a ceramic covering so that the plasma cannot be disrupted by them. The matching network is used to match the impedance of the plasma to a desired output power without any reflections. The oxygen flow direction is controlled by the pneumatic valves. Two of them are mounted after the mass flow controller (Figure 19), so that only one line is set to open while the other one is closed. Normally, the oxygen flows through the line directly connected to the rotary vane pump, referred to as by-pass. Just before the oxidizing step occurs, the pneumatic valve for the by-pass closes and the other one opens leading to an oxygen flow into the reactor through the top electrode grid used to create the oxygen-plasma. Figure 19 displays the same principle as described for the oxygen flow direction as well for the argon flow, purging step.

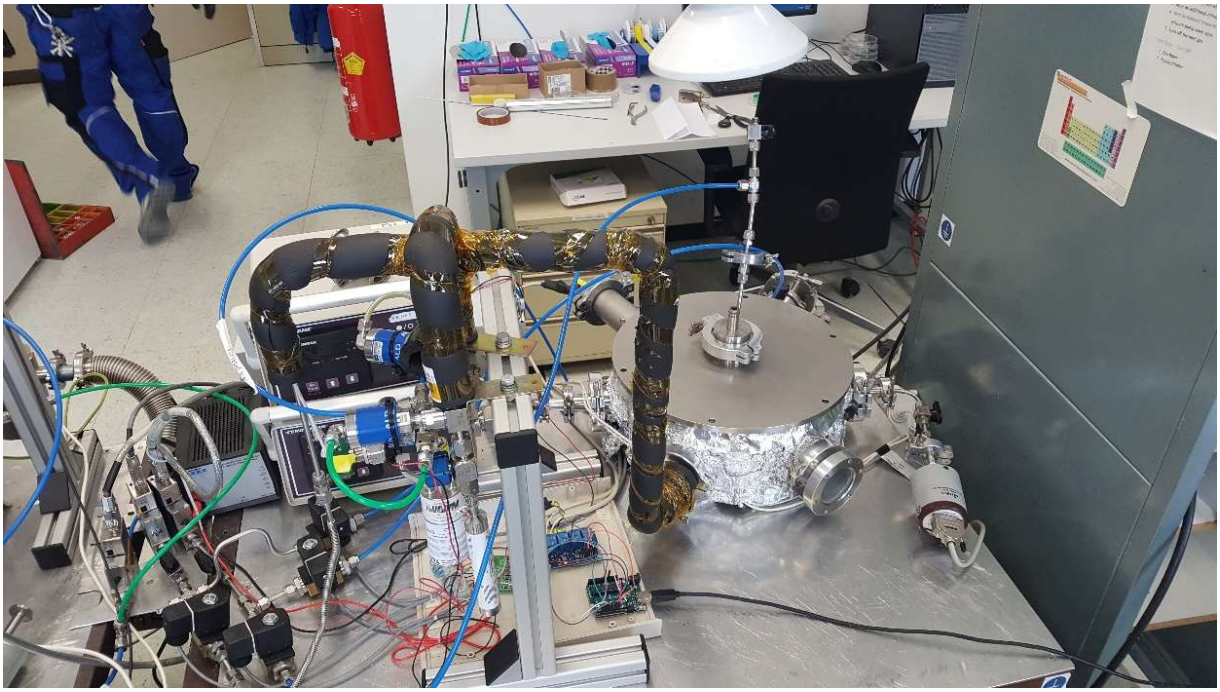

Figure 20: Experimental setup. On the left side, the mass flow controllers connected to the pneumatic valves and the manual valves are shown. In the middle of the figure, the big diethylzinc reservoir as well as the small trimethylaluminium reservoir can be seen. Above them, the ALD valves connected to the actuators (left) are mounted. Below them, the Arduino and the relays module are shown. On the right side, the custom-built reactor connected to a relative gauge is shown. On the back side, the butterfly valve connected to the vacuum system (right) as well as the heating connection to the heating stage (left) are mounted. The heated lines are below the black heating isolation.

4.1.2 ALD VALVE

An actuator, connected to an ALD valve, shown in Figure 20 above the precursor reservoirs, controls the opening and closing via the up and down movement of the valves diaphragm within 5 ms by the usage of compressed air having a pressure of 5 bar [22].

4.1.3 PRECURSORS

The precursor diethylzinc (DEZ / chemical formula: $(C_2H_5)_2Zn$) is utilised for the formation of zinc oxide (ZnO) layers, whereas trimethylaluminium (TMA / chemical formula: $(CH_3)_3Al$) is used to form aluminium oxide (Al_2O_3) ones. The DEZ reservoir (EC No. 209-161-3) is bought from Dockweiler Chemicals GmbH and the TMA reservoir (PCode: 1002183055 663301-25G) comes from the ALDRICH Chemistry, shown in Figure 20. The vapour pressure for DEZ is about 30mbar at room temperature while the vapour pressure for TMA is only about 12mbar leading to the possibility of deposit AZO thin films without a bubbler system [23], [24]. The precursors are liquid at room temperature and highly flammable as well as pyrophoric, catching fire spontaneously if exposed to air [25], [26]. For safety reason a type D fire extinguisher at the working place is installed and the requirement to have someone else nearby is established.

4.1.4 ALD-MLD-CONTROLLER PROGRAM

In section 2.5.2 the doping process relating to ALD has been explained. In relation to that, this section describes the computer program used on the one hand to set the parameters, necessary to create AZO thin films on a substrate, and on the other hand to computationally control the procedure.

As shown in Figure 19, this program controls the Arduino as well as the multi gas controller via a serial connection. The computer program, called ALD-MLD-controller, is shown in Figure 21, a picture made during a deposition process of an AZO thin film having a cycle ratio of 30:1 and deposited at elevated temperature (150°C). The total number of cycles is 310. Table 2 presents the devices connected to the Arduino at the relative port. The commands to open a line/ start a process, close a line/ end a process and to wait until a new command is in progress are shown in Table 3. Finally, the process sequence represented with the capital letters "A,B,C,D,E,F,G" containing all other information like the port numbers and commands have to be defined.

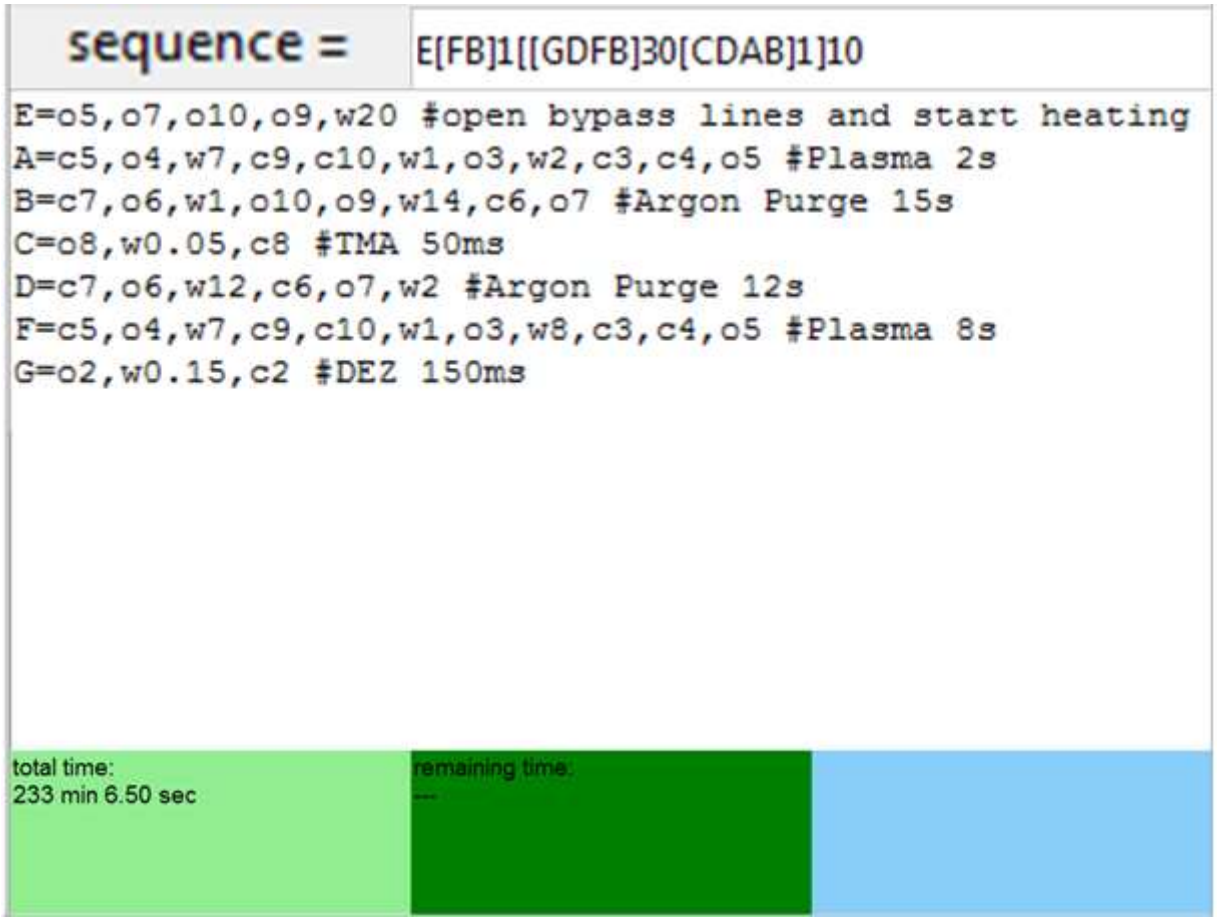

Figure 21: ALD-MLD-controller, which is the program used to control the deposition procedure to get AZO thin films

Table 2: Connection plan of the Arduino

Arduino Port	Device
2	ALD Valve DEZ
3	Plasma
4	Oxygen
5	Oxygen Bypass
6	Argon
7	Argon Bypass
8	ALD Valve TMA
9	Heating Stage inside the reactor
10	Heating Plate of the corpus of the reactor

Table 3: Commands to the Arduino

Command	Performance
“o”	open line / start process
“w5”	wait for 5 s
“c”	close line / end process

The letters of Table 3 have to be combined with the number mentioned in Table 2 leading to the corresponding line opening/ process starting or closing/ ending. The number associated with the command “w” instead corresponds to a waiting time in seconds. This know-how enables a brief explanation of the sequences:

- “E” characterize the initial sequence, opens the oxygen and the argon bypass. Moreover, the heating process, at first the corpus (100 °C) and then the heating stage inside (150 °C) are heated up to the desired temperature.

- “F” describes the plasma-step for DEZ. It is found that 8 s for the plasma-time is the minimum for being in saturation. The oxygen bypass is closed and the line into the reactor is opened to enables the creation of oxygen plasma. After waiting for 7 s, the heating process is stopped. 1 s before and also during the plasma exposure, no heating process occurs to not disturb the oxidizing process. The plasma process is stopped after 8 s by closing the oxygen flow into the reactor and opening the oxygen bypass.

- “A” qualifies the plasma-step for TMA doing the same procedure as explained for “F”. The difference is the waiting time, the one for being in saturation for oxidizing the TMA. It is reduced to the found minimum of 2 s.

- “B” depicts the purging time after the plasma exposure of the precursors. The argon bypass is closed and the line for introducing the argon into the reactor opens. The heating system is started again (beginning with the corpus). A waiting time of in total 15 s ensures no side-products in the reactor before initiating the precursor flow. The purge ends by redirecting the argon flow to the rotary vane pump, using the by-pass line.

- “G” characterize the precursor exposure time for DEZ. The ALD valve connected to the DEZ reservoir opens for 150 ms [12].

- “C” describes the precursor exposure time for TMA leading to an opening of the ALD valve connected to the TMA reservoir for the found optimum time of 50 ms.

- “D” qualifies the purging after the precursor exposure. A redirection of the argon flow to purge the excess of the DEZ or TMA and some side-products is done. The minimum time is found to be 12 s.

As shown in the part “results and discussion”, the purging times of the two different precursors differ. Since the Arduino can only handle 7 sequences (“A”, ”B”, ”C”, ”D”, ”E”, ”F”, ”G”) and a maximum of 11 commands each, some reductions and a regrouping is done. The purging times are set to the minimum of the highest purging dose needed leading to that for the deposition of ZnO layers. The shifting of the restarting heating procedure to the argon purge after plasma is due to the limitation of the commands.

The initial sequence, reported in Figure 21, initiates a constant flow of oxygen and argon. Furthermore, the system is heated up to the desired temperatures. Subsequently, the second half-cycle, letters “F” and ”B” in brackets followed by the number 1, starts once to create active sites (explained in section 2.2). 30 cycles starting with the DEZ precursor flow and ending with the oxidizing plasma step separated by the different purging ones, deposits 30 monolayers of ZnO. Moreover, a whole cycle consisting TMA as the precursor and its different plasma exposure time to deposit an Al_2O_3 layer ensues the creation of a super-cycle (explained in section 2.5.2). The 10 times repetition results in a AZO thin film with a cycle ratio of 30:1 consisting 310 cycles in total.

4.1.5 WORKING CONDITIONS

To achieve the desired working pressure, the opening angle of the butterfly valve was set automatically to 35°. It got damaged in such a way that neither the leaking rate could be tested nor the opening angle corresponded to the set value anymore. As a consequence, a manually butterfly valve, was used after the first saturation curves (Figure 2).To obtain the same conditions as with the previous one, the pressure were normalized to that during the argon flow into the reactor. Due to the use of a relatively capacitance manometer the difference, leading to be 86 mTorr, of the base pressure and that during the argon flow was calculated out of the recorded curves. Thus, the new butterfly valve was set manually to an opening angle fulfilling the condition adding 86 mTorr to the measured base pressure.

Moreover, due to the occurred sparks, in consequence of absorbed precursor/water in the reactor, after a few depositions, a time clock was installed to bake out the reactor during the night resulting in a stable plasma. This back out was done during the night, due to the needed cool down time of the reactor to waste no working time.

4.2 EXPERIMENTS

The goal of this master thesis was to produce some AZO thin films with low resistivity. The investigations on that account are listed:

(1) Saturation curves for depositing an aluminium oxide layer
   - 10.1 Precursor dose
   - 10.2 Purging after precursor
   - 10.3 Plasma dose
   - 10.4 Purging after plasma

(2) Varying the cycle-ratio to obtain different Al-contents
   - 10.1 AZO thin films deposited at room temperature
   - 10.2 AZO thin films deposited at elevated temperature (150 °C)

(3) Annealing of the Aluminium doped zinc oxide thin films deposited at room temperature

The saturation curves for ZnO and moreover, further studies containing some changes were investigated in a previous work "Plasma-enhanced atomic layer deposition of zinc oxide thin films" by Dipl. Ing. Julian Pilz [21]. As the work was done with the same reactor setup and under the same conditions, the found optimum recipe was used to deposit AZO thin films and is listed in Table 4.

Table 4: Optimum Recipe for depositing zinc oxide layers

The exposure times in seconds of the different cycle parts (Figure 2) using diethylzinc (DEZ) as a precursor is shown. The plasma dose is a matter of oxygen-plasma.

DEZ Dose [s]	Purge after DEZ [s]	Plasma Dose [s]	Purge after Plasma [s]
0,15	12	8	15

For the investigation substrates had to be prepared. Silicon (Si) wafers with a native silicon dioxide (SiO_2) on top having a thickness between 1.13 nm and 2.49 nm (P1, P2, P3, P4) were cut into pieces of an area 2 cm times 2 cm. This was done via a diamond tip leading to a break of the silicon wafers along their preferential orientation of their crystal structure. Contaminations on the substrate were removed with an isopropanol cleaning followed by a drying step via a carbon dioxide sprayer. Another substrate used was a silicon wafer with thermal silicon dioxide on top having a thickness between 150,00 nm and 151,63 nm (P_th). The pre-cut ones with an area of 2 cm times 2 cm were cleaned in an acetone ultrasonic bath

for 10 min followed by the same cleaning steps (isopropanol and carbon dioxide) as before. The third kind of substrates having an area 2 cm times 2.5 cm were glass ones (P_G1, P_G2) broken by hand after inflicting a small scratch via the diamond tip and cleaned by the same way then the silicon wafers with native silicon dioxide on top. The Si-wafers having a thermal SiO_2 layer on top and the glass ones were needed for the resistivity measurements. The prepared samples were put into different positions in the reactor (Figure 22) to get an information about the uniform growth.

After placing the cleaned substrates and closing the reactor, the rotary vane pump and the heating systems, if needed, were turned on. To protect the pressure gauge from an overflow measurement the connected valve was set to open after about 3 min. If a relative pressure of 100 mTorr was achieved, the turbo molecular pump rotating at 1500 MHz during the AZO thin film depositions was switched on. The heating system included on the one hand the heated up to 40 °C heating tapes for the TMA line and DEZ line (corresponding to the heated line in Figure 19) and on the other hand, for depositions at elevated temperature, the heating stage inside heated up to 150 °C and the corpus heated up to 100 °C.

Furthermore, a leaking test was made. If the leak rate was small enough, the working conditions could be set, either automatically to 35° or per hand during an argon flow into the reactor (described in section 4.1.5). Additionally, the connection between the Arduino and the PC was done to start the in the ALD-MLD-controller program written one (example described in section 4.1.4).

For each of the depositions the flow rates for argon and oxygen were set to 20 sccm and the plasma power was fixed to 60 W, due to the previous investigation for depositing ZnO thin films done in the master thesis “Plasma-enhanced atomic layer deposition of zinc oxide thin films” by Dipl. Ing. Julian Pilz [21].

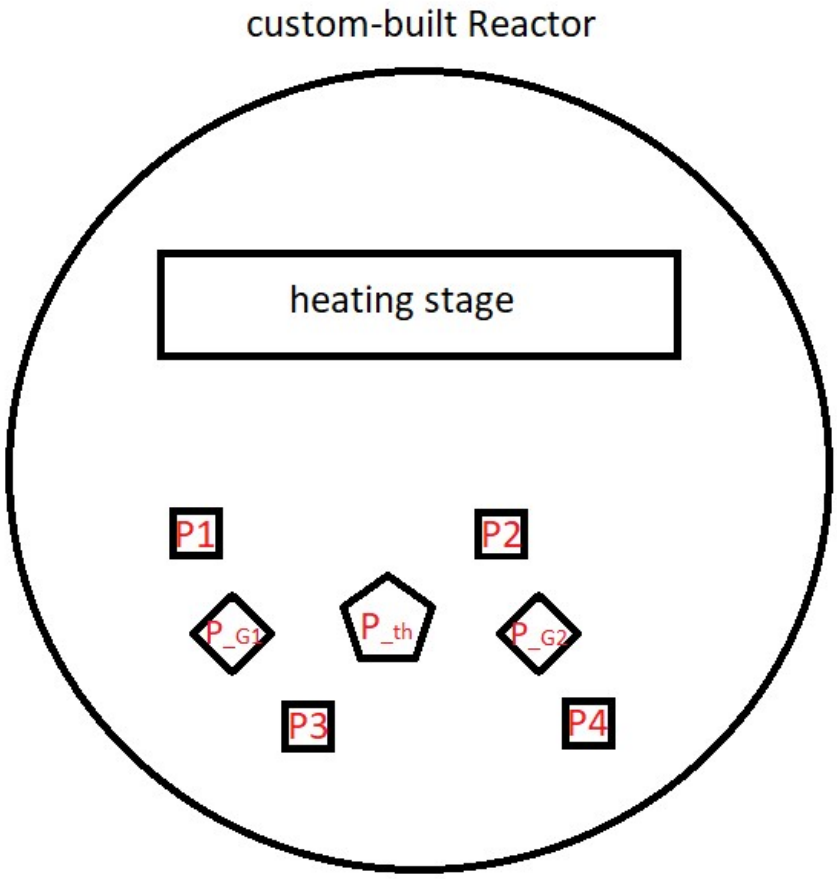

Figure 22: Schematic of the custom-built reactor with the positions of the different substrates. P1, P2, P3 and P4 describe the locating of the Si-wafers with a native silicon dioxide layer on top. P_th describes the position of the Si-wafer with a thermal silicon dioxide layer on top. P_G1 and P_G2 are the places of the used glass substrates. Also the location of the heating stage within the reactor can be seen.

4.2.1 SATURATION CURVES FOR DEPOSITING AN ALUMINIUM OXIDE LAYER

For the investigation of Al_2O_3 layers only 4 silicon wafers with a native SiO_2 layer on top were used. A short refresher to achieve an ALD growth doing all 4 parts of one cycle in saturation (described in section 2.2) is given.

The precursor dose had to be long enough to fully cover the substrate. As a result, and related to be in saturation, no further particle could be bond to the substrate anymore.

The plasma dose had to be long enough to fully oxidize the precursor deposited before.

And **the purging steps** dividing these two parts from each other had to be long enough to prevent for undesired chemical vapour depositions (CVD) during the process.

To optimize the deposition time, finding the minimum time to be in saturation, the following parameters were set:

(1) Each of the deposited thin films consisted of 100 cycles in total.
(2) The opening angle of the butterfly valve was set to 35°.

4.2.1.1 Variation of Precursor dose:

To find the optimum precursor dose, it was decided to take long enough purging times (20 s) and a long enough plasma dose (15 s) to be sure that all of these parameters were in saturation. The first precursor exposure (20 s) fully covered the substrate and was reduced in several steps (Table 5), optimizing the process time, to get the minimum point being still in the saturation.

Table 5: Variation of precursor dose

Trimethylaluminium (TMA) is used as precursor.

TMA Dose [s]	Purge after TMA [s]	Plasma Dose [s]	Purge after Plasma [s]
0.20	20	15	20
0.12	20	15	20
0.10	20	15	20
0.05	20	15	20
0.02	20	15	20

4.2.1.2 Variation of purge after precursor dose:

The optimum purging time necessary to remove the excess of the precursor and the by-products coming up during the chemisorption to the surface had to be long enough to be sure none of these gases were in the reactor during the following plasma step to avoid CVD processes. The steps taken the optimum time for the precursor (0.05 s) into account are shown in Table 6.

Table 6: Variation of the purging time after the TMA dose

TMA Dose [s]	Purge after TMA [s]	Plasma Dose [s]	Purge after Plasma [s]
0.05	20	15	20
0.05	15	15	20
0.05	12	15	20
0.05	10	15	20
0.05	9	15	20

4.2.1.3 Variation of plasma dose

Considering the optimum exposure for the precursor dose (0.05 s) and for the purging time after the precursor (11 s) was to vary the plasma dose shown in Table 7: the minimum time needed to oxidize all of the deposited precursor.

Table 7: Variation of plasma dose

TMA Dose [s]	Purge after TMA [s]	Plasma Dose [s]	Purge after Plasma [s]
0.05	11	15	20
0.05	11	10	20
0.05	11	7	20
0.05	11	5	20
0.05	11	3	20
0.05	11	1	20
0.05	11	0.5	20

4.2.1.4 Variation of purge after plasma dose

Due to the mechanical damage of the automatic butterfly valve (section 4.1.5), the variation of purge after plasma with the set optimum parameters, 0.05 s for the precursor dose, 11s for the purging time after the precursor exposure and 2 s for the plasma dose, was done twice. For the first time, the opening angle of the butterfly valve was set to 35° (Table 8), while for the second time, the opening angle was adjusted manually (Table 9).

Table 8: Variation of the purging time after the plasma dose by an opening angle of 35°

TMA Dose [s]	Purge after TMA [s]	Plasma Dose [s]	Purge after Plasma [s]
0.05	11	2	20
0.05	11	2	15
0.05	11	2	10
0.05	11	2	8
0.05	11	2	5
0.05	11	2	2
0.05	11	2	1

Table 9: Variation of the purging time after the plasma dose by an manually set opening angle

TMA Dose [s]	Purge after TMA [s]	Plasma Dose [s]	Purge after Plasma [s]
0.05	11	2	20
0.05	11	2	15
0.05	11	2	10
0.05	11	2	5

4.2.1.5 Optimum recipe for depositing aluminium oxide thin films

Table 10 presents the optimum recipe found for depositing Al_2O_3 layers used together with the one for depositing ZnO (Table 4) to prepare AZO thin films.

Table 10: Optimum Recipe for depositing aluminium oxide layers

TMA Dose [s]	Purge after TMA [s]	Plasma Dose [s]	Purge after Plasma [s]
0,05	11	2	15

4.2.2 VARYING THE CYCLE-RATIO TO OBTAIN DIFFERENT AL-CONTENTS

To create AZO thin films with different Al-contents, an alternating deposition of n-ZnO-layers to 1-Al_2O_3-layer had to be done (explained in a section 2.5.2). The produced super-cycles are shown in Table 12 (room temperature) and Table 13 (150 °C). Due to the influence of the growth per cycle, the Al-content differed for different deposition temperatures having the same cycle ratio. Consequently, the expected Al-contents were added. Due to the composition of a super-cycle (n-ZnO-layers to 1-Al_2O_3-layer), only the number of ZnO cycles were given.

4.2.2.1 Aluminium doped zinc oxide thin films deposited at room temperature

For the characterization, pure Al_2O_3 and pure ZnO thin films shown in Table 11 were deposited at room temperature. The corresponding Al-content was achieved depending on the stoichiometric of the thin films as shown as an example for Al_2O_3 in Figure 12(a). For the measurements, ideal stoichiometry was considered. Both depositions consists of 100 cycles in total. 4-point probe measurements were done on Al_2O_3 thin films deposited on Si-wafers with a native SiO_2 layer, and on ZnO thin films deposited on Si-wafers having a thermal SiO_2 on top. Due to Al_2O_3 thin films are insulating, while ZnO ones semiconductors, a thicker insulating layer between the Si-wafer and the conductive semiconductor is needed to ensure measuring only the deposited ZnO.

Table 11: Pure thin films of ZnO and Al_2O_3

The chemical names of the deposited materials, Aluminium Oxide (Al2O3) and ZnO (Zinc Oxide) containing their metal content (at%) considering ideal stoichiometry are displayed.

Sample	Content [at%]
Al_2O_3	40
ZnO	50

Due to the influence of the super-cycle the AZO thin film depositions were done by a different number of total cycles (reported in Table 12). The films were deposited on Si-wafers having a native SiO_2 layer on top and moreover on those with a thermal one used for the annealing process. The positions for all depositions at room temperature are shown in Figure 22.

Table 12: Aluminium-doped zinc oxide thin films deposited at room temperature

The total number of deposited cycles depending on the used super-cycle indicated by the number of ZnO-cycles are listed with the corresponding calculated aluminium content (at%) evaluated via formula 7a.

ZnO-cycles	Total cycles	Al-content [at%]
40	287	2.08
35	288	2.36
30	310	2.72
25	312	3.22
20	294	3.95
15	304	5.10
10	297	7.19

4.2.2.2 Aluminium-doped zinc oxide thin films deposited at elevated temperature

For the deposition series at elevated temperature (150 °C) also pure Al_2O_3 and pure ZnO thin films were deposited with the conditions reported in Table 11. Each deposition consisted of two glass substrates and two Si-wafers having a native oxide on top placed in a row (Figure 23) except the pure Al_2O_3 thin films made by using four of those Si-wafers. The depositions done for the AZO thin films at 150 °C are shown in Table 13. In the process, the total number of cycles for the different ratios were the same as for the room temperature series (Table 12).

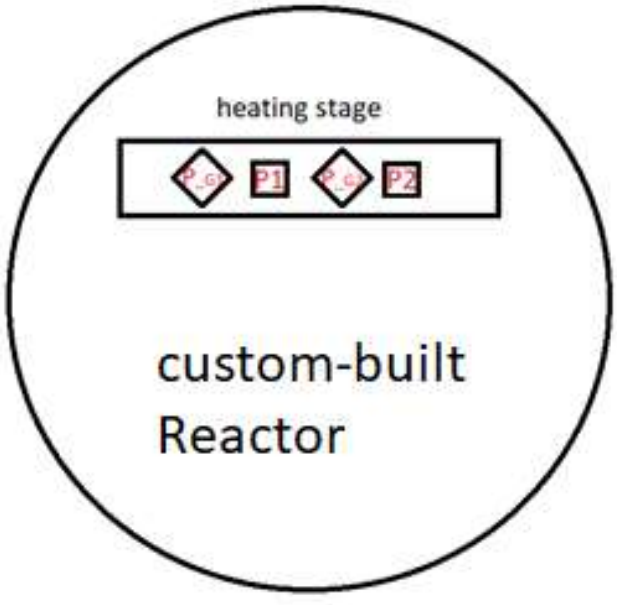

Figure 23: Schematic of the custom-built reactor with the positions of the different substrates used at 150 °C substrate temperature. P1 and P2 describe the locating of the Si-wafers with native silicon dioxide layer on top. P_G1 and P_G2 are the places of the used glass substrates. All of the substrates are placed on the heating stage.

Table 13: Aluminium-doped zinc oxide thin films deposited at 150°C substrate temperature

ZnO-cycles	Al-content [at%]
40	0.69
30	0.91
20	1.35
10	2.61

4.2.3 ANNEALING OF THE ALUMINIUM-DOPED ZINC OXIDE THIN FILMS DEPOSITED AT ROOM TEMPERATURE

Annealing is a heat treatment in which the temperature is increased to a chosen value during a given time to achieve a change in material properties. In this case it is wanted to observe a change in resistivity investigated by 4-point probe measurements. Furthermore, X-ray diffraction was done to study the change of the crystal structure. During the annealing process, the high temperature leads to diffusion processes covered by the dopant self-diffusion that change the distribution of the atoms in the thin film [27].

Due to some investigations of annealing for ZnO thin films by Dorr. Mag. Alberto Perrotta, the holding temperature was set to 600 °C for 375 minutes. The process was performed with a surrounding nitrogen gas flow of 0.3 Lpm within a graphite dome to avoid oxidizing processes. The heating step was done by a heating rate of 100 °C per minute, while the cooling rate depended on the used annealing stage itself. The graphite dome was cooled via an oxygen flow starting after exceeding 200 °C of the heating stage. Consequently, the cooling rate was dependent on that.

Anton Paar GmbH developed the used setup consisted of the annealing stage, DHS 1100 Domed Hot Stage Version Panalytical (Figure 24(a)), and the temperature control unit, TCU 200 (Figure 24(b)). For more information about them, read the “Instruction Manual DHS 1100 Domed Hot Stage Version PANalytical” and “Instruction Manual TCU 200 Temperature Control Unit”.

Figure 24: (a) Domed Hot Stage (DHS 110). (b) Temperature Control Unit (TCU 200)

5) CHARACTERISATION TECHNIQUES

Spectroscopic ellipsometry was used to characterize the thickness and optical constants of the thin films, like the refractive index. For an investigation of the Zn-content and the Al-content, x-ray fluorescence and x-ray photoelectron spectroscopy were performed. Furthermore, X-ray photoelectron spectroscopy has the possibility of measuring the C-Content leading to make a point about the purity of the samples, which is about C impurities occurring if the oxidizing step does not work quite well. To get to know the crystal-structure as well as the crystallite size and their influence on the resistivity, x-ray diffraction is used. The resistivity depending on the Al-content and the deposition temperature is measured via the 4-point probe.

5.1 SPECTROSCOPIC ELLIPSOMETRY (SE)

As mentioned, spectroscopic ellipsometry is used to determine the thickness of the deposited thin films and their optical constants, like the refractive index. Via the thickness and the knowledge of the total number of the deposited cycles, the calculation of the growth per cycle can be done.

The light source used is followed by a polarizer allowing only light with a preference electric field orientation to pass through. Linearly polarized light, two orthogonal light waves are in phase, is created. After the interaction with the sample, a change of the polarization occurs resulting in elliptical polarized light having an arbitrary amplitude and phase. The change of polarisation is parameterized by the amplitude ratio (Ψ) and the phase difference (Δ) for the two separated orthogonal components, parallel (p) and perpendicular (s), with respect of the plane of incidence. Due to the interest of the spectroscopic ellipsometry is primarily of the change of reflection (r) and transmission of the two components, it leads to formula 3 [28]:

$$\frac{r_p}{r_s} = tan\,\Psi * e^{i\Delta} \qquad (3)$$

The presented basic principle of spectroscopic measurements is shown in Figure 25.

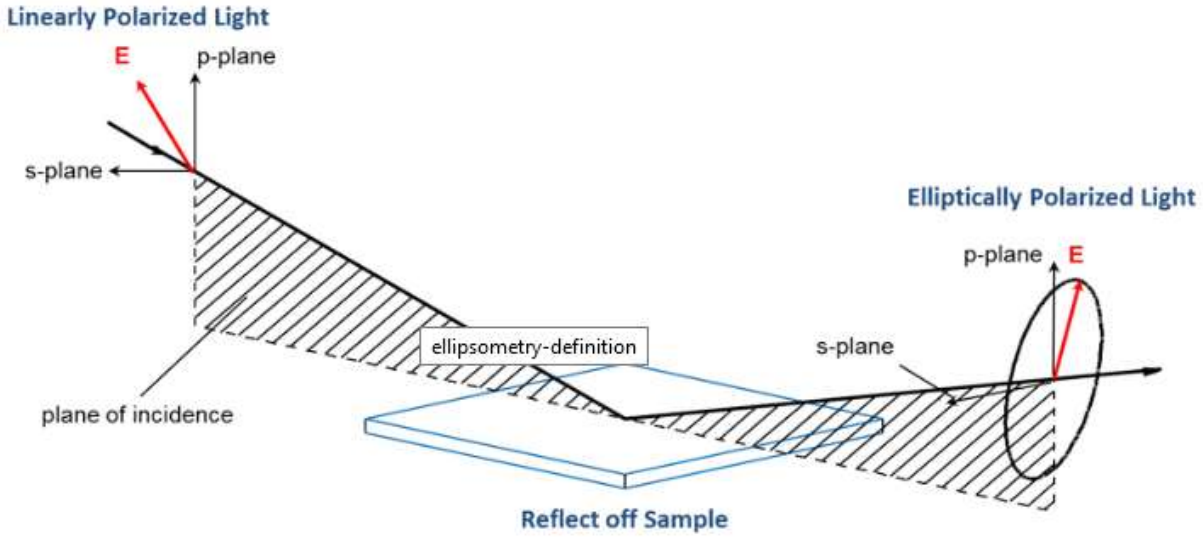

Figure 25: Basic principle of spectroscopic ellipsometry. Image reprinted from [28]

In the laboratory, the J.A. Woollam CO M-200V ellipsometer, having a wavelength range of the incident light between 371 nm and 1000 nm, was used to characterize the samples by taking several incident angles, 65°, 70° and 75°. To get to know the thickness and the refractive index (n), the measured data was fitted by the CompleteEASE software, using a defined model, the Cauchy model [29], due to of dealing with AZO thin films, which were highly transparent for the wavelength (λ) of 550 nm, even if they were highly doped [30]. The drawback of the Cauchy relationship (Formula 4) was the possibility of producing unphysical dispersions due to being not constrained by the Kramers-Kronig consistency ensuring a realistic shape being retained for the optical dispersion. As a consequence, the physical meaning of the used fit parameters like the roughness had to be controlled. Furthermore, the fit parameters for the Cauchy model were A, B and C [29].

$$n(\lambda) = A + \frac{B}{\lambda^2} + \frac{C}{\lambda^4} \qquad (4)$$

Due to for the measurements strong correlated fit parameters B and C, the $\frac{C}{\lambda^4}$-term could be neglected, as mentioned in the previous work “Plasma-enhanced atomic layer deposition of zinc oxide thin films” by Dipl. Ing. Julian Pilz [21].

5.2 X-RAY DIFFRACTION (XRD)

X-ray diffraction is a method used to characterize the crystal structure and furthermore, to get to know the crystallite size by using the Scherrer formula (formula 6). This section explains the fundamentals of x-ray diffraction and the setup used to do the investigation.

5.2.1 XRD FUNDAMENTALS

This section explains the fundamentals of x-ray diffraction occurring if the inter-planar distance of the planes is in the range of the wavelengths exposed to the sample, which is for crystals between 0.15 nm and 0.4 nm corresponding to x-rays with a photon energy between 3 keV and 8 keV. Moreover, the for the investigation used classical θ/2θ setup is delineated. A detailed description for the x-ray diffraction can be found in the book "Thin Film Analysis by X-Ray Scattering" by Mario Birkholz [31].

During the exposure of x-rays to the sample, three different kinds of scattering, the photoelectric effect, Thomson scattering and Compton scattering occurs. For diffraction only the Thomson scattering, an elastic one, happen if the particle kinetic energy and the photon frequency does not change during the interaction with the sample, is used. The interaction of the incident x-rays with different inter-planar distances of the sample leads to interference effects. Constructively interferences, described by the Bragg equation (formula 5), invented by W.H. Bragg and W.L. Bragg in 1913, occur if the phase shift of two adjacent planes is a multiple of 2π. θ_B is the Bragg-angle for which positive interference is observed, d_{hkl} represents the inter-planar distance and λ is the wavelength of the x-rays. Furthermore, the Bragg equation, visualised in Figure 26, is used for the investigation of the change of the inter-planar distances while enhancing the Al-content (sections 10.1.1 and 10.3.1).

$$2d_{hkl}\,sin(\theta_B) = \lambda \qquad (5)$$

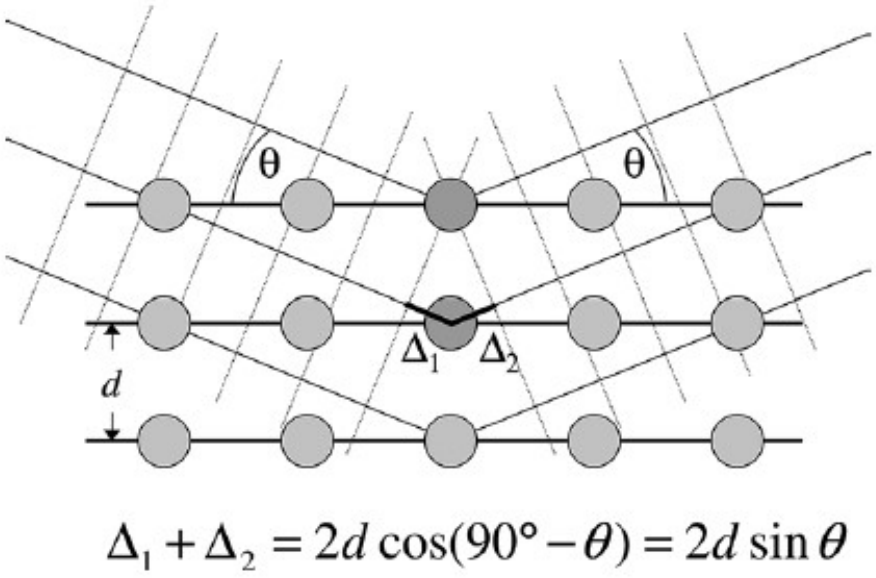

Figure 26: Visualization of Bragg's equation. Maximum scattered intensity is observed when the phase shifts add to a multiple of the incident wavelength λ. Image reprinted from [31]

Figure 27 represents the schematic of the θ/2θ setup. The incident angle θ, the one between the incident x-ray beam and the surface of the investigated sample changes during the measurement, while the 2θ angle, representing the one occurring between the incident beam and the diffracted one, is fixed. Moreover, the scattering vector (**Q**), the difference of the incident wave vector ($\mathbf{K}_0$) and the diffracted one (**K**), pointing along the bisection of the incoming and scattered beam, is shown. Due to the fixed 2θ angle only lattice planes oriented parallel to the surface plane contribute to the Bragg reflection.

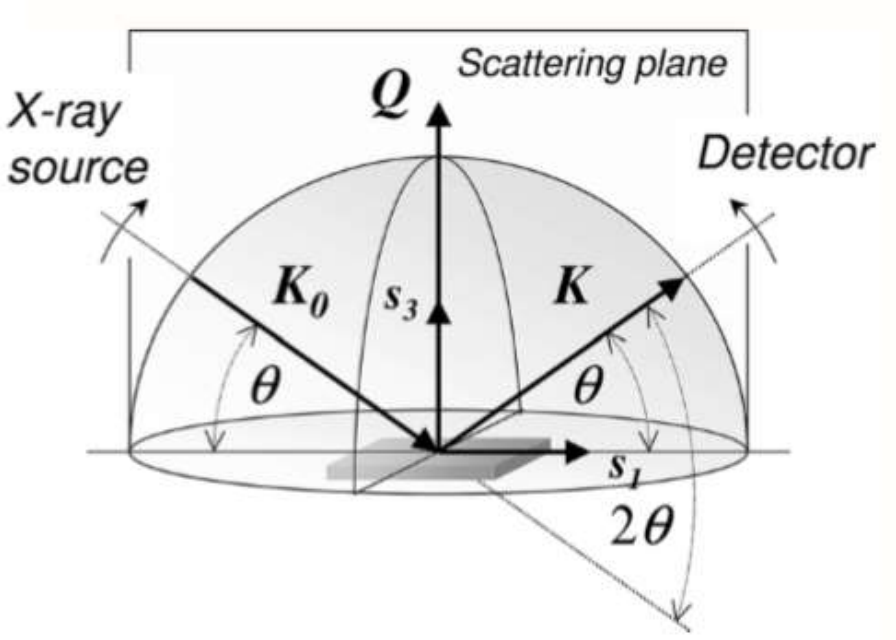

Figure 27: Schematic representation of a ϑ/2ϑ scan from the viewpoint of the sample reference frame {$\mathbf{s}_i$}. Image reprinted from [31]

AZO thin films are polycrystalline ones having a wurtzite structure (Figure 8), as ZnO is the main compound. Consequently, they have various crystallites oriented in different directions according to the surface, leading to the observation of crystal planes with different Miller indices. Figure 13 shows so-called preferential orientation changes, during the increase of the deposition temperature. A preferential orientation occurs, if some of the different crystal planes are favoured, while the crystal arises. At lower temperature, the (100) orientation is preferred, while during the increase of the substrate temperature, the favoured orientation changes to (002).

A further investigation done with the XRD pattern was to calculate the crystallite size (D_{sph}) of the researched orientations (100) and (002). For such an estimation, the Scherrer formula (formula 6) for spherical crystallites was used. Moreover, the irradiation wavelength (λ), the measured full width half maximum of the 2θ angle ($\beta_{2\theta}$) and the peak position (θ_0) had to be known. Due to the experimental setup, some broadening effects occurred, which were not considered [21].

$$D_{sph} = \frac{4}{3} \left(\frac{\pi}{6}\right)^{\frac{1}{3}} \frac{\lambda}{\beta_{2\theta} \cos(\theta_0)} \tag{6}$$

5.2.2 XRD – SETUP

The XRD measurements were done with the Panalytical Empyrean diffractometer at the institute, whose setup is shown in Figure 28. The diffractometer consisted of an x-ray tube creating a Cu-K_α-radiation with a wavelength λ = 1.5406 Å. Furthermore, a divergence slit ($\frac{1}{8}$°) decreasing the beam divergence and a mask (10 mm) reducing the focal spot size to irradiate only the sample were used. The anti-scatter slit (P7.5) at the right avoided influences of scattering with air-molecules and aperture edges and a PIXCEL 3D detector measured the intensities of the different Bragg reflections.

To align the system, a 2θ scan was done at the beginning. Moreover, after changing the sample, a z-scan corresponding to the height of the sample stage, and an Ω-scan determining the lattice geometry of the crystals, were alternatingly repeated until the samples were perfectly aligned. During the alignment, the divergence slit ($\frac{1}{32}$°) and the anti-scatter slit (0.1 mm) were changed and the detector operated in receiving slit 0D mode. Additionally, the beam attenuator hindering to inflict damage to the detector by an automatic turn on was involved, if a certain threshold intensity was exceeded. [21]

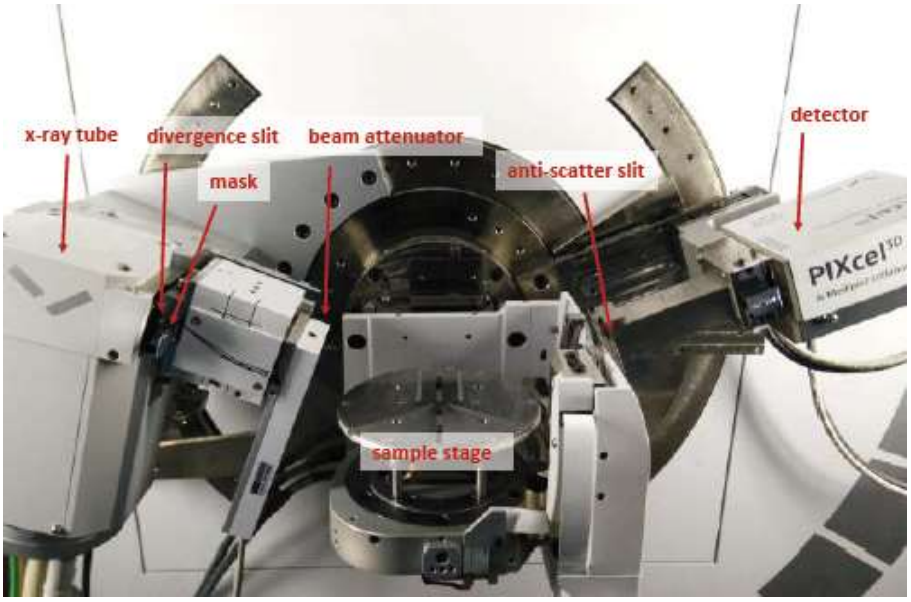

Figure 28: Experimental setup of the Panalytical Empyrean diffractometer. Image reprinted from [21]

5.3 X-RAY FLUORESCENCE (XRF)

X-ray fluorescence is a method used to characterize the composition of the AZO thin films. The fundamentals, the used setup and the analysis for the measurements are discussed.

5.3.1 XRF FUNDAMENTALS

This section explains the fundamentals of fluorescence. When x-rays interact with matter three main processes can take place: absorption, producing fluorescent radiation, transmittance and scattering, as mentioned in section 5.2.1. Moreover, how characteristic x-rays are produced to characterise the composition of the sample, is indicated. A detailed description for x-ray fluorescence can be found in the script „Theory of XRF, Getting acquainted with the principles“ by Peter Brouwer [32].

The fluorescence depends on the thickness, density and composition of the sample as well as on the energy of the x-rays produced by a source, irradiating the sample. The elements present in the sample emits characteristic fluorescent x-ray radiation with discrete energies. By measuring those energies and their intensities, the present elements and their amount can be determined, qualitative analysis.

To get to know the characteristic x-rays, leading to a so-called fingerprint of the chemical composition of the sample, the classical model of an atom (Figure 29), describing the atom as a nucleus surrounded by electrons grouped in shells or orbitals, has to be considered. Each shell, except the innermost one (K-shell) consists of sub-shells containing 2 electrons (spin-up and spin-down). The energy of an electron depends on the shell it occupies and on the element to which it belongs. If an atom is irradiated, the x-ray photons produced by the x-ray tube can expel electrons from the inner shells of an atom, if the binding-energy is exceeded. This produces initial vacancies corresponding to an unstably excited state. To reach a stable

configuration again, electrons of the outer shells are transferred to these initial vacancies. The energy difference of each is emitted via an X-ray photon, seen as a line in the spectrum.

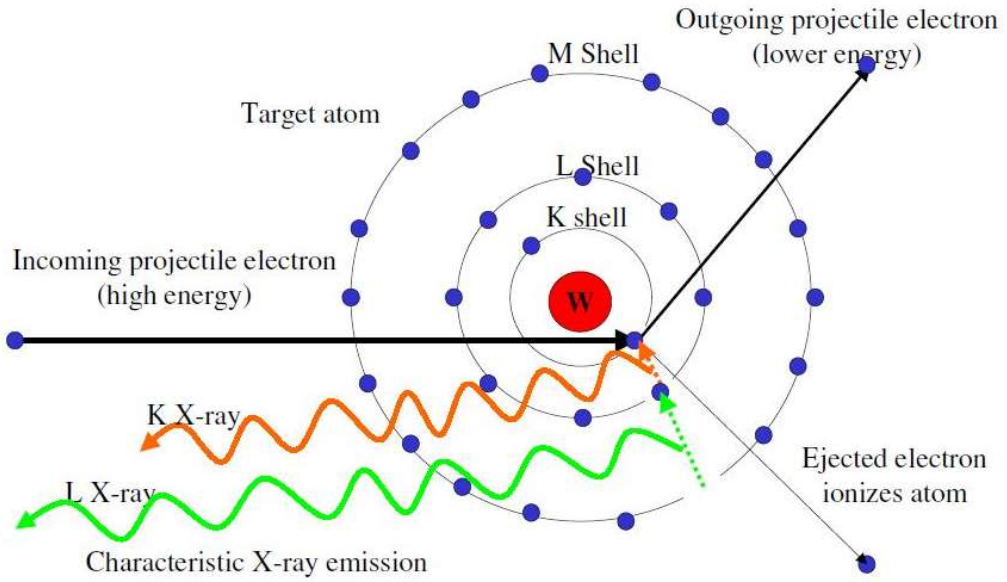

Figure 29: Production of characteristic x-rays. Image reprinted from [33]

5.3.2 XRF-SETUP

To do quantitative analysis via XRF, the Epsilon 1 of PANalytical, allowing with little to no sample-preparation a quantification for the elements sodium to americium, was used. To discuss the setup, the manuals, “Epsilon 1 User’s Guide” from PANalytical [34] and “Epsilon 1, Flexible and accurate elemental analysis“ from PANalytical [35] were used.

The measuring chamber (Figure 30) consisted of a measuring station and a reference-sample needed to do a gain measurement every 24 hours. As a result, a so called ‘snapshot’ of the stable instrument leading to a warm up of about 30 min, was taken.

The measuring station consisted of an x-ray tube, a protection foil, a clamping ring to fix the protection foil, a filter wheel, placed between the source and the sample, and a high resolution energy dispersive detector. The detector, a highly sensitive silicon drift one measuring the energy of an incoming photon by the amount of ionisation it produced in the detector material, and the x-ray tube (15W and 50 kV), producing a spectrum of the silver anode used for exciting the elements, were encapsulated by a dome composed of aluminium, located below the protection foil. The filter wheel consisted of different filters used to reduce the intensity of interfering lines and backgrounds leading to an enhancement of the signal to noise ratio [32]. A further specification of the filters is not necessary, due to not using them during the measurement to determine the composition in wt%.

Figure 30: Measuring chamber Epsilon 1

5.3.3 XRF-ANALYSIS

This section illustrates on the one hand, the analysation of the results (wt%) obtained from the XRF measurements, and on the other hand, the calculation of the theoretical values (at%) of the Al(Zn)-content depending on PEALD, the chosen method to deposit the thin films.

For the theoretical calculation of the Al-content, formula 7a was used. Atomic percent (at%) is defined as the ratio of the atoms interested in to atoms in total in a compound. As, there had been two different layers, the molar mass (M) of the two individual layers (Al_2O_3 and ZnO) as well as their densities (ρ) and their individual growth per cycle (GPC), due to the layer-by-layer deposition, had to be taken into account. Furthermore, the cycle ratio of (n)-ZnO to one Al_2O_3, leading to various super-cycles, had to be kept in mind. The calculation was done while considering ideal stoichiometry of each of the layers. Moreover, the formula took into account the changed Al-content while varying the temperature, leading to a modification of the GPC, and the cycle ratio.

$$at\%_{Al} = \frac{\frac{2*GPC_{Al_2O_3}*\rho_{Al_2O_3}}{M_{Al_2O_3}}}{\frac{2*n*GPC_{ZnO}*\rho_{ZnO}}{M_{ZnO}} + \frac{5*GPC_{Al_2O_3}*\rho_{Al_2O_3}}{M_{Al_2O_3}}} \quad (7a)$$

The same formula slightly changed, leading to formula 7b, was taken for determining the Zn-content.

$$at\%_{Zn} = \frac{\frac{n*GPC_{ZnO}*\rho_{ZnO}}{M_{ZnO}}}{\frac{2*n*GPC_{ZnO}*\rho_{ZnO}}{M_{ZnO}} + \frac{5*GPC_{Al_2O_3}*\rho_{Al_2O_3}}{M_{Al_2O_3}}} \quad (7b)$$

To be able to compare the XRF results (wt%) with the calculated Al-content (at%), formula 8a was designed. Considering an ideal stoichiometry, 40 at% of aluminium would be in a pure Al_2O_3 thin film. By multiplying the measured samples (wt%) of different cycle ratios with 40 at% and dividing them by the measured al-content (wt%) of the pure Al_2O_3 thin film, the Al-content in at% for the samples of different cycle ratios could be calculated. The impact of the GPC on the Al-content is taken into account by normalizing the measured samples to their thickness, due to depositing super-cycles leading to non-equal total cycles. Considering the same measured high amount of aluminium in pure ZnO thin films and in pure Si-wafers (Table 14), this amount was subtracted from the prepared AZO samples. Moreover, a measurement with bulk zinc, leading to no aluminium content (Table 14), was done to verify formula 8a.

The reason of the high aluminium content was ascribed to the composition of the dome (Al) encapsulating the detector and the x-ray tube (section 5.3.2). The $K_{\alpha 1}$ fluorescence produced by Si-wafers (1739 eV) irradiated on the aluminium of the dome (K-edge = 1560 eV) resulted in this mentioned high content.

Further investigations, contained in Table 14, led to a different amount of aluminium while using Si-wafers having a native oxide of few nm (Si) and Si-wafers with a thermal oxide of about 150 nm on top (Si (2)). As a consequence, thicker SiO_2 on top, leading to a reduced probability of irradiating the aluminium dome, resulted in a reduced amount of Si-$K_{\alpha 1}$ fluorescence.

Only samples deposited at room temperature were shown, as the same behaviour was found for depositing the thin films at 150 °C.

Table 14: Zn-content and Al-content of pure Al_2O_3 thin films, pure ZnO thin films, Si-wafers used as substrate and bulk zinc as a reference sample. The thin films are deposited at room temperature

The Zn- and Al-Content (wt%) of the samples measured via XRF are listed.

Sample	Zn-content [wt%]	Al-content [wt%]
Al_2O_3	0.002 ± 0.001	1,650 ± 0,016
ZnO	0.022 ± 0.001	1,180 ± 0,004
Si	0.004 ± 0.001	1,184 ± 0,004
Si (2)	0.002 ± 0.001	1,003 ± 0,004
Zn	98.630	-

$$at\%_{Al} = \frac{40 * mean\ value\ of\ the\ sample\ series\ \left[\frac{\text{wt\% } Al_{Sample} - \text{wt\% } Al_{ZnO}}{t_{Sample}}\right]}{mean\ value\ of\ the\ sample\ series\ \left[\frac{\text{wt\% } Al_{Al_2O_3} - \text{wt\% } Al_{ZnO}}{t_{Al_2O_3}}\right]} \quad (8a)$$

To be able to do investigations on Zn-content, this formula had to be slightly changed as well, leading to formula 8b:

$$at\%_{Zn} = \frac{50 * mean\ value\ of\ the\ sample\ series\ [\frac{\text{wt\% } Zn_{Sample} - \text{wt\% } Zn_{Al_2O_3}}{t_{Sample}}]}{mean\ value\ of\ the\ sample\ series\ [\frac{\text{wt\% } Zn_{ZnO} - \text{wt\% } Zn_{Al_2O_3}}{t_{ZnO}}]} \quad (8b)$$

5.4 X-RAY PHOTOELECTRON SPECTROSCOPY (XPS)

This section describes x-ray photoelectron spectroscopy by use of the webpage "https://www.colorado.edu/physics/phys3340/phys3340_sp13/CourseInformation/Modern/XPS.pdf" [36] and the master thesis "Plasma-enhanced atomic layer deposition of zinc oxide thin films" by Dipl. Ing. Julian Pilz [21]. Furthermore, XPS would be compared to XRF.

XPS is based on the photoelectric effect, Albert Einstein came up with in 1905. The kinetic energy of the ejected electron (E_k), detected by an energy dispersive detector and delineated by the law of energy conversion (formula 9), is the difference of the injected photon energy (hv) and the binding energy of an electron in the solid (E_B) as well as the work function (Φ), that must be exceeded to reach the vacuum level, to set the electron free. The energy loss of the electrons is exponential while leaving the sample, due to some exchanges. As a result, only electrons, tightly bond or weakly bond valence ones, near the surface can be ejected. This leads to a surface sensitive method, where the analysing depth is a few Å to a few nm depending on the incident angle of the x-rays. A further main difference to XRF is the used monochromatic x-rays to be able to determine the binding energy.

$$E_k = hv - E_B - \Phi \quad \rightarrow \quad E_B = hv - E_K - \Phi \quad (9)$$

For the XPS investigations, a spectrum over the whole range of the binding energy (typically 0 eV to 1200 eV), called survey spectrum, was done to be able to determine the composition of the thin films. Therewith, all elements except hydrogen could be detected, leading to a major field of applications compared to XRF (section 5.3.2). To be able to determine the zinc and aluminium content in the samples, the binding energies of the distinct core levels of the deposited elements like aluminium, zinc, oxygen and carbon are listed in Table 15.

Table 15: Binding energies of the distinct core levels used for the elemental analysis

The investigated core states of the deposited elements characterised by XPS as well as their corresponding energies and sensitivity factors are listed.

Element	Core state	Energy [eV]	Sensitivity factor
Al	2p	74	0.5371
C	1s	285	1
O	1s	531	2.93
Zn	$2p_{3/2}$	1022	9.8

The peak positions were characteristic for each element due to the different binding energies for the core level electrons. The intensity divided by a specific sensitivity factor depending on the photoemission cross-section of the core levels and on the instrument setup, resulted in the number of any kind of atoms, part of the composition. To determine the relative atomic concentration of an element A (C_A), their intensities (I_A, I_n) and sensitivity factors (S_A, S_n) combined with formula 10 were used.

$$C_A = \frac{\frac{I_A}{S_A}}{\Sigma_n \frac{I_n}{S_n}} \tag{10}$$

Beside the survey spectrum, two high resolution scans, before and after sputtering, recorded in FAT (Fixed Analyzer Transmission) mode at a pass energy of 117.40 and 29.35 eV, were done to investigate in the chemical states listed in Table 15. In the set conditions, the analyzer energy resolution (FWHM, full width at half-maximum height), measured on the silver Ag $3d_{5/2}$ photoemission line, was 0.7 eV for a pass energy of 29.35 eV. The sputter process, made with argon ions for 1 min of 1 kV and 1 µA by a raster size 2 * 2 cm^2, was necessary to clean the surface, to remove the whole carbon content.

The measurements were provided by Dr. Antonella Milella at the University of Bari, Italy. For the investigation, a scanning XPS microprobe (PHI 5000 Versa Probe II, Physical Electronics), equipped with a monochromatic Al K_α X-ray source (1486.6 eV) operated at 15 kV with a spot of 100 µm and a power of 24.8 W, was used. All spectra were acquired at a take-off angle of 45°, with respect to the sample surface. The elemental and chemical state analysis by use of the high resolution scans and the survey spectra were provided using the software CasaXPS.

5.5 4-POINT PROBE

This section explains the fundamentals of 4-point probing, a common technique to do some resistivity measurements, and the used setup. A short introduction into the fundamentals of this technique is provided with the support of the paper “Measurement of Sheet Resistivities with the Four-Point Probe” by F. M. SMITS [37].

5.5.1 4-POINT PROBE FUNDAMENTALS

The 4-point probe method is used to determine the resistivity of samples. Normally it is used for bulk ones, but after some treatments beforehand thin films can be investigated as well.

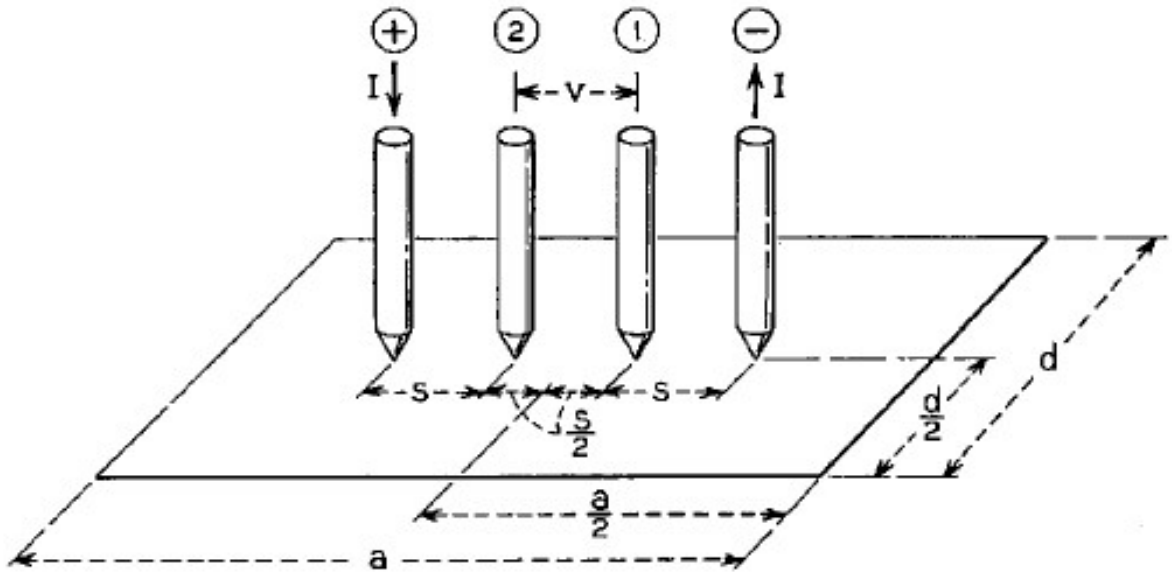

Figure 31: Arrangement of four-point probe on a rectangular sample. Image reprinted from [37]

A schematic for a 4-point probe on a rectangular sample, considering equal spacing (s) between the 4 probes and an arrangement of them in a line, is shown in Figure 31. The two outer probes are used to inject a fixed current (I). The voltage (V) for this purpose is measured with the two inner probes to get out the sheet resistance (ρ_S), correlated with the thickness (t) of the thin film to the resistivity (ρ), as shown in formula 11. The correlation factor ($F(\frac{t}{s})$) approaching to unity, if the thickness converges zero.

$$\rho = \rho_S t = \frac{V}{I} t \frac{\pi}{\ln 2} F(\frac{t}{s}) \qquad s>>t \qquad (11)$$

A logarithmic potential arises, if a fixed current is injected into an infinite sheet. To get the infinite relation working for a finite thin film, a treatment considering a potential for a dipole, represented by the two outer probes, and the method of images are done. As a result, only non-conducting boundaries are treated. The principle of “system of images” for a rectangular sample shape is shown in Figure 32. Due to the arrangement in a line and equally spacing of

the infinite number of current sources, the potential distribution is simplified to geometrical series and leads to a sheet resistivity represented in formula 12. Due to its dependency on the length (a) and width (d) of the sample as well as the equal spacing (s), the constant $C(\frac{a}{d};\frac{d}{s})$ is defined by this equation and tabulated in Table I of the paper "Measurement of Sheet Resistivities with the Four-Point Probe" by F. M. SMITS [37]. In consequence of having a spacing of 1.5 mm and a quadratic sample shape, resulting in a relation of $\frac{a}{d} = 1$ with a length(width) d = 2 cm for the setup, the constant was chosen to be 4.3.

$$\rho_S = \frac{V}{I} C(\frac{a}{d};\frac{d}{s}) \tag{12}$$

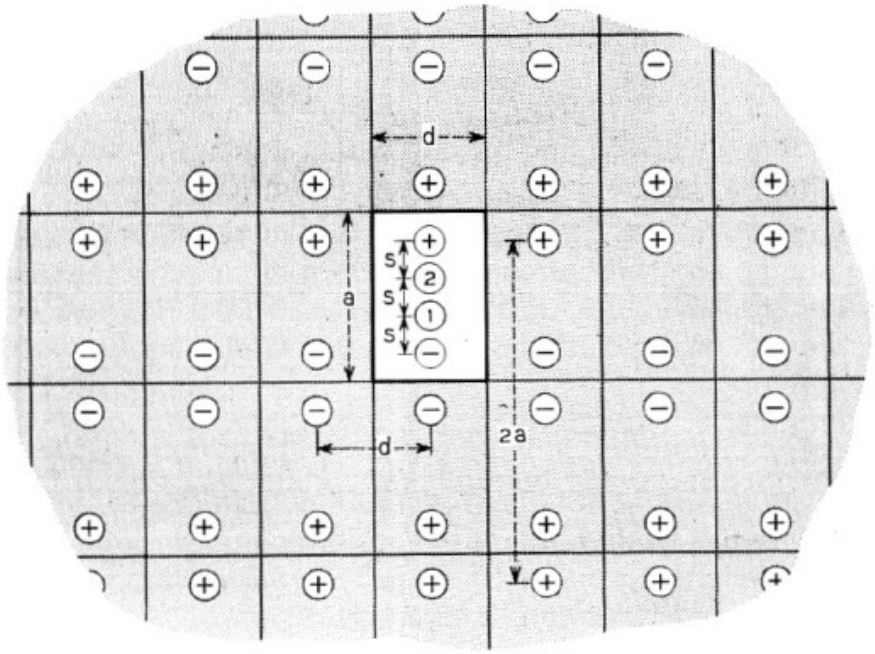

Figure 32: System of images. Image reprinted from [37]

5.5.2 4-POINT PROBE SETUP

To be able to perform 4-point probe measurements without destroying the deposited thin films, a new setup was designed, as shown in Figure 33. The main components were the four hemispheric and spring-loaded probes, having an equal spacing of 1.5 mm. Spring-loaded probes were chosen to achieve an equal force through all of them on the deposited films. The hemispheric shape of the bottom of the probe allowed to do not penetrate too deep into the films (with thickness in the range 50 nm - 90 nm), resulting otherwise into measuring the insulating SiO_2 layer of the thermal Si-wafers or the glass substrates. A source meter (KEITHLEY 2614B SourceMeter), controlled by a program called python, were used to set the fixed injection current and the chosen voltage range (-20 V to +20 V). The program was written by Dipl. Ing. Julian Pilz. The voltage values were averaged over 10 measurements at the same injection current. Furthermore, a 2-point probe at the same fixed current and a current measurement at the just-determined voltage was done validate the 4-point probe

measurement. As a consequence, the measured current had to equal the current injected for the 4-point probe measurement.

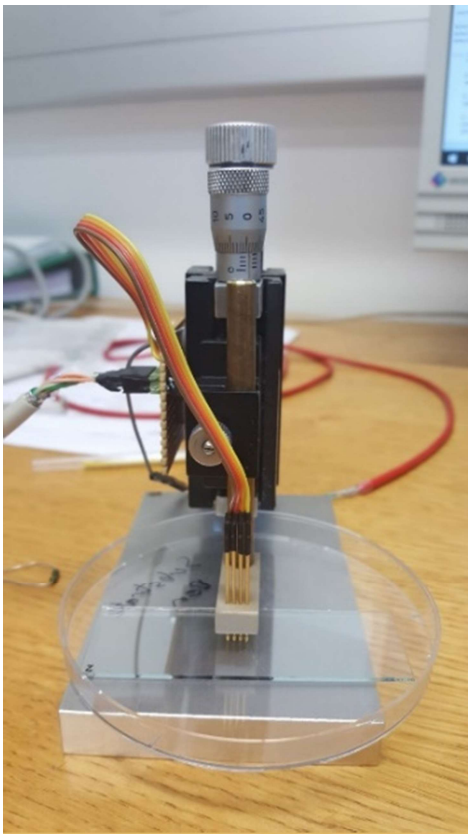

Figure 33: Setup for the 4-point probe, placing the sample in such a way that the described conditions are fulfilled.

Part III

RESULTS AND DISCUSSION

This part covers all results gained via the different characterisation techniques. The saturation regimes to deposit aluminium oxide using trimethylaluminium as precursor are shown at the beginning. Afterwards the behaviour of aluminium doped zinc oxide by two different deposition temperatures and different amount of aluminium content is compared. Moreover, investigations on the growth per cycle, the refractive index and the aluminium content as well as the zinc content while changing the cycle ratio are discussed. Furthermore, some conclusions are drawn for comparing the determination of the contents while using two different methods, X-ray fluorescence and X-ray photoelectron spectroscopy. At the end of this part, the crystal structure and the resistivity of the deposited aluminium doped zinc oxide thin films are shown. Moreover, the influence of the deposition temperature, the aluminium content and the effect of the annealing are discussed.

6) DETERMINATION OF THE SATURATION REGIMES OF ALUMINIUM OXIDE

In this chapter the use of the spectroscopic ellipsometry (SE) to determine the minimum time needed to be in saturation for depositing a cycle of aluminium oxide (Al_2O_3), produced by plasma-enhanced atomic layer deposition (PEALD), is described. As explained in section 2.2, one cycle deposited by PEALD consisted of four parts:

1. Precursor dose
2. Purging after precursor dose
3. Co-reactant dose
4. Purging after co-reactant dose

To do investigation, the thickness of the deposited Al_2O_3 thin films were measured with the spectroscopic ellipsometry (section 5.1), using a Cauchy model for fitting, to obtain values. The measured thickness values were divided by the fixed number of total cycles to calculate the growth per cycle (GPC), given in angstrom (Å). The total number deposited for the analysation of the Al_2O_3 thin films was 100. GPC was a mean value of the different sample positions shown in Figure 22. As a result, a standard deviation arose as well.

To get to the minimum of the different saturation regimes, long enough times had to be used for the first deposition. Afterwards, a stepwise reduction of the different times (section 4.2.1) was done.

6.1 PRECURSOR DOSE

As precursor trimethylaluminium (TMA) was used. The dose had to be long enough to fully cover the surface area. Consequently, it was started with a precursor dose of 200 ms to be sure to be in saturation. While reducing the precursor dose (TMA-time), a plateau between 50 ms and 120 ms was observed. This plateau corresponded to the saturation regime described in section 2.2. The gained difference, compare Figure 34 with Figure 2, was the further increase of the GPC while increasing the TMA-time from 120 ms to 200 ms. The observed CVD like growth for the 200 ms TMA time was due to the too low purging time after the precursor dose for such a high amount of TMA exposure. As a result, a higher standard deviation compared to all other measurements of this series occurred.

The minimum time needed to be in saturation was 50 ms and resulted in a GPC of 2.273 Å/cycle (Figure 34).

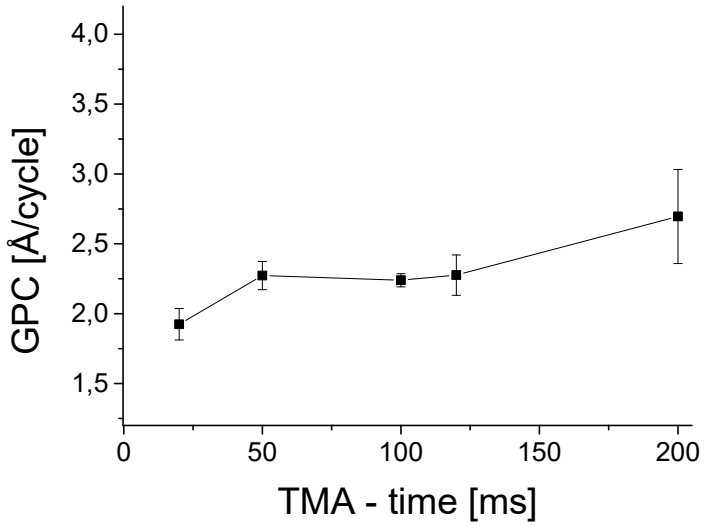

Figure 34: Saturation of the growth per cycle by varying the precursor dose (trimethylaluminium).

6.2 PURGING TIME AFTER PRECURSOR TIME

As purging gas, argon with a flow rate of 20 sccm, was used. The purging time had to be long enough to avoid non-self-limiting CVD processes as for the 200 ms of precursor exposure in Figure 34.

The purging time is shown in Figure 35, consisting of two different scalings due to a big increase of the GPC in the course of 9 s, leading to a CVD process, and 10 s, being in saturation. During the depositions of Al_2O_3 layers, some contaminations occurred after three to four deposition processes, leading to sparks in the reactor during the plasma dose resulting in an unstable plasma. As a consequence, the reactor was backed out. The high amount of contamination while depositing the thin film consisting 9 s of purging after the used precursor had led to a cleaning via isopropanol and a further back out process for 48 h. Due to a high waste of deposition time and TMA, no further investigation was done. To be sure to operate in saturation, it was decided to set the purging time after the precursor dose to 11 s for finding the optimum recipe.

The limitation of the Arduino to 7 sequences and 11 commands each sequence (section 4.1.4) led to a further increase of the purging time to 12 s while depositing AZO thin films.

The minimum purging time of 11 s resulted in a GPC of 2.217 Å/cycle.

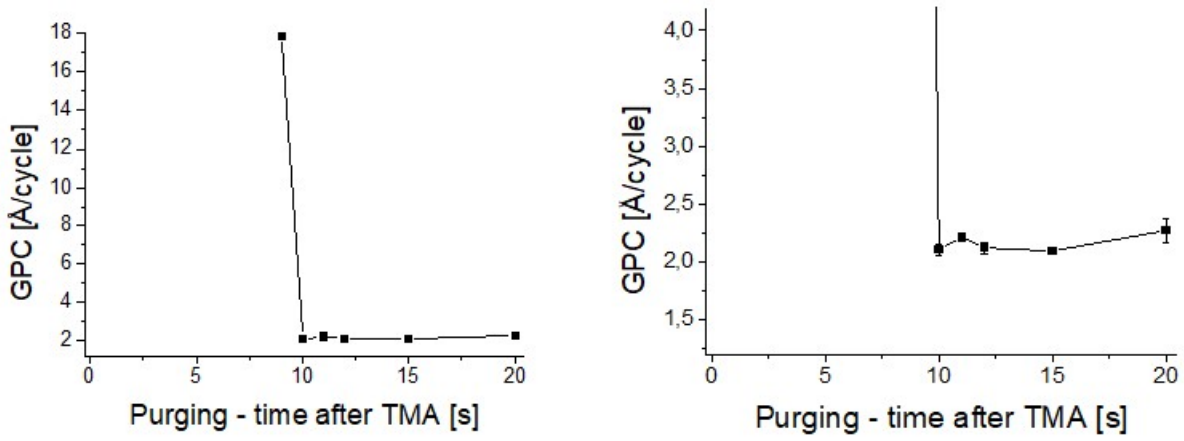

Figure 35: Saturation of the growth per cycle by varying the purging time after precursor dose. Argon gas is used for purging. Two different scalings are used to show the deviation as well as the sharp increase between 9 s and 10 s of purging time.

6.3 PLASMA DOSE

To determine the optimum plasma dose, an oxygen plasma of a RF-power of 60 W was used due to the pre-work "Plasma-enhanced atomic layer deposition of zinc oxide thin films" by Dipl. Ing. Julian Pilz [21]. The plasma dose had to be long enough to fully oxidize the precursor TMA. The different plasma times with an oxygen flow rate of 20 sccm were shown in Figure 36.

To be sure to fully oxidize the precursor a plasma time of 2 s was chosen, resulting in a GPC of 2.276 Å/cycle.

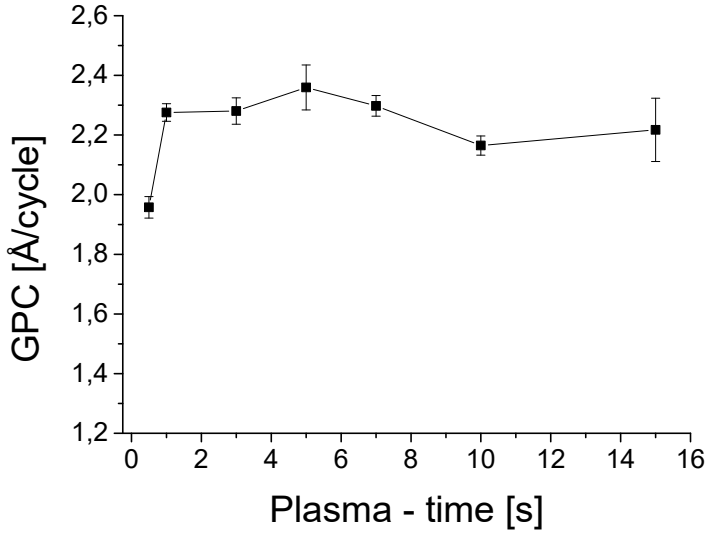

Figure 36: Saturation of the growth per cycle by varying the plasma dose. (oxygen plasma of RF-power of 60 W)

6.4 PURGING TIME AFTER PLASMA TIME

The purging time after plasma dose, using again argon with a flow rate of 20 sccm as purging gas, was shown twice in Figure 37 due to the use of two different butterfly valves (section 4.1.5). The automatic butterfly valve showed a saturation until 5 s of purging, resulting in a GPC of 2.354 Å/cycle, while the manual one indicated an increase of the GPC, 2.492 Å/cycle for the saturation regime, after 10 s. Due to the damaging of the automatic butterfly (section 4.1.5), the data points below 10 s of purging were not trustable.

To ensure to be in saturation and based on the limits of the arduino (section 4.1.4), the purging time after plasma dose was set to 15 s resulting in a GPC of 2.509 Å/cycle.

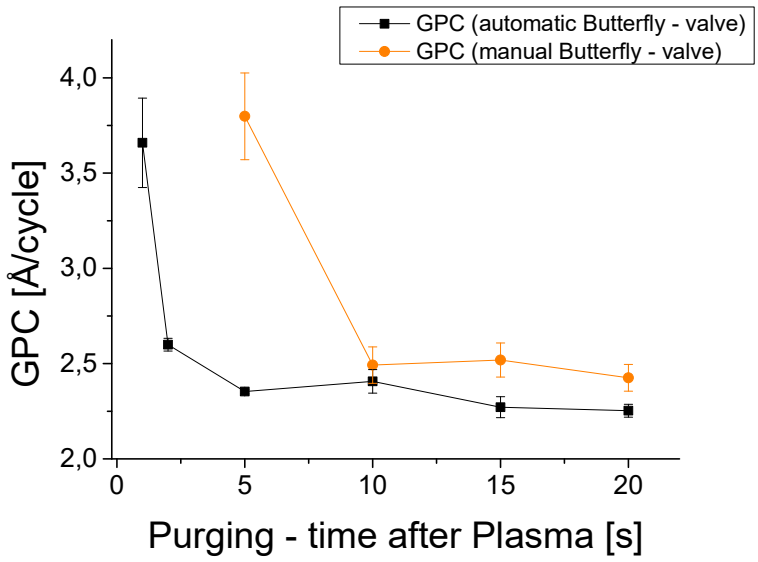

Figure 37: Saturation of the growth per cycle by varying the purging time after plasma dose for the automatic and manual butterfly valve.

6.5 OPTIMUM RECIPE

Figure 38 shows the high resolution measurements of the carbon peak (~283 eV) in counts per seconds (CPS) related to the binding energy of the measured electrons (eV) for the sample having a cycle ratio of 20:1 deposited at 150 °C for (a) after sputtering and (b) before sputtering. As mentioned in section 2.2 and 4.2, the depositions were done with the optimum recipe for depositing ZnO layers (Table 4) and Al_2O_3 layers (Table 10). To control the well-performing deposition process, fully oxidized precursors, the XPS measurements before and after sputtering were compared, leading, as desired, to no carbon content after sputtering.

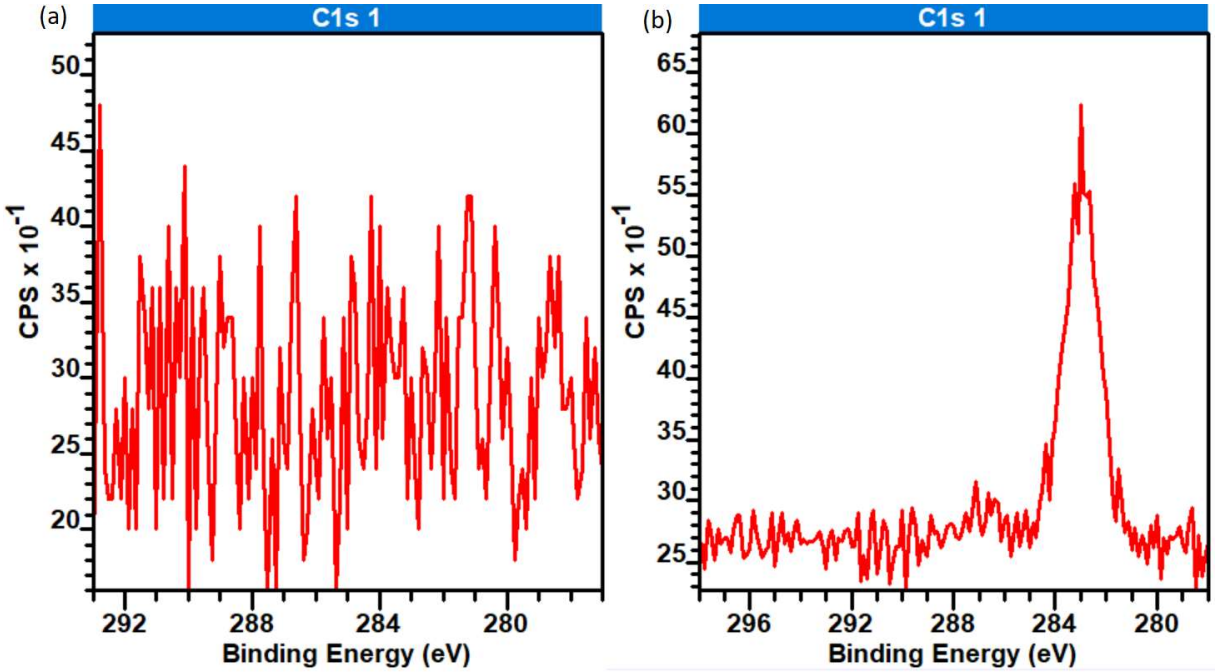

Figure 38: High resolution measurements of the carbon peak (~283 eV) shown in counts per seconds (CPS) related to the binding energy of the measured electrons (eV) for the sample having a cycle ratio of 20:1 deposited at elevated temperature (150 °C) for (a) after sputtering and (b) before sputtering.

7) GROWTH PER CYCLE

The growth per cycle was influenced by many parameters, like the temperature and the cycle ratio as shown in section 3.1 and 3.2. While being in saturation, the GPC would be constant during repeating the depositions under the same conditions, as the same monolayer was deposited. During the change of the pre-conditions, like the cycle ratio or the temperature, the composition of the monolayer changed and as a consequence also the growth per cycle. Operations on saturations were still done, as no carbon content was shown after sputtering for all of the other samples. Figure 38 served only as an example.

This chapter show the increase of the GPC for ZnO while increasing the deposition temperature from room temperature (RT) up to 150 °C and the contrast behaviour for the GPC of Al_2O_3 while increasing the deposition temperature the same way. Thus, only these two temperatures were investigated.

The second part of this chapter investigates into the GPC change while changing the cycle ratio at those two different deposition temperatures.

7.1 GPC – TEMPERATURE DEPENDENCE

Table 16 contains the different growth rates of the two materials (Al_2O_3 and ZnO) deposited at two different temperatures (RT and 150 °C). While for room temperature the GPC for Al_2O_3 (2.509 Å/cycle) was larger than that for ZnO (1.604 Å/cycle), it was more or less reversed for 150 °C, due to there the GPC of ZnO (2.743 Å/cycle) was greater than that for Al_2O_3 (1.367 Å/cycle).

Such a behaviour was shown as well in other papers and consequently illustrated for ZnO in Figure 9 and for Al_2O_3 in Figure 11. A similar relation between the GPC of ZnO and Al_2O_3 deposited at 150 °C was described in the paper “Structural, electrical, and optical properties of atomic layer deposition Al-doped ZnO films” by Parag Banerjee et al. [5]. There, the GPC for Al_2O_3 was also half of the GPC of ZnO, as tabulated in Table 16.

Table 16: Growth rate change for aluminium oxide and zinc oxide at two different temperatures, 25 °C and 150 °C.

The growth per cycle evaluated with dividing the via spectroscopic ellipsometry measured thickness (Å) by the total number of cycles corresponding to the two different temperatures, 25 °C referred as room temperature, and 150 °C referred as elevated temperature, is listed.

Sample	Deposition Temperature [°C]	Growth per Cycle [Å/cycle]
Al_2O_3	~25	2.509
Al_2O_3	150	1.367
ZnO	~25	1.604
ZnO	150	2.743

7.2 GPC – CYCLE RATIO DEPENDENCE

The growth per cycle depends on the percentage of zinc oxide cycles, closely related to the cycle ratio, deposited during the preparation of AZO thin films (section 3.2.1). Due to the deposition technique, PEALD, a layer-by-layer deposition, alternating Al_2O_3 and ZnO layers had to be deposited to create the samples (section 2.5.2).

The GPC was evaluated by measuring the thickness using spectroscopic ellipsometry and divided by the total number of cycles listed in Table 12.

7.2.1 GPC AT ELEVATED TEMPERATURE

Figure 39 shows the GPC depending on the aluminium content at elevated deposition temperature of 150 °C. The GPC for pure ZnO thin films, corresponding to an Al-content of 0 at%, was 2.743 Å/cycle, while that for pure Al_2O_3 ones, having an Al-content of 40 at%, was 1.367 Å/cycle. As a consequence, a decrease of the GPC was expected.

Different Al-Contents resulted in a different growth rate for both layers (ZnO and Al_2O_3), leading to a variation of the GPC for each cycle of the super-cycles deposited at elevated temperature (Figure 18). The Al-content of 4.0 at% corresponded to a cycle ratio of 10:1 and a percentage of ZnO cycles of approximately 91 %. Consequently, the depositions occurred above the negative growth leading to no observation of etching. The enhanced growth rates of ZnO after the first four to six layers, as discussed in section 3.2.1, led to an enhanced GPC for low doping concentrations as it is illustrated for an Al-content of 1.72 at% in Figure 39. A similar behaviour of the shown change of the GPC while varying the Al-content is pictured in the paper “Atomic layer deposition of Al-doped ZnO thin films” by Tommi Tynell et al. [38].

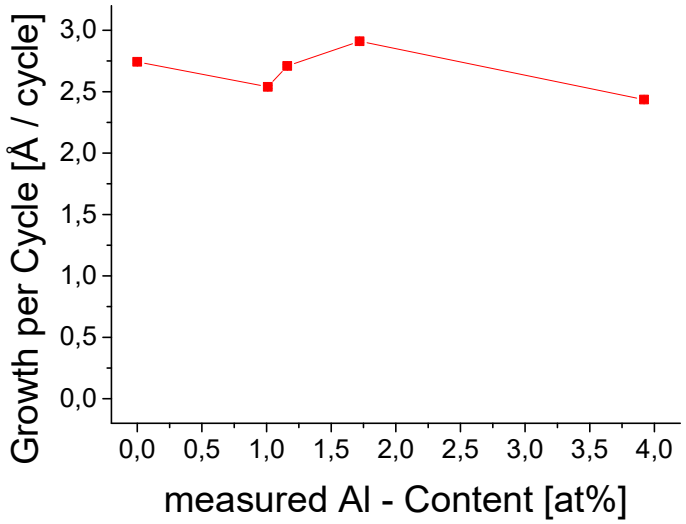

Figure 39: Growth per cycle given in Å/cycle depending on the measured Al-content given in at% for depositions at 150 °C.

7.2.2 GPC AT ROOM TEMPERATURE

The GPC for pure Al_2O_3 thin films (2.509 Å/cycle) deposited at room temperature was higher than that for pure ZnO ones (1.604 Å/cycle). As a result, the GPC was almost continuously increased while increasing the Al-content (Figure 40), leading to the conclusion that the growth rates for such a low deposition temperature, compared to the high one shown in Figure 39 and discussed in section 3.2.1, did not depend anymore on the cycle ratio.

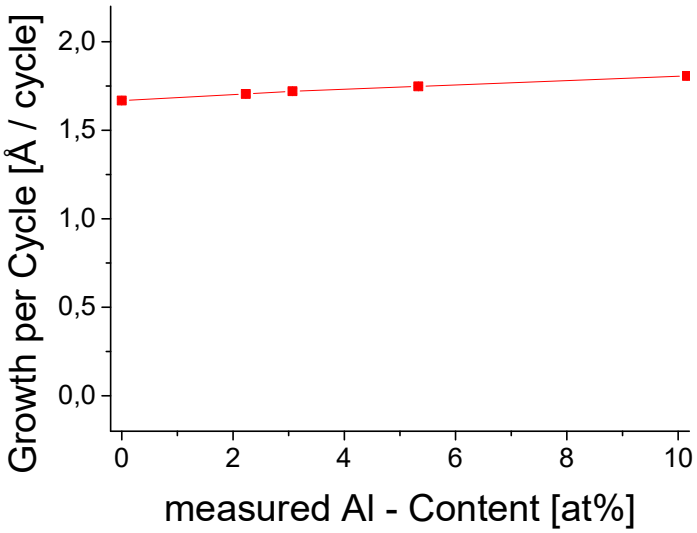

Figure 40: Growth per cycle given in Å/cycle depending on the measured Al-content given in at% for depositions at room temperature.

8) REFRACTIVE INDEX

The refractive index was changed while changing the composition of the AZO thin films due to the refractive index of Al_2O_3 differed from ZnO and while increasing the deposition temperature. The pure samples, consisting 100 cycles, used to create the AZO ones (Table 17) showed an increase of their refractive indices, used for a film density change, for depositing them at 150 °C instead of room temperature [29]. As shown in Figure 12, the film density was increased for Al_2O_3 while increasing the deposition temperature. Related to that behaviour, also the refractive Index and so the film density of ZnO was increased until a constant value of the GPC was reached, as reported in the paper "Plasma-Enhanced Atomic Layer Deposition of Semiconductor Grade ZnO Using Dimethyl Zinc" by Pieter C. Rowlette et al. [39]. Furthermore, lowering the hydrogen content was often associated with an increase of the refractive index.

Table 17: Refractive index measured via spectroscopic ellipsometry for aluminium oxide and zinc oxide at two different temperatures, 25 °C and 150 °C.

Sample	Deposition Temperature [°C]	Refractive Index
Al_2O_3	~25	1.615
Al_2O_3	150	1.716
ZnO	~25	1.860
ZnO	150	1.975

Figure 41 shows the decrease of the refractive index for depositing the AZO at room temperature (Figure 41(a)) and at 150 °C (Figure 41(b)), while increasing the aluminium content due to the lower refractive index of Al_2O_3 compared to ZnO. Furthermore, the higher refractive index for depositions at elevated temperature (150 °C) was shown in the different scaling. For the deposition done at 150 °C, indicating a problem coming up again during the discussion of the zinc content (Figure 43), the refractive index showed a local minimum for an aluminium doping concentration of 1.01 at%.

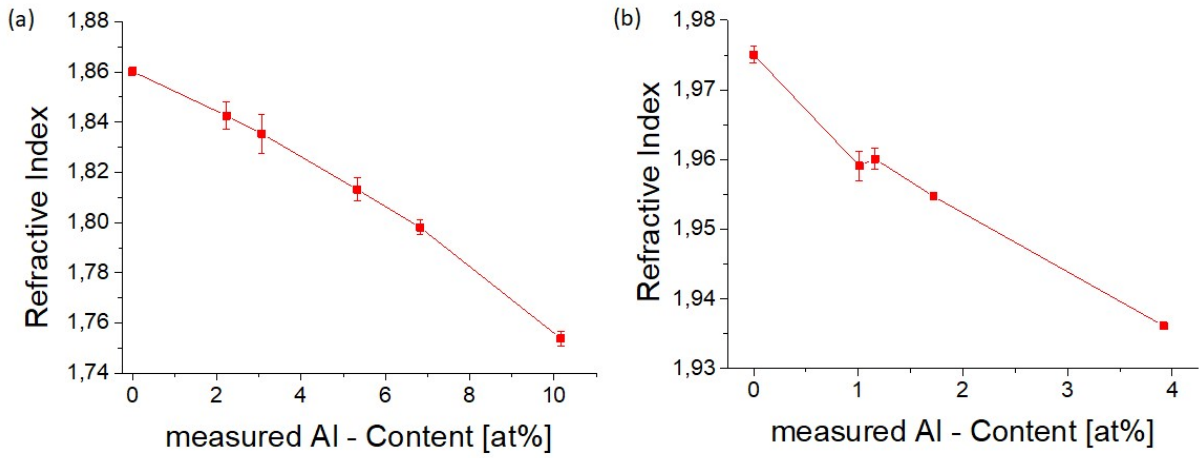

Figure 41: Refractive Index related to the aluminium content in at% (a) for depositions at room temperature (b) for depositions at 150 °C

9) DETERMINATION OF THE CHEMICAL COMPOSITION

To determine the aluminium content and the zinc content X-ray fluorescence, using the two formulas 8a and 8b, and X-ray photoelectron spectroscopy, using formula 10, were done. Furthermore, theoretical values were calculated with formulas 7a and 7b. A sample series containing different aluminium contents were prepared. Due to the deposition technique PEALD, the amount of doping concentration was controlled by changing the cycle ratio (section 2.5.2). The prepared super-cycles are listed in Table 12 and Table 13.

9.1 ALUMINIUM CONTENT

Figure 42 show the calculated aluminium content (at%), evaluated via formula 7a and shown in blue, and the measured one (at%), done with XRF, determined via formula 8a and shown in red, deposited at room temperature and 150 °C. Reducing the cycle ratio, depositing less ZnO cycles before depositing one Al_2O_3 layer, led to an increase of the aluminium content (section 2.5.2) demonstrating the well-performed PEALD doping process.

Depending on the GPC behaviour of ZnO and Al_2O_3 (section 7.1), the Al-content of the at 150 °C prepared samples showed a lower Al-content than the equivalent deposition series at room temperature (Table 16). Considering the formulas 7a and 8a, the GPC dependency for evaluating the aluminium content was taken into account and predicted a different behaviour for the different deposition temperatures.

The deviations of the calculated to the measured Al-content had different issues. One of them was the change of the aluminium oxide growth rates while varying the cycle ratio (section 3.2.1). The differences caused by the consideration of ideal stoichiometry, the behaviour of Al_2O_3 shown in Figure 12(a) serves as an example, and the setup, the measuring chamber of the XRF consisting of an aluminium dome encapsulated the detector and the x-ray tube (section 5.3.3), were further reasons. The $K_{\alpha 1}$ fluorescence of the Si (1739 eV) irradiating the aluminium of the dome (K-edge = 1560 eV) was taken to be the same for each sample, leading to the subtraction of the aluminium content of the pure ZnO thin film (section 5.3.3), resulting in a deviation to the calculated one, due to a possible change of the probability of such a second excitation.

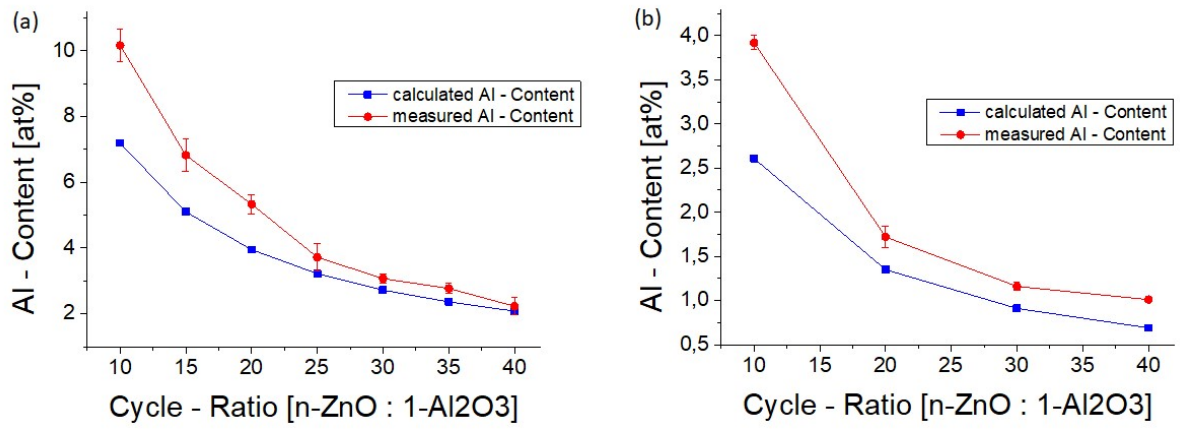

Figure 42: Aluminium content (at%) depending on the cycle ratio for the calculated aluminium content (blue) as well as the measured aluminium content (red) (a) for depositions at room temperature (b) for depositions at 150 °C

9.2 ZINC CONTENT

The calculated zinc content (at%) evaluated with formula 7b (violet) and the measured one (at%) with formula 8b (brown) for the prepared samples are shown in Figure 43(a) (room temperature) and Figure 43(b) (150 °C).

Comparing the corresponding figures of Figure 43 to Figure 42, one the one hand, enhancing the aluminium content resulting in a decrease of the zinc content can be demonstrated. Due to the pictured increase of the Al-content and as a consequence, the decrease of the zinc content, while reducing the cycle ratio from 40:1 to 10:1, concluded to a well-performed doping process. On the other hand, the increased deviation of the measured aluminium content above the calculated one while decreasing the cycle ratio resulted in a deviation of the measured zinc content below the calculated one leading to a relation between the two contents.

Moreover, for the deposited series at elevated temperature, the different growth rates of the GPC while varying the cycle ratio, changing the Al-content (Figure 42), were correlated to the zinc content. By comparing Figure 43(b) to Figure 39, an increased zinc content leading to a higher GPC could be shown.

By relating Figure 43(b) to Figure 41(b) the local minimum of the refractive index for an aluminium doping concentration of 1.01 at%, a cycle ratio of 40:1, could be explained. Considering the lower refractive index for ZnO compared to Al_2O_3 as shown in Table 17, the reduced deposited Zn-content, resulting in a decreased deposition of ZnO layers and further to a lower GPC, led to a reduced refractive index for the composition having a cycle ratio of 40:1 deposited at 150 °C.

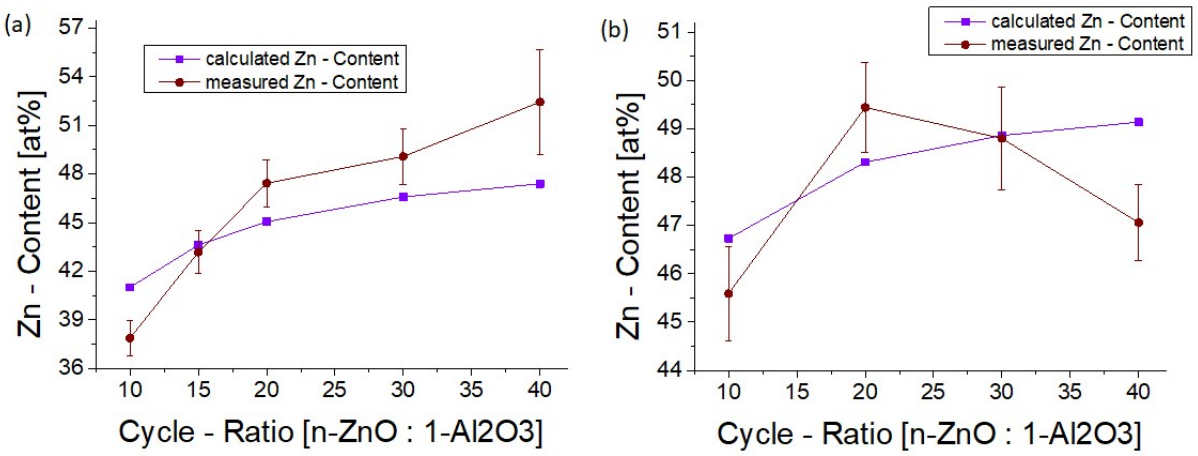

Figure 43: Zinc content (at%) depending on the cycle ratio for the calculated zinc content (brown) as well as the measured zinc content (violet) (a) for depositions at room temperature and (b) for depositions at 150 °C

9.3 COMPARISON WITH CHEMICAL COMPOSITION MEASURED BY XPS

Due to achieving low resistivity semiconductors while varying the Al-content is the main point of the thesis, XPS was chosen to be the second method to investigate the deposited contents and furthermore, to be able to measure the oxygen one in the deposited thin films.

The results of the XPS, the Al-content (pink), the Zn-content (blue), the C-content (black) and the oxygen content (red) are shown in Figure 44 related to the deposited cycle-ratio at (a) room temperature and (b) 150 °C. As a result, a strong relation between the carbon content and the oxygen one was pointed out.

For the analysis of Figure 44 (a) and (b), the thicknesses of one super-cycle for the different cycle ratios (40:1, 30:1, 20:1 and 10:1), indicated by the number of ZnO cycles, depending and the deposition temperature are shown in Table 18.

Table 18: Thickness of one super-cycle depending on the cycle ratio at two different temperatures, 25 °C and 150 °C.

The thickness of one super-cycle is calculated by multiplying the GPC with the numbers of cycles for one of it in nm.

ZnO-cycles	Deposition Temperature [°C]	Thickness of one super-cycle [nm]
40	150	10.414
30	150	8.401
20	150	6.111
10	150	2.684
40	~25	7.011
30	~25	5.363
20	~25	3.675
10	~25	1.991

Due to XPS is a surface sensitive analysis method, as discussed in section 5.4, a maximum detection depth of only few nm could be reached. The detection depth depended mostly on the incident angle of the X-rays and was assumed to be maximal 10 nm. Considering a carbon layer on top with at least 2 nm to 4 nm thickness, no second Al_2O_3 layer for the 30:1 and 40:1 ratio at elevated temperature deposited samples could be measured. As a consequence, the Al- and Zn-content should stay constant. Moreover, Figure 44(b) shows a constant Al- and Zn-content for the cycle ratios 10:1 and 20:1, leading to the conclusion, that only one Al_2O_3 layer was measured, resulting in a penetration depth lower than 2.684 nm below the carbon contamination layer. Due to a pictured decrease of the Al- and Zn-content between the 20:1 and the 40:1 ratio, the sensitivity of the XPS, coming from the exponential decay of the leaving probability of the measured electrons, had to be taken into account leading to a decrease of the contents while a thicker carbon contamination layer was present.

Figure 44(a) shows a similar behaviour than discussed for Figure 44(b). The only main difference, the big increase of the Al-content from a cycle ratio 20:1 to 10:1, led to two possibilities, a connection to the decrease of the carbon-content on the one hand, and a measuring of a second Al_2O_3 layer due a 1.991 nm thick super-cycle on the other. Due to the carbon contents for both 10:1 ratios, deposited at room temperature and 150 °C, were about 30 at%, the assumption of measuring a second layer was forced.

Due to many different influences, like finding a representative back ground, having a high noise to signal ratio, and the influence of the different amount of carbon contamination, the deviation for the contents are not shown in Figure 44. Moreover, the surveys were only done before sputtering, leading to an impossibility of considering the influence of the carbon contamination.

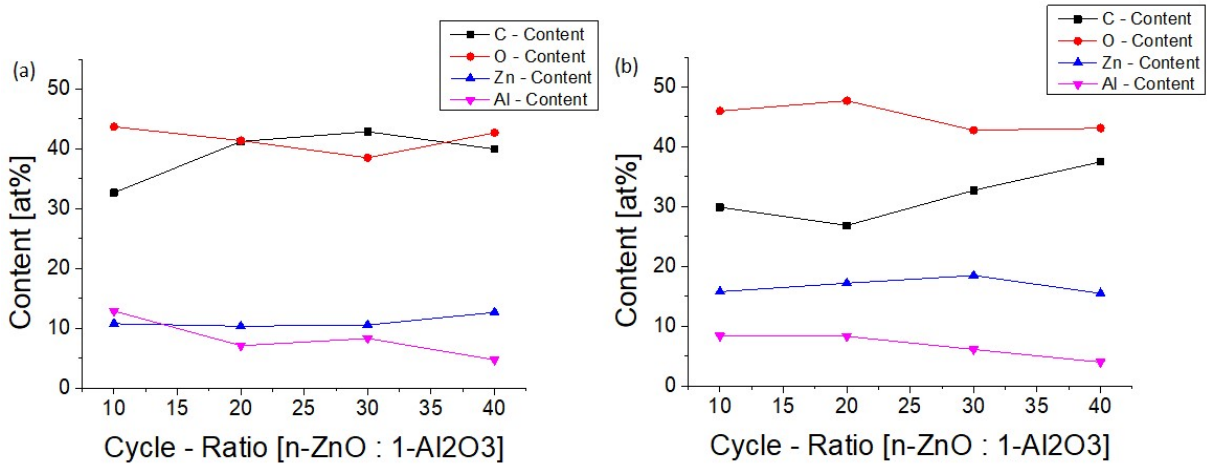

Figure 44: The aluminium content (pink), the zinc content (blue), the carbon content (black) as well as the oxygen content (red) are shown related to the deposited cycle-ratio at (a) room temperature and (b) elevated temperature (150 °C).

Another issue after sputtering is shown in Figure 45 picturing the high resolution scans of the aluminium peak presenting the counts per second (CPS) related to the binding energy of the measured electrons (eV) for the sample having a cycle ratio of 20:1 deposited at 150 °C for (a) after sputtering and (b) before sputtering. The aluminium peaks were normally visible at 73 eV (Al $2p_{3/2}$) and 74 eV (Al $2p_{1/2}$). Due to some charging of the surface during the

measurements, the peaks were shifted to 1-2 lower eV, corrected only for the survey measurements by shifting the carbon peak from 283 eV – 284 eV to 285 eV. Such a shifting was not necessary for this high resolution scans due to only the measured intensities of aluminium before and after sputtering are pointed out to indicate the sensitivity of the aluminium atoms to the sputter-process. Due to the aluminium peak was almost invisible after sputtering, only the survey before sputtering was investigated to get to know the composition.

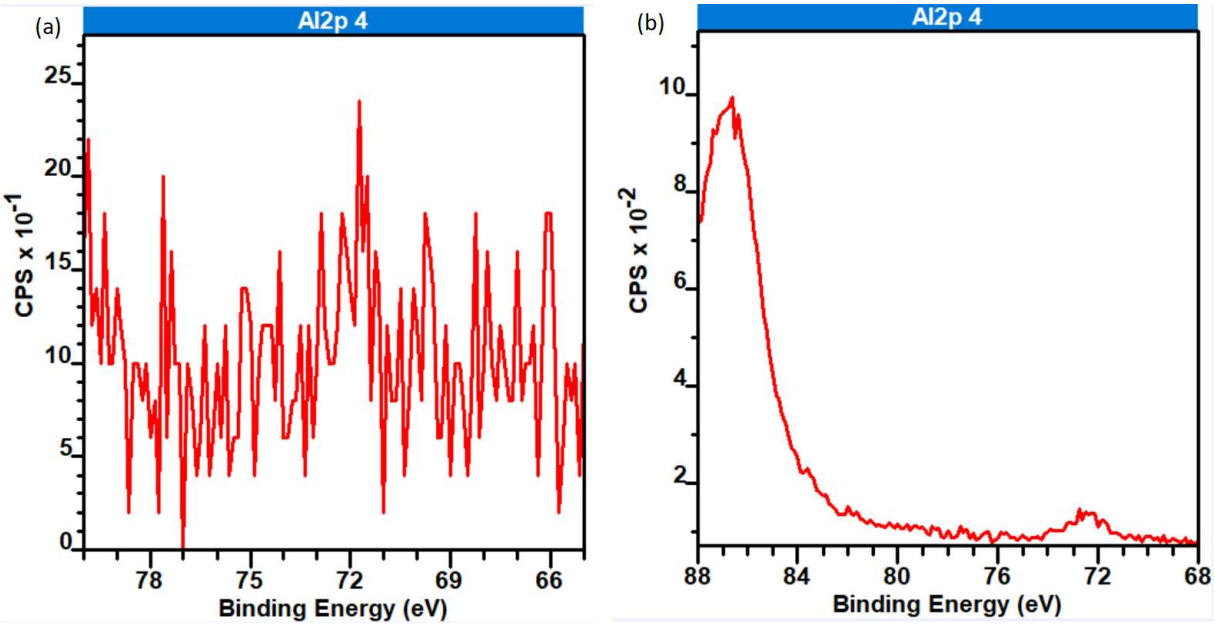

Figure 45: High resolution measurements of the aluminium peak (~72,5 eV) shown in counts per seconds (CPS) related to the binding energy of the measured electrons (eV) for the sample having a cycle ratio of 20:1 deposited at elevated temperature (150 °C) for (a) after sputtering and (b) before sputtering.

The Al-content measured with XPS shows higher values than expected due to the with XRF measured and the calculated one (comparing Figure 44 to Figure 42). Moreover, the layer-by-layer deposition and the exponential decay of the probability of electrons leaving the sample and getting measured as well as not knowing exactly how many ZnO layers were measured, it could be concluded, that XPS was due to its surface sensitivity not the right choice to measure the Al-content of AZO thin films deposited by PEALD.

9.4 OXYGEN PEAK

Some investigation of the O 1s peak, shown in Figure 46, was done to distinguish between three different components, the oxygen bound to hydrogen (blue), the oxygen bound to zinc or to aluminium (black) and the oxygen vacancies one (red), related to the cycle-ratio for (a) room temperature and (b) 150 °C.

To determine the fractions of the O 1s peak, considering this peak as 100 % leading to a strong correlation between the fraction contents, the program (CasaXPS) was used. A comparison of Figure 46(a) and (b) shows a higher hydrogen content for depositions at room temperature due to the fraction of O-H. An example for the found behaviour, reducing the H-content while increasing the deposition temperature, is reported for depositing Al_2O_3 layers in the paper "Plasma-enhanced and thermal atomic layer deposition of Al_2O_3 using dimethylaluminium

isopropoxide, $[Al(CH_3)_2(\mu\text{-}O^iPr)]_2$, as an alternative aluminium precursor" by Stephen E. Potts et al. [13].

While the deposition at room temperature showed more or less a constant value for the oxygen bound to zinc or to aluminium, except the outlier for a cycle ratio of 30:1, the deposition at 150 °C pointed out a decrease of this fraction after a constant value between the 40:1 and 20:1 cycle ratio. The increase of the aluminium content above 2 at% (Figure 42(b)) was correlated to a creation of zinc vacancies, leading to a decrease of the O-Zn/O-Al fraction and a decrease of the zinc content, as mentioned in the paper "Aluminium-doped zinc oxide films grown by atomic layer deposition for transparent electrode applications" by G. Luka et al. [30]. As a consequence, the decrease shown in Figure 43(b) for the cycle ratio of 10:1, could be explained.

Furthermore, such a decrease of the Zn-content was shown for the deposition at room temperature (Figure 43(a)), but not recognized in Figure 46(a). This might be due to the samples deposited at low temperature (Figure 46(a)), compared to the high one (Figure 46(b)) had different behaviours as shown by comparing to their corresponding figures, Figure 39 and Figure 40. For the samples deposited at 150 °C, the GPC was dependent on the different Al-contents (Figure 39) while no influence on the GPC depending on the cycle ratio of the AZO thin films deposited at room temperature was indicated.

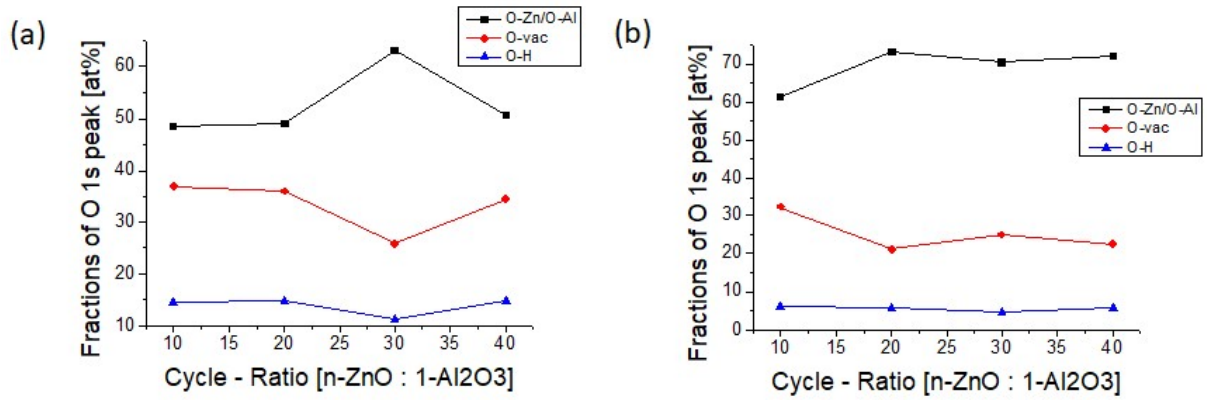

Figure 46: The oxygen hydrogen bound to zinc component (blue), the oxygen bound to zinc or oxygen bound to aluminium component (black) as well as the oxygen vacancies component (red) of the oxygen 1s peak are shown related to the deposited cycle-ratio at (a) room temperature and (b) elevated temperature (150 °C).

10) CRYSTAL STRUCTURE AND RESISTIVITY

As discussed in section 3.1.1 the conductivity, reversed proportional to the resistivity, depended on the deposition temperature due to different preferential orientations of the ZnO crystal structure. While for lower deposition temperatures the observed preferential orientation was the (100) direction, higher temperatures led to change to the (002) direction. Furthermore, the conductivity changed while varying the Al-content (section 3.2) resulting in a minimum of the resistivity due to the increase of the free charge carrier concentration and the decrease of their mobility, if a certain amount of free charge carriers leading to an increase of scattering events was exceeded. Those effects on the resistivity as well as the change in crystallite size and inter-planar spacing, due to the variation of the aluminium doping concentration, are shown in this chapter. Moreover, the results of the investigation of annealing is presented.

10.1 CRYSTAL STRUCTURE OF THE ELEVATED TEMPERATURE SERIES

Figure 47 shows the XRD-pattern of a θ/2θ-scan, done with the Panalytical European diffractometer at the institute. The investigation for the sample series deposited at elevated temperature (150 °C) was done, as the x-axis, indicated between 27 to 58 degrees. The deposited doping concentrations, or cycle ratios, were a pure ZnO (cyan) sample as well as a 40:1 (green), a 30:1 (blue), 20:1 (red) and a 10:1 (black) cycle-ratio sample. The red lines show the peak position of a ZnO reference measurement. The reference peak positions for the (002) direction and the (110) direction were slightly shifted to higher 2θ-values compared to the measured ZnO sample. Moreover, no (102) peak was observed for the whole sample series, but an (101) peak occurred while reducing the cycle ratio.

The polycrystalline wurtzite-structure from ZnO having a preferential orientation of the (002)-direction was pointed out. By enhancing the doping concentration, reducing the cycle ratio from 40:1 to 10:1, the peak intensity was decreased, as shown in Figure 14 as well, leading to a change of the preferential orientation from the (002)- to the (100)-direction. As a result, not only the deposition temperature influenced the preferential orientation, also the aluminium doping concentration did.

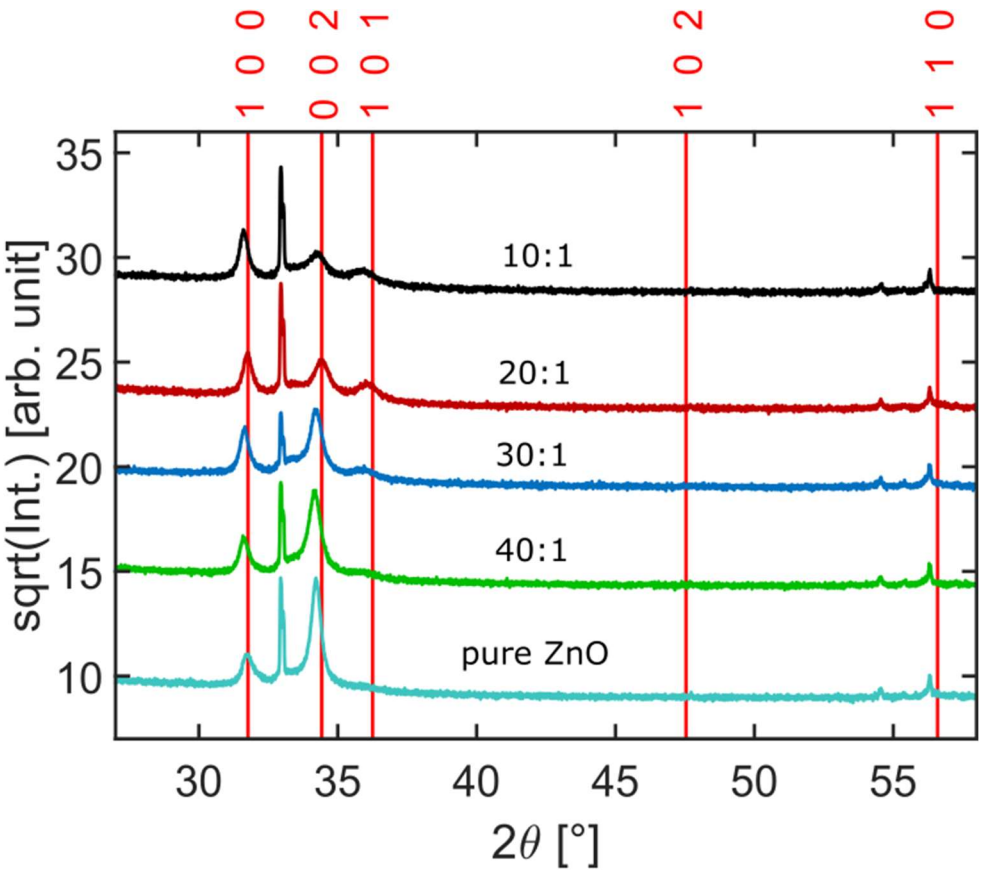

Figure 47: ϑ/2ϑ – scan of aluminium doped zinc oxide thin films having various Al-content and are deposited at an elevated temperature of 150 °C. Consequently, the cycle-ratios are written above each measured XRD-pattern. The red lines show the peak position of a ZnO reference measurement.

10.1.1 INTER-PLANAR SPACING OF THE SAMPLE SERIES DEPOSITED AT ELEVATED TEMPERATURE

For the investigation of the inter-planar distance, the Bragg-equation (formula 5) was used. Figure 48 shows the inter-planar spacing (d_{hkl}) of the ZnO-(100)-direction (black), the ZnO-(002)-direction (red) and the Si-(200)-direction (blue) depending on the aluminium content (at%).

In a specular X-ray diffraction, the occurrence of the Si-(200)-direction peak is a basis-forbidden reflection as mentioned in the paper “High-resolution characterisation of the forbidden Si 200 and Si 222 reflections” by Peter Zaumseil [40]. Under certain conditions this Si peak, appearing at about 2θ = 33°, occurs as a result of multiple diffraction. Due to the measuring range (27 degrees to 58 degrees), the forbidden Si-(200) peak was used as a reference peak. As a consequence, if the sample were well aligned, the peak stays constant while varying the doping concentration.

As the fits indicate in Figure 48, no change of the inter-planar spacing, ~2.82 Å for the ZnO-(100)-direction and ~2.62 Å for the ZnO-(002)-direction, while varying the aluminium content was observed.

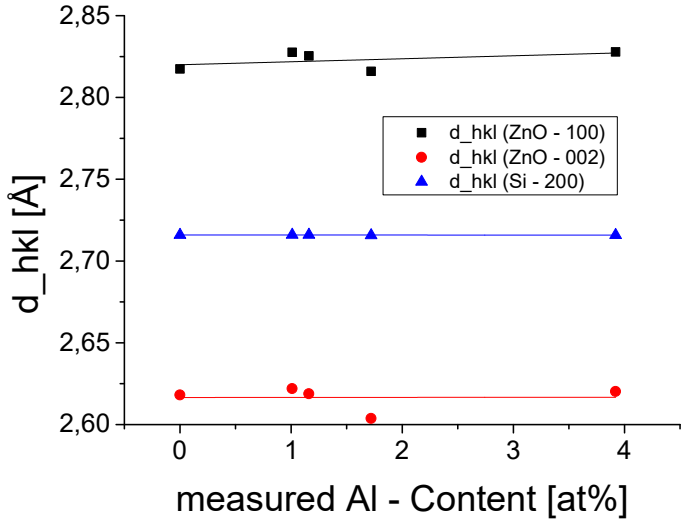

Figure 48:Inter-planar spacing (d_{hkl}) change, given in Å, in relation to measured aluminium content (at%) for the sample series deposited via plasma enhanced atomic layer deposition at elevated temperature (150 °C). The inter-planar distance of the ZnO-(100)-direction (black), the ZnO-(002)-direction (red) and the Si-(200)-direction (blue), as a reference measurement, are shown.

10.1.2 CRYSTALLITE SIZE OF THE SAMPLE SERIES DEPOSITED AT ELEVATED TEMPERATURE

For the investigation of the crystallite size, the Scherrer formula for spherical crystallites (formula 6) was used. Figure 49(a) shows, using the basis-forbidden Si-(200) peak (section 10.1.1) as reference peak, the crystallite size (D_{sph}) of the ZnO-(100)-direction (black), the ZnO-(002)-direction (red) and the Si-(200)-direction (blue) depending on the Al-content (at%).

A decrease of the crystallite size of the ZnO-(002)-direction could be observed while increasing the Al-content. The pure ZnO (0 at% Al-content) led to a crystallite size of 299 Å, while the AZO thin film sample with a cycle ratio of 10:1 (~3.92 at% Al-content) led to a reduced crystallite size of 111 Å.

While the ZnO-(002)-direction showed a big impact on varying the Al-content, the ZnO-(100)-direction showed a dramatically less one. Consequently, a rescaling (Figure 49(b)) was done. The pure ZnO led to a crystallite size of 230 Å for the ZnO-(100)-direction, while the AZO thin film sample, having an Al-content of approximately 3.92 at%, led to an enhanced crystallite size of 301 Å.

As a result, increasing the Al-content of the prepared samples led to a huge decrease of the crystallite size for the ZnO-(002)-direction, while that for the ZnO-(100)-direction was increased at the same time much less.

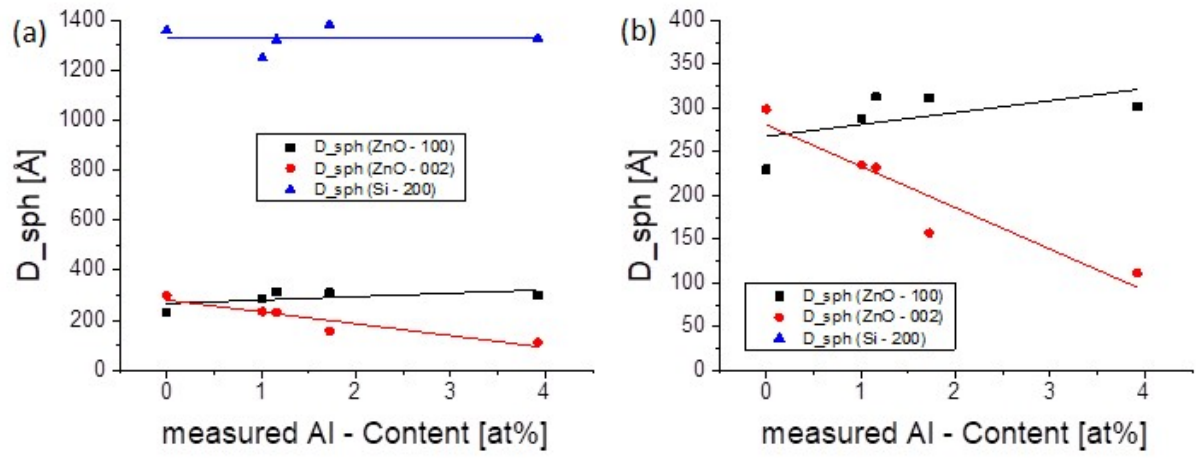

Figure 49(a): Crystallite size (D_{sph}) change, given in Å, depending on the aluminium content (at%) for the sample series deposited via plasma enhanced atomic layer deposition at elevated temperature (150 °C). The crystallite size of the ZnO-(100)-direction (black), the ZnO-(002)-direction (red) and the Si-(200)-direction (blue), as a reference measurement, are shown. (b) shows the same as (a) but having a different scaling, pointing out the increase of the ZnO-(100)-direction and excludes as a consequence the basis-forbidden Si-(200)-direction.

10.2 RESISTIVITY OF PLASMA-ENHANCED ATOMIC LAYER DEPOSITION DEPOSITED ALUMINIUM-DOPED ZINC OXIDE THIN FILMS AT ELEVATED TEMPERATURE

The goal of the master thesis is the optimization of AZO deposition obtaining low resistivity by using PEALD. However, PEALD led to higher resistivities (Figure 50) than compared to thermal ALD (Figure 16) as discussed in section 3.1.1.

Figure 50 shows the resistivities obtained by the 4-point probe measurements, discussed in section 5.5, for various measured aluminium doping concentrations (at%). The resistivity found for pure ZnO (0 at% Al-content) deposited using PEALD (2540 Ωcm) was lower than that (> 10^4 Ωcm) reported in the paper "Structural, optical, electrical and resistive switching properties of ZnO thin films deposited by thermal atomic layer deposition thermal and plasma-enhanced atomic layer deposition" by Jian Zhang et al. [6]. Furthermore, Figure 50 shows a minimum of the resistivity for a measured aluminium content of 1.16 at% corresponding to a cycle ratio of 30:1. Followed by the minimum, the 20:1 ratio sample (1.72 at% Al-content), indicated a higher resistivity than the pure ZnO.

Compared to Figure 47, showing a change of the preferential orientation from the ZnO-(002) to ZnO-(100)-direction, led to the suggestion, pointed out in section 10.4, that for achieving low resistivity the ZnO-(002) orientation should be preferred.

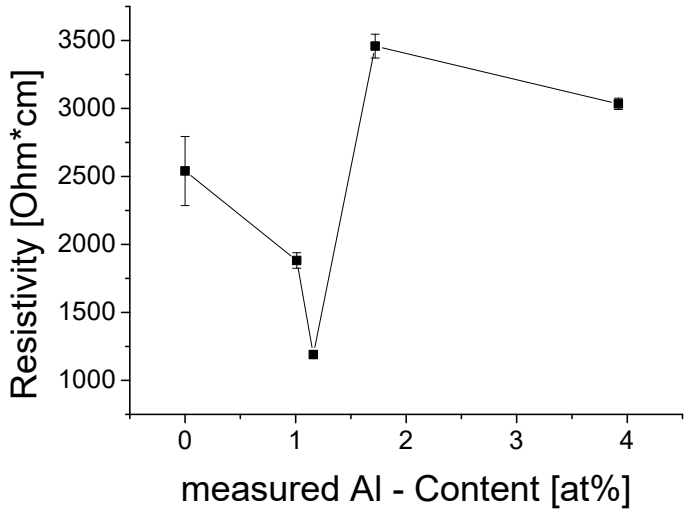

Figure 50: The resistivity as a function of measured aluminium content (at%) of aluminium doped zinc oxide films deposited by plasma enhanced atomic layer deposition on glass substrates. The samples are deposited at elevated temperature of 150 °C.

Figure 51 shows the ratio of oxygen to zinc and aluminium (O:Zn/Al), evaluated with a calculator written in excel, as a function of measured Al-content (at%) for the samples deposited at 150 °C. To calculate the amount of oxygen bound to carbon and the remaining one, the fitted areas of different C compounds lying at different energies, computed with the program CasaXPS by investigating the high resolution scans, and the amount of carbon as well as oxygen for the different samples, calculated from the surveys, were needed. Using the remaining oxygen and dividing it by the amount of zinc, weighted by 1 (ZnO), plus the amount of aluminium, weighted by 1.5 (Al_2O_3), resulted in the ratio seen in Figure 51. By comparing this figure to Figure 50 a minimum at the same measured Al-content (1.16 at%) for the ratio and the measured resistivity is pointed out.

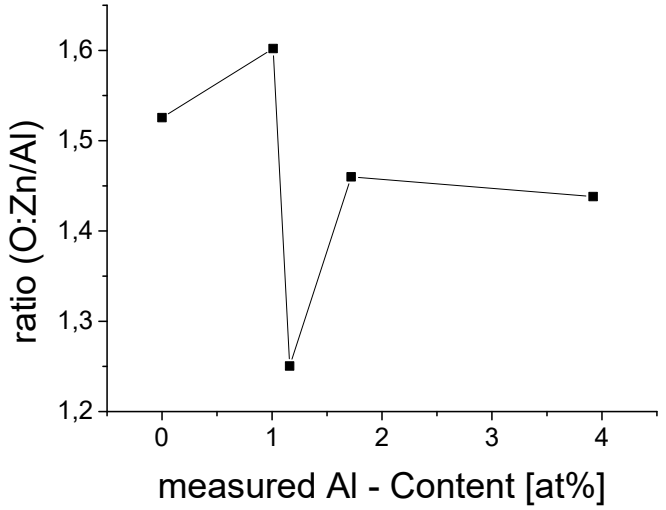

Figure 51: The ratio of oxygen to zinc or aluminium as a function of measured aluminium content (at%) of aluminium doped zinc oxide films deposited by plasma enhanced atomic layer deposition on silicon substrates having a native oxide layer on top. The samples are deposited at elevated temperature of 150 °C.

10.3 CRYSTAL STRUCTURE OF THE ROOM TEMPERATURE SERIES

Figure 52 shows the XRD-pattern of a θ/2θ-scan, between 27 degrees to 58 degrees, for the investigation of a sample series deposited at room temperature. The cycle ratios, were a 40:1 (dark green), a 35:1 (pink), a 30:1 (intense blue), a 25:1 (light red), a 20:1 (cyan), a 15:1 (light green) and three 10:1 cycle-ratios differing due to annealing. The black one was annealed at 600 °C for 375 min and the dark red one for 250 min, while the blue one remained untreated. The violet lines show the peak position of a ZnO reference measurement. The reference peak positions for the (110) direction were slightly shifted to higher 2θ-values compared to the measured ZnO sample. Moreover, neither a (102) and a (101) peak nor a (002) peak occurred for the whole series as shown in this figure.

The polycrystalline wurtzite structure having a preferential orientation of the (100)-direction was pointed out. Comparing this to Figure 47, the preferential orientation change, as mentioned in the sections 3.1.1 and 3.2, due to different deposition temperatures could be shown. Furthermore, as no (002)-, (101)- and (102)-directions were observed and only a small (110) peak occurred, it could be concluded that PEALD at room temperature led to a high oriented (100) crystal. While increasing the Al-content, indicated by the cycle ratio, a peak shift of the preferential (100)-direction to higher 2θ-values occurred. The behaviour shown in Figure 52 was also described in the paper “Structural, electrical, and optical properties of atomic layer deposition Al-doped ZnO films” by Parag Banerjee et al. [5]. Moreover, annealing at 600 °C, by comparing the three different 10:1 cycle ratios, seems to not influence the crystal structure very much due to having the same peak positions. Nevertheless, a small change in the intensity, while varying the cycle ratio, is indicated.

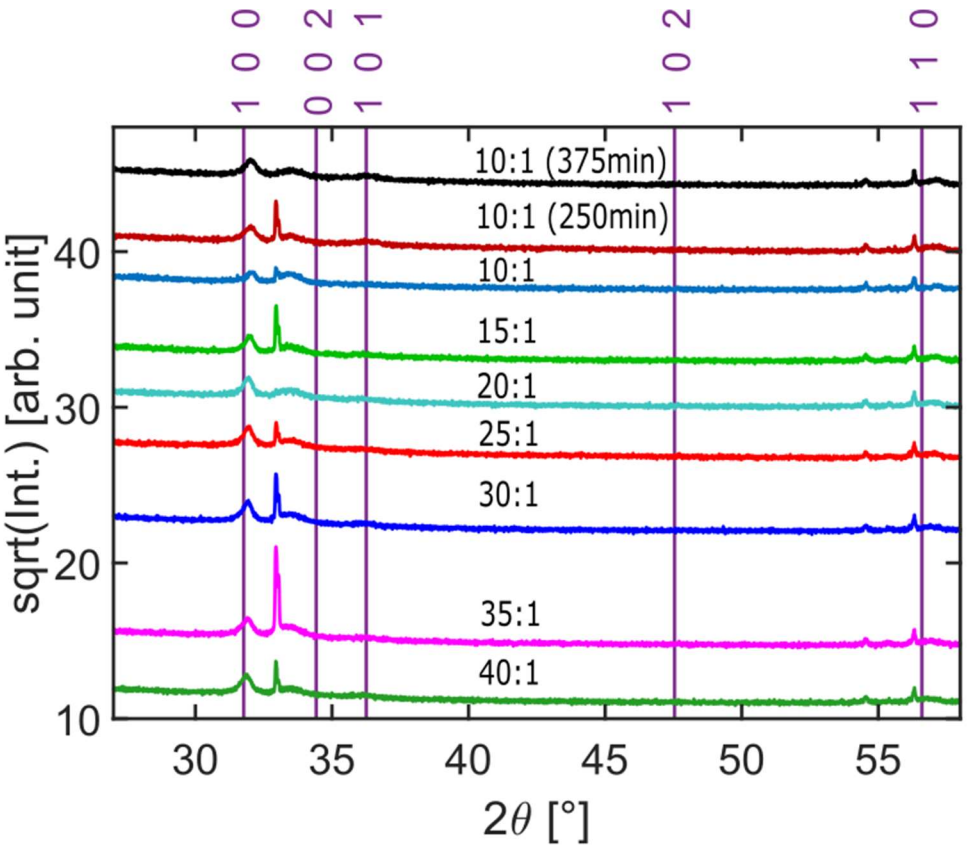

Figure 52: ϑ/2ϑ – Scan of aluminium doped zinc oxide thin films having various Al-content are deposited at room temperature. Consequently, the cycle-ratios are written above each measured XRD-pattern. For the 10:1 ratio also different annealing times for an annealing temperature of 600 °C are mentioned. The violet lines show the peak position of a ZnO reference measurement.

10.3.1 INTER-PLANAR SPACING OF THE SAMPLE SERIES DEPOSITED AT ROOM TEMPERATURE AND THE INFLUENCE OF ANNEALING THEM

Figure 53 shows, using the basis-forbidden Si-(200) peak (section 10.1.1) as reference peak, the inter-planar spacing (d_{hkl}) of the ZnO-(100)-direction (black), the ZnO-(100)-direction after annealing at 600 °C for 375 min (red) and the Si-(200) direction (blue) depending on the Al-content (at%).

The inter-planar distance for both ZnO-(100)-directions, the one annealed at 600 °C for 375 min (red) and the other one remained untreated (black), showed the same results, namely a decrease while decreasing the Al-content (at%). The AZO sample with a cycle ratio of 40:1 (~2.23 at% Al-content) led to an inter-planar distance for the (100) direction of about 2.81 Å, while the thin film with a cycle ratio of 10:1 (~10,16 at% Al-content) led to a reduced one of about 2.79 Å.

By comparing the depositions done at room temperature (Figure 53), the inter-planar spacing changed, to the one at 150 °C (Figure 48), the inter-planar spacing remains constant, while varying the Al-content, was pointed out.

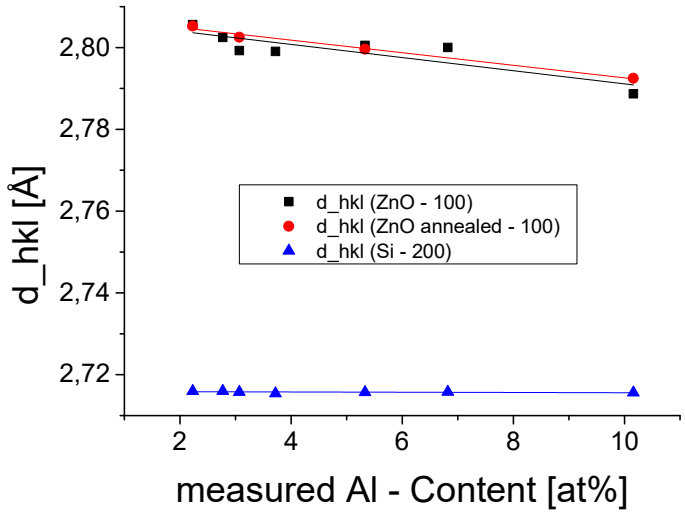

Figure 53: Inter-planar spacing (d_{hkl}) change, given in Å, in relation to measured aluminium content (at%) for the sample series deposited via plasma enhanced atomic layer deposition at room temperature. The inter-planar distance of the ZnO – (100) direction (black), the ZnO – (100) direction after annealing at 600 °C for 375 min (red) and the Si – (200) direction (blue), as a reference measurement, are shown.

10.3.2 CRYSTALLITE SIZE OF THE SAMPLE SERIES DEPOSITED AT ROOM TEMPERATURE AND THE INFLUENCE OF ANNEALING THEM

Figure 54(a) shows, using the basis-forbidden Si-(200) peak (section 10.1.1) as reference peak, the crystallite size (D_{sph}) of the ZnO-(100)-direction (black), the ZnO-(100)-direction after annealing at 600 °C for 375 min (red) and the Si-(200)-direction (blue) depending on the Al-content (at%).

The AZO thin film with a cycle ratio of 40:1 (~2.23 at% Al-content) led to a crystallite size of 242 Å for the ZnO-(100)-direction while the sample with a cycle ratio of 10:1 (~10.16 at% Al-content) led to an enhanced crystallite size of 279 Å.

Compared to Figure 49, the same behaviour for the ZnO-(100)-direction is shown. Nevertheless, the increase of the crystallites were higher than those for the deposited AZO thin films at room temperature (Figure 54).

Annealing in contrast led to a reduction of the crystallite size, comparing the annealed samples (red) to the samples remained untreated (black) in Figure 54(b), to 235 Å for the ZnO-(100)-direction while increasing the Al-content to approximately 10.16 at%.

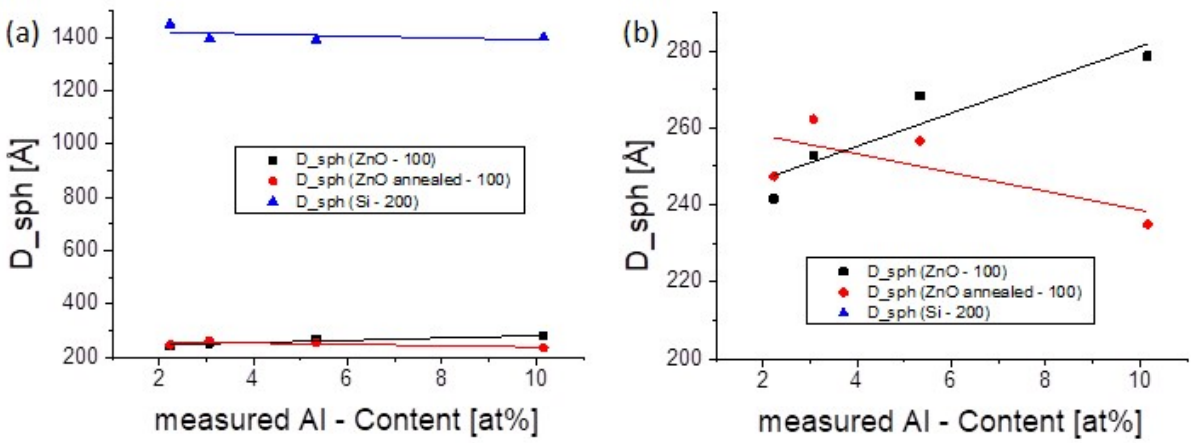

Figure 54: (a) Crystallite size (D_{sph}) change, given in Å, in relation to measured aluminium content (at%)for the sample series deposited using plasma enhanced atomic layer deposition at room temperature. The crystallite size of the ZnO – (100) direction (black), the ZnO – (100) direction after annealing at 600 °C for 375 min (red) and the Si – (200) direction (blue), as a reference measurement, are shown. (b) shows the same as (a) but has a different scaling to see the effect more in detail and excludes as a result the basis-forbidden Si – (200) direction.

10.4 RESISTIVITY OF PLASMA-ENHANCED ATOMIC LAYER DEPOSITION DEPOSITED ALUMINIUM DOPED ZINC OXIDE THIN FILMS AT ROOM TEMPERATURE AND THE INFLUENCE OF ANNEALING

To measure the resistivity of the deposited AZO thin films the 4-point probe method consisted of the setup shown in Figure 33 was used. Due to the limitation of the setup, the results for the resistivities measured for the samples deposited at room temperature using PEALD led to an overflow, a higher sheet resistance than 1 TΩ. As a consequence, insulation layers were produced.

To enhance the resistivity of the samples, annealing, leading to a decrease of the resistivity of the AZO thin films in orders of magnitude (Figure 55), at 600 °C for 375 min was done. The investigation, done for the same cycle ratios as for the samples deposited at 150 °C (compare Table 12 to Table 13), resulted after the annealing procedure in a decrease of the resistivity to 9 Ωcm for an Al-content of 2.23 at%.

The same cycle ratio resulted in an enhanced Al-content for the lower deposition temperature due to the different GPC. As a consequence, the resistivity may further decrease until an Al-content of 1.16 at% was reached.

Compared to Figure 50 led to the conclusion that enhancing the deposition temperature and annealing the AZO thin films result in a decrease of the resistivity. Furthermore, the expected minimum of the resistivity while varying the Al-content was found for the two investigated deposition temperatures (Figure 55 and Figure 50).

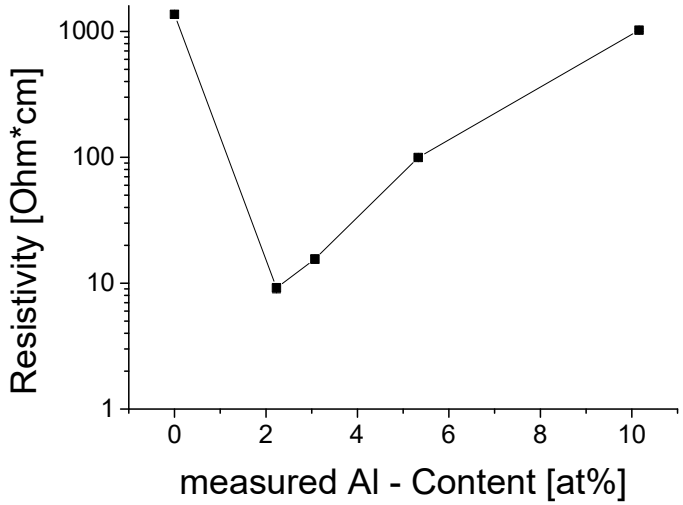

Figure 55: The resistivity as a function of measured aluminium content (at%) of aluminium doped zinc oxide films deposited by plasma enhanced atomic layer deposition on silicon substrates having an approximately 150 nm thick thermal silicon oxide layer on top. The samples are deposited at room temperature and have been annealed afterwards at 600 °C for 375 min.

11) CONCLUSION

This thesis demonstrated the possibility to deposit aluminium doped zinc oxide using plasma-enhanced atomic layer deposition and a minimum for the resistivity was found while varying the aluminium content. Furthermore, the influence of the deposition temperature on the crystal structure and the resistivity was pointed out.

11.1 PLASMA-ENHANCED ATOMIC LAYER DEPOSITION

- PEALD led to a uniform and self-limiting process as shown in chapter 6) for the growth per cycle, depending on the different times according to the 4 steps of a cycle. The uniform growth was demonstrated with the small deviation, coming up due to different positions in the reactor (Figure 22 and Figure 23). The self-limiting process was pointed out with the saturation curves done for the used precursor trimethylaluminium for depositing aluminium oxide layers.

- The oxidizing process of the used precursors, trimethylaluminium and diethylzinc, worked well, due to the vanishing carbon content after sputtering demonstrated by Figure 38.

- The doping procedure by varying the cycle ratio of zinc oxide to aluminium oxide layers from 40:1 to 10:1 pointed out the possibility of controlling the amount of deposited aluminium content (Figure 42). For the determination of the aluminium and the zinc content x-ray fluorescence and x-ray photoelectron spectroscopy were used. Section 9.3 demonstrated that x-ray photoelectron spectroscopy was not useful to determine the contents of the layer-by-layer deposited thin films using plasma-enhanced atomic layer deposition due to its surface sensitivity, leading to many troubles like the unknown number of measured layers (Figure 44). In contrast, x-ray fluorescence showed good congruities with the calculated aluminium contents (Figure 42).

- The growth per cycle was shown to be dependent on the deposition temperature, 2.509 Å/cycle for aluminium oxide and 1.604 Å/cycle for zinc oxide if deposited at room temperature and the reversed behaviour if deposited at 150 °C leading to 1.367 Å/cycle for aluminium oxide and 2.743 Å/cycle for zinc oxide.
  Furthermore, while doping two different behaviours are shown, a constant increase of the growth per cycle for higher aluminium contents deposited at room temperature due to the higher growth rates of aluminium oxide and aluminium content dependent growth rates for the prepared samples at 150 °C.

- The measured refractive index, showing a decrease while increasing the aluminium content due to the lower refractive index of aluminium oxide compared to zinc oxide, could be related to the deposited zinc and aluminium content.

11.2 CRYSTAL STRUCTURE AND RESISTIVITY

- A change of the preferred orientation of the crystal structure could be achieved by varying the deposition temperature leading to the ZnO-(002)-direction if deposited at 150 °C and to the ZnO-(100)-direction if deposited at room temperature.

- The crystallite size of the preferred orientation for depositing the aluminium doped zinc oxide at 150 °C resulted in a decrease whereas the ZnO-(100)-direction increased slightly, while increasing the aluminium content. Furthermore, an increase of the preferred ZnO-(100)-direction for the samples deposited at room temperature was shown, whereas the annealed thin films led to a decrease of the preferential orientation.

- The inter-planar distance for both investigated ZnO-directions, (100) and (002), of the prepared thin films deposited at 150 °C showed a constant behaviour, whereas the inter-planar distance, for the annealed as well as the remained untreated samples, deposited at room temperature pointed out a lowering of the ZnO-(100)-direction while increasing the aluminium content.

- The resistivity, pointing out a minimum while varying the aluminium content (Figure 50 and Figure 55), showed a decrease for depositing the aluminium doped zinc oxide thin films at elevated temperatures (compare depositions at room temperature and at 150 °C). A further annealing step, done at 600 °C for 375 min, resulted in a huge decrease of the resistivity (section 10.4). The minimum of the resistivity was shown for an aluminium content of 1.16 at% if deposited at 150 °C and for an aluminium content of 2.23 at% if deposited at room temperature including a following annealing step.

BIBLIOGRAPHY

[1] C. Jagadish and S. Pearton. “Zinc Oxide Bulk, Thin Films and Nanostructures”. In: Elsevier, Oxford, UK (2006).

[2] J. N. Duenow, T. A. Gessert, D. M. Wood, T. M. Barnes, M. Young, B. To, and T. J. Coutts. “Transparent conducting zinc oxide thin films doped with aluminum and molybdenum”. In: Journal of Vacuum Science & Technology A: Vacuum, Surfaces, and Films 25, 955 (2007).

[3] T. Minami, H. Nanto, and S. Takata. “Highly Conductive and Transparent Aluminum Doped Zinc Oxide Thin Films Prepared by RF Magnetron Sputtering”. In: Japanese Journal of Applied Physics, Volume 23, Part 2, Number 5.

[4] 4F. K. Shan, G. X. Liu, W. J. Lee, and B. C. Shin, ”The role of oxygen vacancies in epitaxial-deposited ZnO thin films”. In: Journal of Applied Physics 101, 053106 (2007).

[5] Parag Banerjee, Won-Jae Lee, Ki-Ryeol Bae, Sang Bok Lee, and Gary W. Rubloff. “Structural, electrical, and optical properties of atomic layer deposition Al-doped ZnO films.” In: *JOURNAL OF APPLIED PHYSICS 108, 043504 (2010).*

[6] H. C. M. Knoops, S. E. Potts, A. A. Bol, and W. M. M. Kessels. “Atomic Layer Deposition.” In: vol. 3. Handbook of Crystal Growth: Thin Films and Epitaxy: Second Edition. 2014, pp. 1101–1134.

[7] Nicola Pinna and Mato Knez. Atomic layer deposition of nanostructured materials. John Wiley & Sons, 2012.

[8] Assoc. Prof. Dr. Anna Maria Coclite. Supporting Documents “Oberflächen- und Dünnschichtphysik” (2016)

[9] https://www.halbleiter.org/en/waferfabrication/doping/. Accessed: 04.04.2018

[10] Jian Zhang, Hui Yang, Qi-long Zhang, Shurong Dong and J.K. Luo. “Structural, optical, electrical and resistive switching properties of ZnO thin films deposited by thermal atomic layer deposition thermal and plasma-enhanced atomic layer deposition”. In: Applied Surface Science 282 (2013), pp. 390–395.

[11] J. W. Elam and S. M. George. “Growth of ZnO/Al2O3 Alloy Films Using Atomic Layer Deposition Techniques”. In: Chem. Mater. (2003), 15, pp. 1020-1028.

[12] W J Maeng, Jae-won Lee, Ju Ho Lee, Kwun-Bum Chung and Jin-Seong Park. “Studies on optical, structural and electrical properties of atomic layer deposited Al-doped ZnO thin films with various Al concentrations and deposition temperatures”. In: Journal of Applied Physics, 44 (2011) 445305 (7pp).

[13] Stephen E. Potts, Gijs Dingemans, Christophe Lachaud and W. M. M. Kessels. “Plasma-enhanced and thermal atomic layer deposition of Al_2O_3 using dimethylaluminium isopropoxide, $[Al(CH_3)_2(\mu\text{-}O^iPr)]_2$, as an alternative aluminium precursor”. In: Journal of Vacuum Science & Technology A: Vacuum, Surfaces, and Films 30, 021505 (2012).

[14] Hadis Morkoç and Ümit Özgür. Zinc Oxide: Fundamentals, Materials and Device Technology. Wiley-VCH Verlag GmbH & Co. KGaA, 2007.

[15] Mi-jin Jin, Junhyeon Jo, Guru P Neupane, Jeongyong Kim, Ki-Seok An, and Jung-Woo Yoo. “Tuning of undoped ZnO thin film via plasma enhanced atomic layer deposition and its application for an inverted polymer solar cell.” In: AIP Advances 3.10 (2013), p. 102114.

[16] Sang-Hee Ko Park, Chi-Sun Hwang, Ho-Sang Kwack, Jin-Hong Lee, and Hye Yong Chu. “Characteristics of ZnO thin films by means of plasma-enhanced atomic layer deposition.” In: Electrochemical and solid-state letters 9.10 (2006), G299–G301.

[17] SF Yu, Clement Yuen, SP Lau, and HW Lee. “Zinc oxide thinfilm random lasers on silicon substrate.” In: Applied physics letters 84.17 (2004), pp. 3244–3246.

[18] B. Hoex, J. Schmidt, P. Pohl, M. C. M. van de Sanden, *and* W. M. M. Kessels. “Silicon surface passivation by atomic layer deposited Al_2O_3“. In: Journal of Applied Physics 104, 044903 (2008).

[19] R. Matero, M. Ritala, M. Leskelä, T. Salo, J. Aromaa and O. Forsén. “Atomic layer deposited thin films for corrosion protection”. In: *Journal de Physique IV France 09 (1999), pp. 493-499.*

[20] D. I. Garcia-Gutierrez, D. Shahrjerdi, V. Kaushik, and S. K. Banerjee. “Physical and electrical characterizations of metal-oxide-semiconductor capacitors fabricated on GaAs substrates with different surface chemical treatments and Al_2O_3 gate dielectric”. In: Journal of Vacuum Science & Technology B, Nanotechnology and Microelectronics: Materials, Processing, Measurement, and Phenomena 27, 2390 (2009)

[21] Julian Pilz. “Plasma-enhanced atomic layer deposition of zinc oxide thin films”. Master thesis (2017)

[22] Swagelok. Diaphragm Valves for Atomic Layer Deposition. https://www.swagelok.com/downloads/WebCatalogs/en/MS-02-301.PDF. Accessed: 19.04.2018.

[23] National Institute of Standards and Technology. Diethylzinc VapourPressure. http://webbook.nist.gov/cgi/cbook.cgi?ID=C557200&Mask=4&Type=ANTOINE&Plot. Accessed: 19.04.2018.

[24] https://en.wikipedia.org/wiki/Trimethylaluminium. Accessed: 27.03.2018

[25] Sigma Aldrich. Diethyl Safty Data Sheet. http://www.sigmaaldrich.com/catalog/product/aldrich/668729. Accessed: 19.04.2018.

[26] Written on the TMA-reservoir (PCode: 1002183055 663301-25G)

[27] http://www.iue.tuwien.ac.at/phd/puchner/node24.html. Accessed: 02.04.2018

[28] J. A. Woolam Co. Ellipsometry Tutorial. https://www.jawoollam.com/resources/ellipsometry-tutorial/ellipsometry-measurements. Accessed: 19.04.2018.

[29] J. A. Woolam Co. CompleteEASE Data Analysis Manual. http://crn2.3it.usherbrooke.ca/guide_sb/appareils/Ellipsometre/CompleteEASE%20Manual.pdf. Accessed: 19.04.2018.

[30] G. Luka, T. A. Kranjewski, B. S. Witkowski, G. Wisz, I. S. Virt, E. Guziewicz and M. Godlewski. ”Aluminium-doped zinc oxide films grown by atomic layer deposition for transparent electrode applications”. In: Journal of Materials Science: Materials in Electronics (2011), Volume 22, Issue 12, pp. 1810-1815.

[31] Mario Birkholz. Thin film analysis by X-ray scattering. John Wiley & Sons, 2006.

[32] Peter Brouwer. “Theory of XRF, Getting acquainted with the principles“. In: PANalytical B.V. (2010).

[33] http://slideplayer.com/slide/6188331/18/images/25/Characteristic+X-Ray+Production.jpg. Accessed: 19.04.2018

[34] PANalytical. “Epsilon 1, Flexible and accurate elemental analysis.pdf“. Downloaded: 06.03.2018

[35] PANalytical. “Epsilon 1, User’s Guide”. 4022 339 20671, (2013).

[36] https://www.colorado.edu/physics/phys3340/phys3340_sp13/CourseInformation/Modern/XPS.pdf. Spring 2007

[37] F. M. Smits. “Measurement of Sheet Resistivities with the Four-Point Probe”. Manuscript received (1957)

[38] Tommi Tynell and Maarit Karppinen. “Atomic layer deposition of ZnO: a review.” In: Semiconductor Science and Technology 29.4 (2014), p. 043001.

[39] Pieter C Rowlette, Cary G Allen, Olivia B Bromley, Amy E Dubetz, and Colin A Wolden. “Plasma-Enhanced Atomic Layer Deposition of Semiconductor Grade ZnO Using Dimethyl Zinc.” In: Chemical Vapor Deposition 15.1-3 (2009), pp. 15–20.

[40] Peter Zaumseil. “High-resolution characterisation of the forbidden Si 200 and Si 222 reflections”. In: Journal of applied crystallography (2015), pp. 528-532